Geotechnical design of offshore wind monopiles under cyclic loading

Aude Péchadre

TU Delft Delft University of Technology

SIEMENS Gamesa RENEWABLE ENERGY

Geotechnical design of offshore wind monopiles under cyclic loading

by

Aude Péchadre

in partial fulfilment of the requirement for the degree of Master of Science
in Offshore & Dredging Engineering
at the Delft University of Technology

To be defended publicly on Tuesday, July 27, 2021 at 10:00 AM

Student number:	5041015	
Project duration:	December 1, 2020 – July 27, 2021	
Thesis committee:	Prof. dr. A.V. Metrikine,	TU Delft, chairman
	Dr. F. Pisanó,	TU Delft, university supervisor
	Dr. ir. R.B.J. Brinkgreve,	TU Delft & Plaxis B.V.
	Ir. S. Panagoulias,	Siemens Gamesa Renewable Energy & TU Delft, company supervisor
	Dr. A. Nernheim,	Siemens Gamesa Renewable Energy, company supervisor

An electronic version of this thesis is available at `http://repository.tudelft.nl/`.

TU Delft Delft University of Technology

SIEMENS Gamesa RENEWABLE ENERGY

Aknowledgements

In December 2020, I started my MSc thesis at Siemens Gamesa Renewable Energy as a graduate student. This period was certainly one of the most challenging time I had to face so far but I am satisfied with the final result. Graduating with an organisation like SGRE provided me with the guidance and expertise I needed for accomplishing the thesis objectives.

I would like to warmly thank my daily supervisors at SGRE Stavros Panagoulias and Axel Nernheim for their close supervision and valuable advice during the whole thesis. I really enjoyed our weekly meetings that helped me to stay motivated and focused. The useful coding tips and friendly messages were very appreciated. I would like to thank Sebastiaan Hermans for giving me te opportunity to graduate with SGRE in the first place.

Furthermore, I would like to thank the members of the TU Delft committee Federico Pisanó and Ronald Brinkgreve for their feedback and guidance throughout the thesis. I am very grateful for their support on my tight graduation schedule.

I would like to thank Dr. Kuo for kindly sharing his Phd thesis with me about the Stiffness Degradation Method (SDM). The document was very helpful for understanding the method and realizing the verification procedure of my study model.

My special thanks go to my family and friends who supported me throughout the thesis rollercoaster. Studying at TU Delft would not have been the same rewarding experience without them. Finally, I would like to thank Bobby for his love and patience during the thesis period. Since december, he learnt as much as me about the cyclic degradation of sand and I am very grateful for his support.

Aude Pechadre
Delft, July 2021

Abstract

For supporting Offshore Wind Turbines (OWT), monopiles are currently the most common foundations. The role of a foundation is to transfer safely the loading to the ground. The wind and the wave loads are considered cyclic because they repetitively apply on the OWT. The North Sea is sand dominated in many areas. During cyclic loading, permanent strains develop in the surrounding soil while the soil stiffness and strength are irreversibly affected. Through time, the accumulation of strains can lead to the soil failure. Thus, assessing the behaviour and stability of monopiles under cyclic loading is essential.

To model the response of monopiles under lateral loading, the traditional design procedure is the use of p-y curves that express the lateral soil resistance in function of the pile deflection. The p-y curves are nowadays recommended to be calibrated on FE models. The Stiffness Degradation Method (SDM) of Achmus et al. (2009) [2] is a numerical strategy that assesses the behaviour of a monopile under cyclic loading. The method estimates the cyclically degraded stiffness based on the results of a static analysis. The soil stiffness is degraded based on a semi-empirical power law that accounts for the number of loading cycles, the stresses in the soil after the static analysis and two model parameters calibrated on cyclic triaxial tests.

The SDM was successfully implemented in PLAXIS 3D via a practical routine coded in Python and the use of soil clusters around the pile. The soil stiffness is degraded by updating the soil material within the clusters. The study model was verified by comparing results with the published reference system of Kuo (2008) [39] for two piles with pile embedded length to pile diameter ratios of 2.7 and 5.3. The results indicate that the study model provides a stiffer pile-soil response than the reference model because the soil stiffness is overestimated. The degraded stiffness overestimation is attributed to the initial stiffness mismatch and the use of soil clusters. The impact on the short pile is greater than on the long pile because the short pile opposes less resistance to the loading and is thus more affected by the stiffness difference.

The study model was validated against three 1-g pile tests for homogeneous uniform and multi-layered dense sand. The numerical results are in agreement with the test data. In the absence of cyclic triaxial tests, the two model parameters were directly calibrated on the pile head displacement of the experiment. The two model parameters have a significant impact on the stiffness degradation. Thus, model parameters from literature were classified from the highest to the smallest estimation of pile lateral displacement.

The results of codified and published approaches (DNV-GL-0126 [24]; Dührkop (2009) [23]; Garnier, 2013 [27]) were compared with the results of the study model. The study model and the method of Garnier (2013) [27] are in agreement. They both account for the loading amplitude, the number of cycles and the pile geometry. The codified procedure [24] and the method of Dührkop (2009) [23] estimate higher lateral displacement compared to the study model. Finally, the 1D model was successfully calibrated with the highest displacement estimate of the study model. With this procedure, the 1D model accounts for the number of cycles, the pile geometry and the loading amplitude.

The study model provides a less conservative approach for determining the pile lateral displacement under cyclic loading. The calibration of the 1D model on the pile deflection curves of the study model is a promising procedure which will require further research.

Contents

Aknowledgements iii

Abstract v

List of Figures xi

List of Tables xv

List of Symbols xvii

List of Abbreviations xxi

1 Introduction 1
- 1.1 General context . . . 1
  - 1.1.1 Offshore wind foundations . . . 1
  - 1.1.2 Cyclic loading . . . 1
  - 1.1.3 Cyclic behaviour of sand . . . 2
  - 1.1.4 Current design practice . . . 2
  - 1.1.5 Numerical models . . . 2
  - 1.1.6 Stiffness Degradation Method (SDM) . . . 2
- 1.2 Thesis objectives and methodology . . . 2
  - 1.2.1 Objective 1: Literature overview . . . 3
  - 1.2.2 Objective 2: FE implementation . . . 3
  - 1.2.3 Objective 3: Verification . . . 3
  - 1.2.4 Objective 4: Validation . . . 3
  - 1.2.5 Objective 5: Design integration . . . 4

2 Literature overview 5
- 2.1 Definition of cyclic loading . . . 5
  - 2.1.1 Definition of cyclic loading . . . 5
  - 2.1.2 Cyclic loading on offshore wind structures . . . 6
- 2.2 Cyclic behaviour of sand . . . 7
  - 2.2.1 Drained conditions . . . 7
  - 2.2.2 Undrained conditions . . . 9
  - 2.2.3 Compression and extension states . . . 11
  - 2.2.4 Impact of one-way and two-way cyclic loading . . . 11
- 2.3 Current design practice for offshore wind monopiles . . . 13
  - 2.3.1 Rigid behaviour of wind monopiles . . . 13
  - 2.3.2 P-y curves . . . 14
  - 2.3.3 Power laws . . . 15
- 2.4 Conclusion . . . 17

3 Stiffness Degradation Method (SDM) 19
- 3.1 Origin of the Stiffness Degradation Method . . . 19
  - 3.1.1 Permanent strains in sand under cyclic loading . . . 19
  - 3.1.2 Stiffness degradation concept . . . 20
- 3.2 Implementation in a FE model . . . 21
- 3.3 Parameters . . . 22
  - 3.3.1 Soil parameters . . . 23
  - 3.3.2 Model parameters . . . 23
- 3.4 Conclusion . . . 23

4 FE implementation of the SDM 25
4.1 Step 1: Model parameters . . . 25
4.1.1 Soil parameters . . . 25
4.1.2 Monopile parameters . . . 25
4.1.3 Loading conditions . . . 26
4.1.4 Project parameters . . . 26
4.2 Step 2: Soil constitutive model . . . 26
4.3 Step 3: Monopile structure . . . 27
4.3.1 Monopile model . . . 27
4.3.2 Interfaces . . . 28
4.3.3 Lateral displacement . . . 28
4.4 Step 4: Soil clusters . . . 28
4.5 Step 5: Phases . . . 30
4.6 Step 6: Stiffness degradation procedure . . . 31
4.6.1 Cyclic stress ratio . . . 31
4.6.2 Stiffness degradation . . . 32
4.7 Step 7: Update of the stiffness . . . 32
4.8 Conclusion . . . 32

5 Verification of the study model 33
5.1 Reference system with L=20m . . . 33
5.1.1 Stiffness degradation . . . 33
5.1.2 Pile deflection . . . 35
5.2 Reference system with L=40m . . . 36
5.2.1 Principal stresses . . . 36
5.2.2 Stiffness degradation . . . 38
5.2.3 Pile deflection . . . 40
5.3 Interpretation . . . 41
5.3.1 Soil model . . . 42
5.3.2 Pile model . . . 42
5.3.3 Beam stiffness . . . 43
5.3.4 Mesh refinement . . . 44
5.3.5 Cluster layout . . . 45
5.3.6 Bottom interface . . . 47
5.4 Conclusion . . . 48

6 Validation of the study model 51
6.1 Pile test of Hettler (1981) . . . 51
6.1.1 Pile test settings . . . 51
6.1.2 Results comparison . . . 52
6.2 Pile test of Achmus et al. (2007) . . . 52
6.2.1 Pile test settings . . . 53
6.2.2 Results comparison . . . 53
6.2.3 Impact of parameters b_1 and b_2 . . . 54
6.3 Pile test of Li et. al (2015) . . . 55
6.3.1 Pile test settings . . . 55
6.3.2 Results comparison . . . 56
6.4 Discussion about 1-g experiments . . . 58
6.5 Conclusion . . . 58

7 Design integration 59
7.1 Reference system . . . 59
7.2 Model adaptation to design framework . . . 60
7.2.1 Homogeneous soil model . . . 60
7.2.2 Multi-layered soil model . . . 61

7.3 Comparison with current design practices . . . 61
7.3.1 Cyclic design practices . . . 61
7.3.2 Static analysis . . . 63
7.3.3 Cyclic analysis . . . 64
7.4 SLS assessment - Total rotation . . . 66
7.5 Calibration of the 1D model with the SDM . . . 67
7.5.1 Highest and most probable estimates . . . 67
7.5.2 Calibration of the SDM results on the 1D model . . . 68
7.6 Conclusion . . . 69

8 Conclusions and Recommendations 71
8.1 Conclusions. . . . 71
8.2 Recommendations . . . 72
8.2.1 Recommendations for the use of the study model . . . 72
8.2.2 Recommendations for future research . . . 73

Bibliography 75

Appendices 81

A Appendix A 83

B Appendix B 85

C Appendix C 87

D Appendix D 89
D.1 Pile test of Hettler (1981) . . . 89
D.2 Pile test of Achmus et al. (2007) . . . 90
D.3 Pile test of Li et al. (2015) . . . 91

E Appendix E 93

F Appendix F 95

List of Figures

1.1 Different offshore foundation types, after Bhattacharya (2014) [11] 1

2.1 Cyclic loading definitions for constant time period and loading amplitude, after Andersen et al. (2013) [6] 5
2.2 Drawing of the loads acting on offshore wind monopile, after Bhattacharya et al. (2017) [12] . . 6
2.3 Relation of wave and wind loading spectra to f_0, f_{1P} and f_{3P}, Kallehave et al. (2015) [34] 7
2.4 Settlements of a foundation under cyclic loading, after Wichtmann (2005) [72] 7
2.5 Behavior of a granular material subjected to drained cyclic triaxial loading. (a) Evolution of the effective mean stress p'_m, deviatoric stress q', axial strain ϵ_1 and void ratio e_1, (b) Evolution of the strain increment per cycle with the number of load cycles; S1, S2 and S3 are initial stress states, after Pasten et al. (2014) [53] 8
2.6 Visualisation of the shakedown theorem, after Shajarati et al. (2012) [63] 9
2.7 Pore pressure as a function of axial strains in an undrained cyclic triaxial test in compression, after Shajarati et al. (2012) [63] 10
2.8 Illustration of phase transformation line (PTL) in a $q - p_m$ space, after Liu (2020) [46] 10
2.9 Effective stress paths during undrained triaxial test in compression (CU) and extension (EU), after De Gennaro et al. (2004) [20] 11
2.10 Classification of cyclic lateral loading conditions on single pile, after Kuo (2008) [39] 12
2.11 Rigid pile deformation about a pivot point (left) and a flexible pile deflection (right) demonstration from Sorensen et al. (2012) [65]) 13
2.12 Beam on non-linear Winkler foundation, after Jalbi et al. (2019) [33] 14
2.13 Soil reaction components applied to the 1D FE model, after Byrne et al., 2015 [17] 15

3.1 Formulation evaluation of Huurman (1996) [30] after Kuo (2008) [39] 20
3.2 Definition of secant shear modulus from Kuo (2008) [39] 20
3.3 Shear modulus response of sand under stress-controlled drained cyclic test, from Kuo (2008) [39] 20
3.4 Schematic degradation of secant modulus under cyclic loading after Kuo (2008) [39] 21
3.5 Schematic sketch of the determination of degradation stiffness in the pile-soil system after Achmus et al. (2009) [2] 22

4.1 View of the PLAXIS 3D model presenting the model and pile dimensions 25
4.2 Elastic-perfectly plastic assumption of Mohr-Coulomb model, after Ti et al. (2009) [67] 26
4.3 Layer-dependent stiffness (Mohr-Coulomb) and stress-dependent stiffness (SDM) in function of the depth at initial stress conditions for $\kappa = 600$ and $\lambda = 0.55$ 27
4.4 Monopile structure of the study model - View of the PLAXIS 3D pile model 27
4.5 Definition of the soil clusters layout. Top and bottom pictures are respectively front and top view of the pile 29
4.6 Static analysis: Construction stages of the SDM static analysis 30
4.7 Schematic representation of the procedure for calculating the cyclic stress ratio in a cluster . . . 31
4.8 Schematic representation of the procedure for degrading the soil stiffness 32

5.1 Soil stiffness after N=1, 100 and 10 000 cycles for the pile-soil system with an embedded length $L = 20m$ - Results comparison between the reference system of Kuo (2008) [39] and the study model 34
5.2 Lateral displacement of a monopile after N=1 cycle for L=20m - Results comparison between the reference system of Kuo (2008) [39] and the study model 35
5.3 Lateral displacement of a monopile after N=100 cycle for L=20m - Results comparison between the reference system of Kuo (2008) [39] and the study model 35
5.4 Lateral displacement of a monopile after N=10 000 cycle for L=20m - Results comparison between the reference system of Kuo (2008) [39] and the study model 36

5.5 Major principal stress $\sigma_1^{(0)}$ and minor principal stress $\sigma_3^{(0)}$ at phase 0 for L=40m - Results comparison between the reference system of Kuo (2008) [39] and the study model 37
5.6 Major principal stress $\sigma_1^{(1)}$ and minor principal stress $\sigma_3^{(1)}$ at phase 1 for L=40m - Results comparison between the reference system of Kuo (2008) [39] and the study model 38
5.7 Soil stiffness after N=1, 100 and 10 000 cycles for the pile-soil system with an embedded length $L = 40m$ - Results comparison between the reference system of Kuo (2008) [39] and the study model 39
5.8 Lateral displacement of a monopile after N=1 cycle for L=40m - Results comparison between the reference system of Kuo (2008) [39] and the study model 40
5.9 Lateral displacement of a monopile after N=100 cycles for L=40m - Results comparison between the reference system of Kuo (2008) [39] and the study model 41
5.10 Lateral displacement of a monopile after N=10 000 cycles for L=40m - Results comparison between the reference system of Kuo (2008) [39] and the study model 41
5.11 Lateral displacement of a monopile after N=1 cycle for L=20m - Results comparison between the reference system of Kuo (2008) [39] and the study model with stiff and flexible beams. 43
5.12 Lateral displacement of a monopile after N cycles for L=20m - Results comparison between the reference system of Kuo (2008) [39] and the study model with stiff and flexible beams. 43
5.13 Lateral displacement of a monopile after N=1 cycle for L=20m - Results comparison between the reference system of Kuo (2008) [39] and the study model with two coarseness factors: 0.075 and 0.050 44
5.14 Lateral displacement of a monopile after N cycles for L=20m - Results comparison between the reference system of Kuo (2008) [39] and the study model with two coarseness factors: 0.075 and 0.05 44
5.15 Lateral displacement of a monopile after N=1 cycle for L=20m - Results comparison between the reference system of Kuo (2008) [39] and the study model for two constant layer depths: $a = 2.5$m and $a = 1.5$m. 45
5.16 Lateral displacement of a monopile after N cycles for L=20m - Results comparison between the reference system of Kuo (2008) [39] and the study model for two constant layer depths: $a = 2.5$m and $a = 1.5$m. 45
5.17 Lateral displacement of a monopile after N cycles for L=20m - Results comparison between the reference system of Kuo (2008) [39] and the study model for two cluster width b close to the pile: $b = 2$m and $b = 1$m. 46
5.18 Lateral displacement of a monopile after N cycles for L=20m - Results comparison between the reference system of Kuo (2008) [39] and the study model for three numbers of clusters per ring c: $c = 3$, $c = 4$ and $c = 5$. 46
5.19 Lateral displacement of a monopile after N=1 cycle for L=20m - Results comparison between the reference system of Kuo (2008) [39] and the study model with and without interface at the pile tip 47
5.20 Lateral displacement of a monopile after N cycles for L=20m - Results comparison between the reference system of Kuo (2008) [39] and the study model with and without interface at the pile tip 48

6.1 Pile test settings of Hettler (1981) [29], after Kuo (2008) [39] 51
6.2 Normalized pile head displacement of a monopile after N loading cycles under constant cyclic lateral loading: $H = 66\%H_u$, $H = 36\%H_u$ and $H = 24\%H_u$ - Comparison of the results of Hettler (1981) [29], study model and Kuo (2008) [39] 52
6.3 Pile test settings of Achmus et al. (2007) [1], after Kuo (2008) [39] 53
6.4 Pile head displacement of a monopile after N loading cycles under constant cyclic lateral loading $H = 40\%H_u$ and $H = 10\%H_u$- Comparison of the results of Achmus et al. (2007) [1], study model and Kuo (2008) [39] 54
6.5 Pile head displacement of a monopile after N loading cycles under constant cyclic lateral loading $H = 40\%H_u$- b_2 is kept constant and b_1 is set to respectively 0.08, 0.12 and 0.16 54
6.6 Pile head displacement of a monopile after N loading cycles under constant cyclic lateral loading $H = 40\%H_u$- b_1 is kept constant and b_2 is set to respectively 0.05, 0.5 and 5 55
6.7 Pile test settings of Li et al. (2015) [42] 56
6.8 Pile head displacement of a monopile in function of the monotonic lateral loading - Comparison of the results of Li et al. (2015) [42] and the study model 57

6.9 Pile head displacement of a monopile after N loading cycles under constant cyclic lateral loading $H = 30\%H_u$ - Comparison of the results of Li et al. (2015) [42] and the study model for two sets of parameters: $b_1 = 0.1$, $b_2 = 8$ and $b_1 = 0.05$, $b_2 = 5$ 57

7.1 Calibration of the stiffness parameters κ and λ on the CPT stiffness 60
7.2 Normalised cyclic degradation factor A_{cycl}/A_{stat} in function of depth - Comparison of the cyclic coefficient of the codified procedure and the method of Dührkop (2009) [23] for $N = 10^2$, $N = 10^3$, $N = 10^4$ and $N = 10^5$ loading cycles 62
7.3 Cyclic degradation coefficient r_c in function of depth for $N = 10^3$, $N = 10^4$ and $N = 10^5$ cycles, based on the method of Garnier (2013) [27] 63
7.4 Lateral displacement of a monopile after N=1 cycle (design exercise) - Results comparison between the study models and the 1D model 63
7.5 Lateral displacement of a monopile after $N = 10^2$ cycles (design exercise) - Results comparison between the study models and the method of Garnier (2013) [27], Dührkop (2009) [23] and the codified procedure 64
7.6 Lateral displacement of a monopile after N cycles (design exercise) - Results comparison between the study models and the method of Garnier (2013) [27], Dührkop (2009) [23] and the codified procedure 64
7.7 Pile lateral displacement at mudline after N cycles (design exercise) - Results comparison between the study models and the method of Garnier (2013) [27], Dührkop (2009) [23] and the codified procedure 65
7.8 Total pile rotation after N cycles - Comparison between the homogeneous and multi-layered soil models 66
7.9 Pile lateral displacement at mudline in function of the number of cycles for 5 sets of parameters b_1 and b_2 obtained with the multi-layered soil model 67
7.10 Pile lateral displacement at mudline in function of the number of cycles - Calibration of the 1D model on the highest estimate 68
7.11 Pile lateral displacement in function of depth after N loading cycles - Results comparison between the study model (highest and most probable estimates), the codified procedure and the 1D-model 68

B.1 Calibration of the parameters b1 and b2 on a cyclic triaxial test performed on Zaanweg sand from Huurman (1996) 85

C.1 Pile lateral displacement in function of depth for N=1, 100 and 10 000 cycles - Comparison of the results of the homogeneous soil model (chapter 7) with and without axial load 87

D.1 FE model of the pile test of Hettler (1981) [29] - PLAXIS 3D View 89
D.2 FE model of the pile test of Achmus et al. (2007) [1] - PLAXIS 3D View 90
D.3 FE model of the pile test of Li et al. (2015) [42] - PLAXIS 3D View 91

F.1 Pile head displacement at mudline in function of the number of cycles - Multi-layered soil model 95

List of Tables

3.1 Model parameters b_1 and b_2 calibrated on existing cyclic triaxial tests after Kuo (2008) [39] . . . 23

5.1 Input parameters of the reference system (Kuo, 2008 [39]) . . . 33
5.2 Clusters layout parameters for verifying the study model on the reference system of Kuo (2008) [39] . . . 33
5.3 Number of elements and nodes of the FE models for different coarseness factors . . . 44
5.4 Revised cluster layout for the two reference systems of Kuo (2008) [39] . . . 47
5.5 Recommendations for the cluster layout of the study model . . . 47

6.1 Input parameters of the numerical model Hettler (1981) [29], after Kuo (2008) [39] . . . 52
6.2 Input parameters of the numerical model of Achmus et al. (2007) [1], after Kuo, 2008 [39] . . . 53
6.3 Model parameters b_1 and b_2 of the sensitivity study . . . 54
6.4 Input parameters of the numerical model of Li et al. (2015) [42], after Yang et al. (2018) [74] - Soil parameters . . . 56
6.5 Input parameters of the numerical model of Li et al. (2015) [42], after Yang et al. (2018) [74] - Pile and loading parameters . . . 56

7.1 Soil input parameters for the reference system (CPT data) . . . 59
7.2 Pile input parameters for the reference system . . . 60
7.3 Load input parameters for the reference system . . . 60
7.4 Soil input parameters of the homogeneous model . . . 60
7.5 Degradation coefficients r_c developped by Garnier (2013) [27] . . . 62
7.6 Sets of parameters b_1 and b_2 for determining the highest and most probable estimate of the pile lateral displacement of the reference system . . . 67

A.1 Summary table of cyclic pile tests in chronological order and their parameters . . . 83

D.1 Cluster layout of the FE model representing the settings of the pile test of Hettler (1981) [29] . . . 89
D.2 Load cases of the pile test of Hettler (1981) [29] . . . 90
D.3 Cluster layout of the FE model representing the settings of the pile test of Achmus et al. (2007) [1] 91
D.4 Load cases of the pile test of of Achmus et al. (2007) [1] . . . 91
D.5 Cluster layout of the FE model representing the settings of the pile test of Li et al. (2015) [42] . . . 91

E.1 Soil parameters of the reference models and pile tests on which the study model is validated . . . 93
E.2 Pile parameters of the reference models and pile tests on which the study model is validated . . . 93
E.3 Loading parameters of the reference models and pile tests on which the study model is validated 93

F.1 Classification of the parameters b_1 and b_2 of the literature in ascending order in function of the pile lateral displacement in Figure F.1 . . . 95

List of Symbols

A_{cycl}	Cyclic coefficient of the p-y curves [1]
A_{stat}	Static coefficient of the p-y curves [1]
A, B, C, D	Stress-dependent coefficients of Huurman (1996) [1]
a, b, c	Dimensions of the cluster layout (respectively constant layer depth, cluster width and number of clusters per ring) ([L], [L], [1])
a_1, a_2, b_1, b_2, c_1, c_2, d_1, d_2	Soil specific parameters of Huurman (1996) [1]
B_D	Relative density parameter of the p-y curves [1]
b_y	Model parameter of the logarithmic power law for the pile lateral displacement [1]
b_{theta}	Model parameter of the logarithmic power law for the pile accumulated rotation [1]
c	Cohesion of the soil [1]
D	Monopile diameter [L]
$E_{flex,beam}$	Young's modulus of the flexible beams $[F/L^2]$
E_p	Elastic modulus of the pile $[F/L^2]$
E_s	Secant stiffness modulus of the soil $[F/L^2]$
$E_{stiff,beam}$	Young's modulus of the stiff beams $[F/L^2]$
E_{s1}	Secant stiffness modulus of the soil after 1 cycle $[F/L^2]$
E_{sN}	Secant stiffness modulus of the soil after N cycles $[F/L^2]$
E_{soil}	Young's modulus of the soil $[F/L^2]$
F_D	Parameter accounting for the pile installation in the logarithmic power law [1]
F_I	Parameter accounting for the soil density in the logarithmic power law [1]
F_L	Parameter accounting for the cyclic load in the logarithmic power law [1]
f_0	Structure frequency of an OWT $[1/T]$
f_{1P}	Frequency of the excitation created by the spinning rotor/mass imbalance $[1/T]$
f_{3P}	Frequency of the excitation created by the blades rotation $[1/T]$
G_p	Shear modulus of the monopile $[F/L^2]$
G_s	Secant shear modulus of the soil $[F/L^2]$
H	Lateral static loading [F]
H_B	Base horizontal force [F]
H_{cycl}	Load variation amplitude [F]
H_{max}	Maximum lateral applied force within one loading cycle [F]
H_{min}	Minimum lateral applied force within one loading cycle [F]
H_u	Ultimate resistance of the soil [F]
h	Load excentricity [L]
I_p	Moment of inertia of the pile [L]
$K0$	Coefficient of earth pressure at rest [1]
L	Pile embedded length [1]
L_E	Elastic pile length [L]
M	Static moment capacity of the pile [FL]
M_B	Base moment of the pile [FL]
M_{max}	Maximum moment within one loading cycle [FL]
M_{min}	Minimum moment within one loading cycle [FL]
m	Distributed reaction along the shaft of the pile [1]
N	Number of loading cycles [1]
N_b	Number of blades of an OWT [1]
n_b	Coefficient of soil reaction [1]
p	Lateral soil resistance [F]
p_m, p'_m	Mean (effective) stress in a triaxial test $[F/L^2]$

[Unit]: L: Length F: Force T: Time

p_u	Static ultimate lateral resistance [F]
q'	Deviatoric effective stress in a triaxial test [F/L^2]
R_{inter}	Interface coefficient in PLAXIS 3D [1]
R_d	Soil relative density [1]
r	Cluster layout radius [L]
r_a	Reduction factor of Dührkop (2009) that accounts for the number of cycles [1]
R_{Het}	Loading ratio of Hettler (1981) [1]
r_c	Cyclic degradation factor of Garnier (2015) [1]
T	Pile-soil relative stiffness ratio [1]
T_b	Function depending on the cyclic load magnitude and the soil relative density [1]
T_c	Function depending on the cyclic load ratio [1]
t_p	Wall thickness of the monopile [L]
u_x	Horizontal displacement in the x-direction [L]
u_{z1}, u_{z3}	Vertical displacement in the z-direction of beam 1 and beam 3 [L]
V	Axial static loading [F]
w_p	Unit weight of the monopile [F/L^3]
X	Cyclic stress ratio [1]
$X^{(0)}$	Cyclic stress ratio at phase 0 [1]
$X^{(1)}$	Cyclic stress ratio at phase 1 [1]
y	Pile deflection [L]
y_1	Pile deflection after 1 cycle [L]
y_N	Pile deflection after N cycles [L]
z	Depth [L]
α	Degradation factor of the logarithmic power law [1]
α_y	Model parameter of the exponential power law for the pile lateral displacement [1]
α_θ	Model parameter of the exponential power law for the pile accumulated rotation [1]
β	Parameter accounting for the soil type in the exponential power law [1]
γ'	Effective unit weight of the soil [F/L^3]
γ_N	Cyclic shear strains [1]
$\epsilon_{e,N=1}$	Elastic axial strains after 1 cycle [1]
$\epsilon_{e,N}$	Elastic axial strains after N cycles [1]
ϵ_N	Axial strains after N cycles [1]
$\epsilon_{N=1}$	Axial strains after 1 cycle [1]
$\epsilon_{p,N=1}$	Permanent axial strains after 1 cycle [1]
$\epsilon_{p,N}$	Permanent axial strains after N cycles [1]
ζ_b	Cyclic load magnitude [1]
ζ_c	Cyclic load ratio [1]
η	Soil obliquity [1]
θ_1	Pile accumulated rotation after 1 cycle [°]
θ_{max}	Pile maximum accumulated rotation [°]
θ_N	Pile accumulated rotation after N cycles [°]
κ	Stiffness parameter of the SDM [1]
κ_s	Stiffness ratio [1]
$\kappa_S(N)$	Secant shear stiffness after N cycles [F/L^2]
$\kappa_S(1)$	Secant shear stiffness after 1 cycle [F/L^2]
λ	Stiffness parameter of the SDM [1]
ν	Poisson's ratio of the soil [1]
ν_p	Poisson's ratio of the monopile [1]
ξ	Parameter accounting for the pile installation method in the exponential power law [1]
σ_{at}	Atmospheric pressure [F/L^2]
σ_{cycl}	Cyclic stress [F/L^2]
σ_m	Mean principal stress [F/L^2]
σ_1	Major principal stress [F/L^2]
$\sigma_1^{(0)}$	Major principal stress at phase 0 of the SDM [F/L^2]
$\sigma_1^{(1)}$	Major principal stress at phase 1 of the SDM [F/L^2]

[Unit]: L: Length F: Force T: Time

$\sigma_{1,f}$	Major principal stress at failure in a triaxial test [F/L^2]
$\sigma_{1,f}^{(0)}$	Major principal stress at failure at phase 0 of the SDM [F/L^2]
$\sigma_{1,f}^{(1)}$	Major principal stress at failure at phase 1 of the SDM [F/L^2]
σ_3	Minor principal stress [F/L^2]
$\sigma_3^{(0)}$	Minor principal stress at phase 0 of the SDM [F/L^2]
$\sigma_3^{(1)}$	Minor principal stress at phase 1 of the SDM [F/L^2]
τ_N	Cyclic shear stress [F/L^2]
ϕ	Friction angle of the soil [°]
ϕ_{load}	Parameter accounting for the cyclic load in the exponential power law [1]
ψ	Dilatancy angle of the soil [°]

[Unit]: L: Length F: Force T: Time

List of Abbreviations

1D	1 Dimension
3D	3 Dimensions
1P	Constant rotational speed of an OWT (1st excitation)
3P	2nd excitation for an OWT with three blades
CPT	Cone Penetration Test
CSL	Critical State Line
FLS	Fatigue Limit State
FE	Finite-Element
MSc	Master of Science
No.	Number
OWT(s)	Offshore Wind Turbine(s)
PISA	Pile Soil Analysis
PTL	Phase Transformation Line
SDM	Stiffness Degradation Method
SGRE	Siemens Gamesa Renewable Energy
ULS	Ultimate Limit State
UMAT	User-defined Material

Chapter 1

Introduction

1.1 General context

In 2020, the European Union increased the greenhouse gas emission reduction target to 55% of the total emissions in 1990 (Komusanac, 2019 [38]). The offshore wind is a good alternative to fossil fuel energies as it provides a great space-efficient solution. Moreover, the offshore wind produces higher energy level compared to the onshore wind as the wind speed is higher and the wind direction is more constant.

1.1.1 Offshore wind foundations

To satisfy to the energy demand, the turbine manufacturers increase the rated capacity of the OWTs and thus, their size. Increasing the size of the OWTs require adapted foundations. The choice of the foundation is ruled by the water depth, the soil and the loading conditions. Figure 1.1 presents different types of bottom-founded structures for OWT.

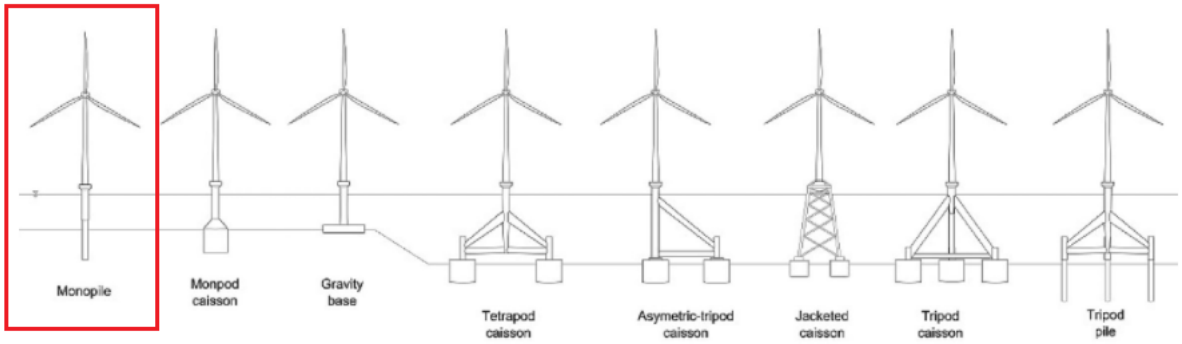

Figure 1.1: Different offshore foundation types, after Bhattacharya (2014) [11]

In Europe, the most common foundation type for OWT is nowadays the monopile as it represents 81% of the installed offshore foundations for OWT (Komusanac, 2019 [38]). A wind monopile is a steel tubular pile with a large diameter which is used until 65m water depth (Arany et al., 2015 [9]). They are installed using driving and/or drilling method. The monopile is favored in the wind industry for its versatility and cost-effective production rate.

1.1.2 Cyclic loading

The role of a wind monopile is to transfer safely the loading to the ground. In offshore conditions, the OWTs experience different types of loading: static and dynamic loading. Whereas static loading remains the same, dynamic loading varies with time. In offshore conditions, the dynamic loads are considered cyclic as they repetitively apply on the offshore structures.
For OWT, there are two types of cyclic loading: the environmental loading and the loading caused by the OWT rotor aerodynamics. The environmental cyclic loading consists of the waves, the wind, the ice sheets that break on the structure or the earthquakes. The waves and the wind are the most common cyclic loading for offshore conditions. The loading caused by the OWT aerodynamics consists of the excitations created by the rotational speed of the spinning rotor (1P) and the blade passing (3P). For the design of the OWT foundations, only the main contributing cyclic loads are considered: the wind and the waves.

1.1.3 Cyclic behaviour of sand

As the OWT monopile transfers the loads to the ground, the impact of cyclic loading on the soil must be assessed. The North Sea is sand dominated in many areas. Sand can be defined as a granular material with particles smaller than gravel but coarser than silt. Because clay and sand behave very differently, this study will focus on the cyclic behaviour of sand.
During cyclic loading, permanent strains develop in sand. Through time, the accumulation of strains can lead to the failure of the soil and thus, the failure of the OWT. As OWTs are designed to be operational for 25 to 30 years, they will experience 10^7 to 10^8 loading cycles. Assessing the stability of an offshore wind monopile under cyclic loading is thus essential.

1.1.4 Current design practice

According to DNVGL-ST-0126 [24], the current design practice is the p-y curve. A p-y curve represents the lateral soil resistance in function of the pile lateral deflection. The p-y curves are calibrated on field tests that are performed on slender piles (Murphy et al., 2018 [49]).
Because of their high diameter, offshore wind monopiles cannot be assumed to behave like slender and flexible piles. Using the p-y curves for the design of offshore wind monopiles overestimates significantly the pile lateral displacement. Thus, the p-y curves are responsible for the overconservative design of offshore wind monopiles and unnecessary costs.

1.1.5 Numerical models

In their last update, design guides advise the use of p-y curves that must be validated with a numerical FE model (DNVGL-ST-0126 [24]). For modelling the soil behaviour under cyclic loading, two main numerical modelling strategies have been developped for FE calculations: implicit and explicit modelling (Niemunis et al., 2004 [52]).
To model the accumulation of plastic strains during cyclic loading, the implicit strategy consists of calculating the permanent strains at every loading cycle (Wichtmann, 2005 [72]). For every cycle, numerical error accumulates which leads to unreliable results and high computation times.
In the explicit procedure, the static analysis is performed with a classical constitutive model (Pasten et al., 2014 [53]). The strains created during cyclic loading are calculated with semi-empirical formulas (Achmus et al., 2009 [2]) or determined from contour diagrams obtained in laboratory (Andersen (2015) [7] , Zorzi et al. (2018) [75]).

1.1.6 Stiffness Degradation Method (SDM)

The Stiffness Degradation Method (SDM) introduced in Achmus et al. (2009) [2] is an explicit numerical method that assesses the behaviour of a monopile in sand under cyclic loading. The concept of the method relies on the stiffness degradation of the soil during cyclic loading. The soil stiffness is degraded with a semi-empirical formula. The SDM is a practical method that corresponds to an early-design procedure as the required input parameters are limited and standard.
The SDM has been verified against pile test data. The method has been developped on the software ABAQUS but it has not been implemented on the FE software PLAXIS 3D yet. PLAXIS 3D is a FE software for geotechnical and civil engineering applications (Brinkgreve, 2013 [15]). Implementing the SDM on PLAXIS 3D would be more convenient for the early-design practice of offshore wind monopiles.

1.2 Thesis objectives and methodology

The main objective of this research is to assess the effects of cyclic loading on an offshore wind monopile in sand. To do so, the following sub-objectives have been determined:

1. **Objective 1 - Literature overview**: Select a numerical method that assesses the cyclic behaviour of a monopile in sand under cyclic loading and corresponds to the early-design procedure requirements of an offshore wind monopile.

2. **Objective 2 - FE implementation**: Ease the method application by implementing the procedure on a widely-used FE software by the mean of an automated routine coded in Python.

3. **Objective 3 - Verification**: Verify the correct implementation of the method.

4. **Objective 4 - Validation**: Identify the strengths and limitations of the study model by comparing results with pile test data.

5. **Objective 5 - Design integration**: Assess the impact of the study model on a reference system.

1.2.1 Objective 1: Literature overview

To fulfil the objective 1, a literature overview has been conducted. The literature overview focuses on answering the scientific questions:

- What is cyclic loading ? What is the behaviour of sand under cyclic loading ?
- What are the current practical methods for the design of offshore wind monopiles? Why do their main principles fail to model the behavior of offshore wind monopiles under cyclic loading?
- Why does the Stiffness Degradation Method (SDM) correspond to the early-design requirements for an offshore wind monopile?

The chapter 2 and chapter 3 present the results of the literature overview. The chapter 2 focuses on answering the two first scientific questions whereas chapter 3 presents the Stiffness Degradation Method (SDM)

1.2.2 Objective 2: FE implementation

To fulfil the objective 2, the FE implementation of the SDM is described. This part of the study focuses on answering the scientific questions:

- What are the main steps of the Stiffness Degradation Method (SDM)?
- How is the Stiffness Degradation Method (SDM) implemented in PLAXIS 3D?

The chapter 4 presents the FE implementation of the SDM.

1.2.3 Objective 3: Verification

To fulfil the objective 3, the results of the study model are compared with the results of a reference system available in the literature. This part of the study focuses on answering the scientific questions:

- Does the study model provide results in agreement with the original model?
- What are the differences between the study model and the original model? What are the causes of the differences?

The chapter 5 presents the verification of the study model.

1.2.4 Objective 4: Validation

To fulfil the objective 4, a description of the validation procedure is presented. This part of the study focuses on answering the scientific questions:

- What are the strengths and limitations of the study model?
- What is the impact of the model parameters on the pile lateral displacement?

The chapter 6 presents the validation of the study model.

1.2.5 Objective 5: Design integration

To fulfil the objective 5, a presentation of the design integration of the study model is included in this research. This part of the study focuses on answering the scientific questions:

- How can the study model be included in the design procedure for assessing the cyclic behaviour of an offshore wind monopile under cyclic loading?
- What is the impact of the study model on the pile lateral displacement compared to current cyclic practice?

The chapter 7 presents the design integration of the study model.

Finally, the chapter 8 will conclude this study by presenting the research conclusions and recommendations.

Chapter 2

Literature overview

This chapter presents the results of the literature overview. First, cyclic loading will be introduced: cyclic loading will be defined and the main cyclic loads for an OWT will be described.
Then, the cyclic behaviour of sand for drained and undrained conditions will be presented. In this section, the difference of behaviour between compression and extension states will be discussed. The section will end by a final discussion about the most detrimental case between one-way and two-way cyclic loading.
Finally, the current design practice for offshore wind monopiles will be investigated: the p-y curves. The new developments of the p-y curves will be presented. The section will end with a presentation of the power laws.

2.1 Definition of cyclic loading

Cyclic loading consists of the repetitive application of a loading. Figure 2.1 illustrates cyclic loading for constant period and amplitude.

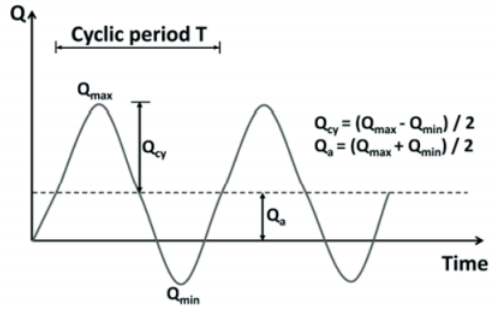

Figure 2.1: Cyclic loading definitions for constant time period and loading amplitude, after Andersen et al. (2013) [6]

In this section, cyclic loading will be presented. First, cyclic loading is defined. Then, the cyclic loads that apply on OWTs will be introduced.

2.1.1 Definition of cyclic loading

Cyclic loading is characterized by the following parameters (Puech et al., 2012 [58]):

- **The cyclic loading amplitude**
  Depending on the nature of the cyclic event, the loading amplitude varies in time (Andersen, 2015 [7]). Cyclic loading can be characterized by its mean loading amplitude (Puech et al., 2012 [58]). To simplify cyclic loading during the design, the cyclic loading amplitude is often assumed constant. In this case, the loading oscillates around the mean value, between a maximum and minimum amplitude.

- **The loading time period**
  Cyclic loading varies significantly in period and duration depending on the nature of the loading. For example, waves have a time period of 10 to 20s whereas tidal forces have a period of 12hours and more (Andersen, 2015 [7]). To simplify cyclic loading during the design, the loading time period is often assumed constant.

- **The rate of loading**
  Depending on the environmental conditions and the location of the structure, an offshore structure will experience different periods of rest during or between cyclic events (Puech et al., 2012 [58]).

- **The number of cycles** N
  A wind monopile will experience 10^7 to 10^8 loading cycles through its lifetime (Leblanc et al., 2010 [40]).

2.1.2 Cyclic loading on offshore wind structures

An OWT experiences two types of cyclic loading: the environmental loading and the loading caused by the OWT rotor aerodynamics. The environmental loading includes the wind, the waves, the ice and the earthquakes. As the ice and the earthquakes are less common and create very specific issues, only the wind and the waves are presented in this section. Thus, the main cyclic loads on an OWT are the following (Bhattacharya et al., 2017 [12]):

- **Wind load**
  The wind loads act at hub height on the rotor-nacelle assembly and on the tower of the OWT.
  At hub height, the wind and the spinning blades create the thrust force. The wind force acting on the tower is the drag force. The magnitude of the wind dynamic loads depends on the rotor diameter, the wind speed, the turbulence and the controlling mechanism (Bhattacharya, 2014 [11] ; Arany et al., 2017 [10] ; Jalbi et al., 2019 [33]).

- **Waves**
  The waves act on the foundation at and below the water surface until a certain water depth. The magnitude of the waves force depends on the significant wave height and period (Bhattacharya, 2014 [11]).

- **Rotor aerodynamics**
  The spinning rotor has a rotational speed of 1P. In the case of misalignment in the rotor-nacelle system, an excitation of frequency f_{1P} is generated by the mass imbalance (Adhikari and Bhattacharya, 2012 [3]; Bhattacharya, 2014 [11]).
  When the blades rotate and pass in front of the tower, it creates an excitation of $N_b f_{1P}$ where N_b is the number of blades and f_{1P} is the rotor frequency. Thus, for an OWT with 3 blades, the rotor blade passing creates an excitation of frequency f_{3P} (Adhikari and Bhattacharya, 2012 [3]).

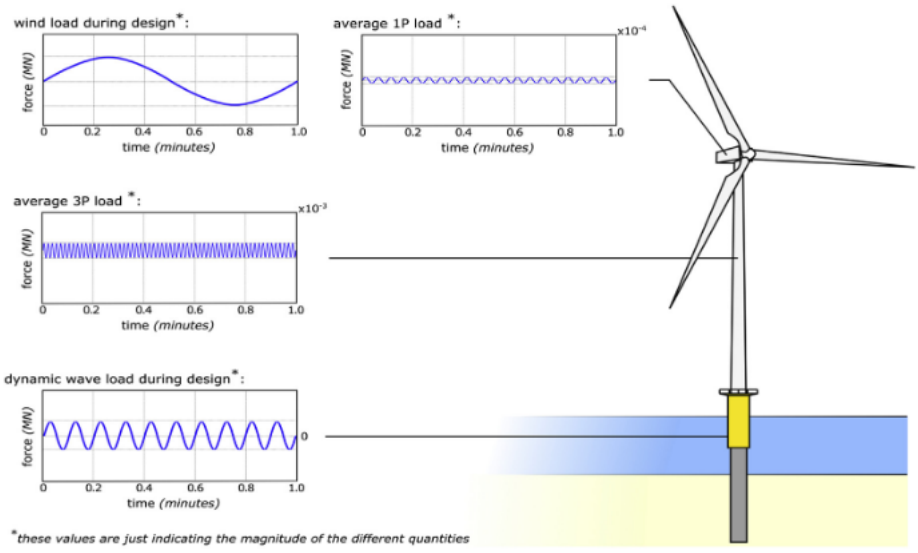

Figure 2.2: Drawing of the loads acting on offshore wind monopile, after Bhattacharya et al. (2017) [12]

Figure 2.2 presents the difference of amplitude and period between the main cyclic loads acting on an OWT (Bhattacharya et al., 2017 [12]). The wind and the waves have the highest loading amplitude.

The dynamic design of an OWT is ruled by the frequency ranges of the dynamic loading (Bhattacharya, 2014 [11]; Arany et al., 2017 [10]). Resonance happens when the structure frequency f_0 lies around the frequency of the loading energy peak. As resonance increases significantly the risk of failure, this situation must be avoided. To avoid the resonance of the structure with dynamic loads, the frequency of the system f_0 (wind turbine and support structure) must be different from the energy peak frequency of the loading (Bhattacharya, 2014 [11]; Arany et al., 2017 [10]).

Figure 2.3 presents the typical frequency range f_0 for an OWT. Most of the OWTs have a system frequency between f_{1P} and f_{3P} range. This is called a soft-stiff design (Bhattacharya, 2014 [11]).

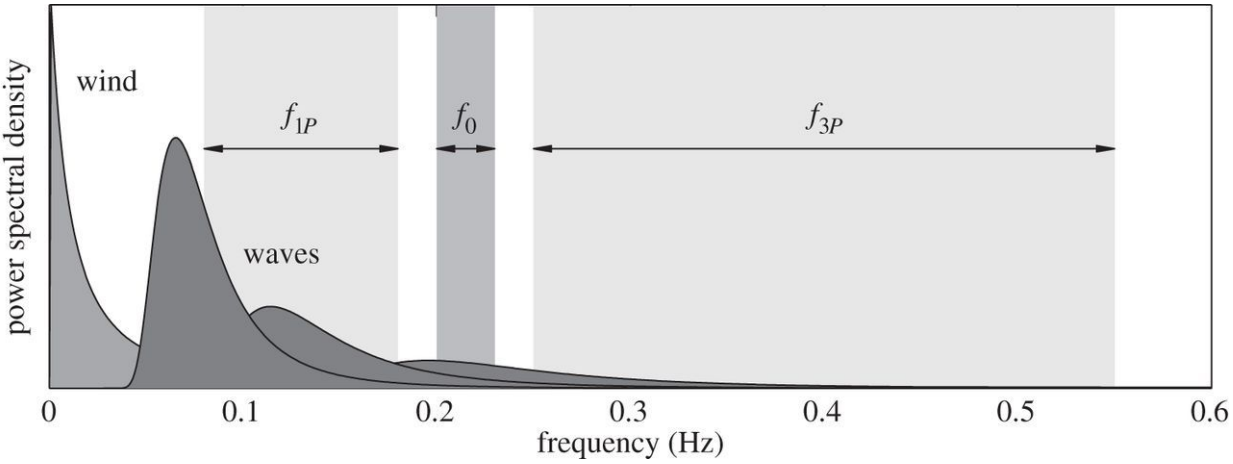

Figure 2.3: Relation of wave and wind loading spectra to f_0, f_{1P} and f_{3P}, Kallehave et al. (2015) [34]

As the wind and the waves have the highest amplitude (Figure 2.2), they have the biggest impact on the structure (Arany et al., 2015 [9]). Thus, only the loading caused by the wind and the waves will be considered in the following sections.

2.2 Cyclic behaviour of sand

During cyclic loading, the stress-strain behaviour of the soil is hysteretic (Figure 2.4). Because of the non-linear, anisotropic and time-dependent nature of the soil (Brinkgreve, 2005 [14]), the strain loops created by cyclic loading are not closed and permanent strains develop (Wichtmann, 2005 [72]). The soil properties like the soil stiffness, the shear strength and the void ratio are affected (Shajarati et al., 2012 [63]).

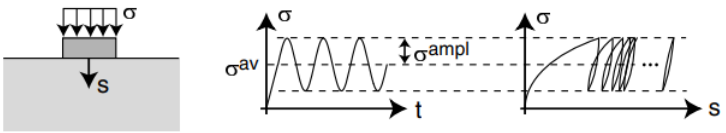

Figure 2.4: Settlements of a foundation under cyclic loading, after Wichtmann (2005) [72]

In this section, the behaviour of sand under cyclic loading will be discussed. First, the drained and undrained behaviour of sand under cyclic loading will be presented. Then, the difference between the compression and extension states will be discussed. Finally, the impact of one-way and two-way cyclic loading will conclude the section.

2.2.1 Drained conditions

The sand is assumed drained if there is sufficient time between the loading cycles for drainage to occur. For modelling the long-term behaviour of sand, the loading time period is high and thus, there is sufficient time

between the loading cycles for drainage to occur. During extreme events, the loading time period shortens. In this case, only highly permeable sand can be assumed drained.
Figure 2.5 presents the drained behaviour of sand under cyclic triaxial loading in compression. At a certain stress level, plastic deformations will increase significantly (Liu, 2020 [46]). This threshold is difficult to precisely define as the plastic strains develop gradually (Alonso-Marroquin and Herrmann, 2004 [5]). Once the plastic threshold is reached, permanent volumetric strains and permanent shear strains develop significantly. This accumulation process depends on the soil type and density, the initial effective stress, the cyclic stress amplitude and obliquity ($\eta = \frac{p'_m}{q'}$ in Figure 2.5) and the number of cycles (Chong and Santamarina, 2016 [19]).

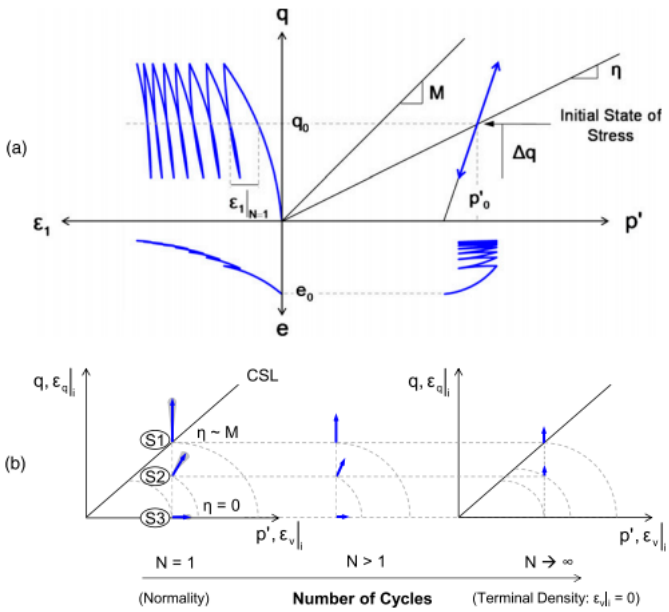

Figure 2.5: Behavior of a granular material subjected to drained cyclic triaxial loading. (a) Evolution of the effective mean stress p'_m, deviatoric stress q', axial strain ϵ_1 and void ratio e_1, (b) Evolution of the strain increment per cycle with the number of load cycles; S1, S2 and S3 are initial stress states, after Pasten et al. (2014) [53]

According to the shakedown theory, drained cohesionless soils under cyclic loading can behave as follows (Venkatesh et al., 2018 [71]):

- **Elastic behaviour**
  If the stress level is located in the elastic range, the deformations are assumed elastic and remain the same at the end of each cycle (Liu, 2020 [46]). Elastic behaviour is observed for very small strains.

- **Elastic shakedown**
  During elastic shakedown, the stress level exceeds the elastic domain and thus, permanent strains develop. The stress level is approximately the same in all the directions and the permanent strains are mainly volumetric. After a finite number of cycles, the permanent volumetric strains stabilise towards a constant value (Pasten et al., 2014 [53]). Once this constant value is reached, the volumetric deformations are only elastic: the strains remain the same after each cycle. This state corresponds to the terminal density where the soil reaches a stable fabric layout (Narsilio and Santamarina, 2008 [51]). This phase happens for low cyclic stress levels (Venkatesh et al., 2018 [71]).

- **Plastic shakedown**
  During plastic shakedown, the stress level cannot be assumed the same in all directions: a major stress direction is identified. In contrary to elastic shakedown, during plastic shakedown, the soil has an hysteretic behaviour. Permanent volumetric and shear strains develop in the soil. Like during elastic shakedown, after a finite but higher number of cycles, both volumetric and shear permanent strains reach a constant value (Liu, 2020 [46]): the stress-strain loops finally close. However, residual stresses can remain in the soil.

- **Ratcheting**
  During ratcheting, plastic volumetric and shear strains develop. The stress-strain loops stretch to the right (Figure 2.4). Whereas the permanent volumetric strains reach the terminal density state after a finite number of cycles, the permanent shear strains increase until failure happens. Failure happens when the stress level is high or the stress state is towards the critical state line (CSL) (Pasten et al., 2014 [53]).

Figure 2.6 presents the different shear stress-strain paths of the shakedown theory (Goldscheider, 1977 [28]).

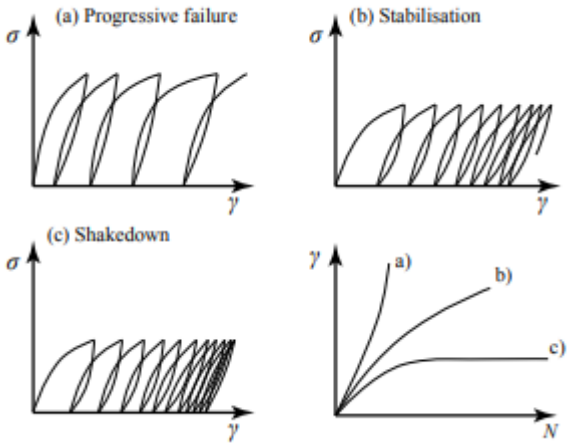

Figure 2.6: Visualisation of the shakedown theorem, after Shajarati et al. (2012) [63]

During cyclic loading, the soil experiences both permanent volumetric strains and permanent shear strains (Figure 2.5). Whereas the permanent volumetric strains will always reach a constant value after a finite number of cycles (terminal density state), the permanent shear strains will either reach a constant value (plastic shakedown) or increase until failure (ratcheting). The difference between plastic shakedown and ratcheting depends mainly on the type of soil, the load level and the stress direction. The shear strains are the determining strains to monitor during cyclic loading as they can cause failure.

2.2.2 Undrained conditions

The sand is assumed undrained if there is not sufficient time between the loading cycles for drainage to occur. The behaviour of the sand is generally assumed undrained during extreme events like storms. In undained conditions, excess pore pressure builds up in the soil (Andersen, 2015 [7]). As the stress level increases, pore pressure and permanent deviatoric strains develop simultaneously in the soil (Liu, 2020 [46]).
Figure 2.7 presents the behaviour of dense and loose sands during an undrained cyclic triaxial test in compression. The excess pore pressure is either positive or negative:

- **Compaction or contraction: positive excess pore pressure**
  In the case of contractive behaviour, as excess pore pressure increases, the effective stresses decrease and soil looses in strength and stiffness (Shajarati et al., 2012 [63]).

- **Dilatation: negative excess pore pressure**
  In the case of dilative behaviour, as negative pore pressure develops, the effective stresses increase and the soil gains in strength and stiffness (Shajarati et al., 2012 [63]).

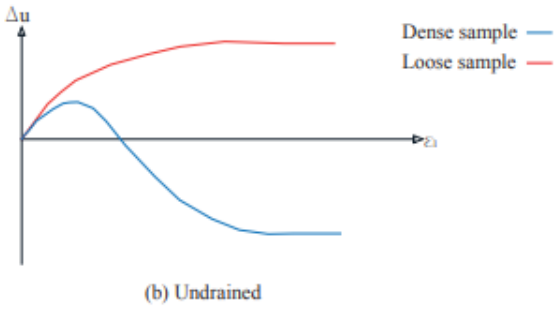

Figure 2.7: Pore pressure as a function of axial strains in an undrained cyclic triaxial test in compression, after Shajarati et al. (2012) [63]

During a cyclic triaxial test in compression, loose sand experiences only contractive behaviour (Figure 2.7). A final positive pore pressure is reached after a finite number of cycles. Dense sand experiences a brief contractive behaviour, followed by a final dilatation phase. After a finite number of cycles, a constant negative pore pressure is reached.
Undrained sand can experience three types of failure during cyclic loading (Liu, 2020 [46]):

- **Cyclic liquefaction**
  Liquefaction happens when the sand softens and reaches a state in which it can behave like a viscous fluid (Della et al., 2014 [21]). It is caused by a sudden increase of pore pressure and shear force that decrease significantly the soil strength. For sand, liquefaction happens during contractive behaviour, thus, mostly for loose sands. Liquefaction is responsible for important runaway deformations within the soil, leading to failure (Liu et al., 2019 [45]).

- **Cyclic mobility**
  The limit between dilative and contractive regimes is represented by a Phase Transformation Line (PTL). Figure 2.8 represents the PTL line.

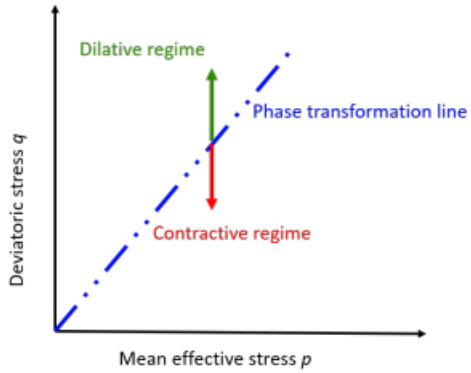

Figure 2.8: Illustration of phase transformation line (PTL) in a $q - p_m$ space, after Liu (2020) [46]

  In case of load reversal from compression to extension stress states (two-way loading), dense sand alternatively contracts and dilates when crossing the Phase Transformation Line (PTL). During the contractive phase, the pore pressure increases and the soil looses in strength. Then, during the dilative phase, the pore pressure dissipates and the soil regains in strength (Chern, 1985 [18]).
  By crossing the PTL line frequently, the soil alternates loss and gain of strength in a short period of time. This process increases the accumulation rate of deviatoric strains in the soil (Chern, 1985 [18]).
  Cyclic mobility generally occurs for dense or medium dense sands (Liu et al., 2019 [45]).

- **Strain accumulation in the presence of static preshear**
  If the soil is pre-loaded and experiences a static shear stress, deviatoric strains accumulate when cyclic loading is applied afterwards. The accumulation of deformations lead to a serviceability failure (Liu, 2020 [46]).

2.2.3 Compression and extension states

In offshore conditions, the soil can experience both compression and extension states.
In triaxial tests, the sign convention is the following: compression stresses are positive whereas extension stresses are negative. The soil has a different behaviour in compression and extension (Rascol, 2009 [59], Jagodnik et al., 2020 [32]). Sands in extension cannot reach the same critical state as in the compression (Jagodnik et al., 2020 [32]). The difference of behaviour observed in triaxial compression and extension tests (cyclic and monotonic) can be explained as follows:

- **Different stress paths**
  The stress path in a triaxial test in compression is different from the stress path in a triaxial test in extension. In a triaxial test in compression, the deviatoric stress is positive ($q > 0$). The major principal stress is the axial stress and the minor principal stress is the radial stress. In a triaxial test in extension, the deviatoric stress is negative ($q < 0$). Thus, the major principal stress is the radial stress and the minor principal stress is the axial stress (De Gennaro et al., 2004 [20]). Thus, even an homogeneous soil has a different behaviour in extension and compression.

- **Anisotropy of the soil**
  The soil properties are non-homogeneous in space directions. During deposition process, the gravity plays a major role in the creation of the soils which leads to an inherent anisotropy. The mechanical properties of the soil are generally stronger in the vertical direction than in the horizontal direction (Gennaro et al., 2004 [20]). This anisotropy could also be partly caused by the sample preparation technique (Vaid et al., 1989 [70]).

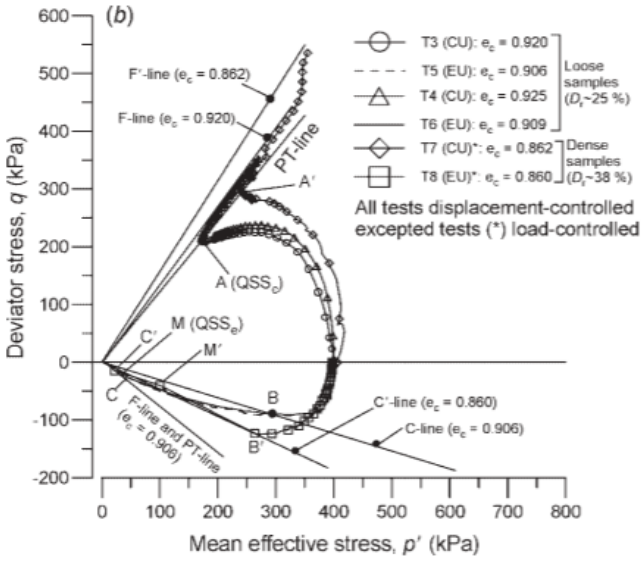

Figure 2.9: Effective stress paths during undrained triaxial test in compression (CU) and extension (EU), after De Gennaro et al. (2004) [20]

Figure 2.9 presents the stress paths in compression and extension in an undrained triaxial test. On Figure 2.9, at identical mean effective stress (p'_m), the critical state line (CSL) is reached for a smaller deviatoric stress amplitude $|q|$ in extension than in compression.

2.2.4 Impact of one-way and two-way cyclic loading

During numerical simulations and lab experiments, cyclic loading can be applied in one-way or two-way loading:

- **One-way loading**:
  If a loading cycle consists of one-direction loading, the loading is called one-way loading. One-way loading is simulated in the soil by a compression stress state (Kuo, 2008 [39]).

- **Two-way loading**:
  If a loading cycle consists of the alternation of one-direction loading and its opposite, the loading is called two-way loading. Two-way loading is simulated by the alternation of compression and extension stress states within one cycle (Kuo, 2008 [39]).

On Figure 2.10, the principle of one-way and two-way loading within one cycle is presented (Kuo, 2008 [39]). Even though the dynamic environmental loading is never one-way or two-way loading in offshore conditions (Arany et al., 2017 [10]), multiple experiments simulating one-way and two-way loading have been carried out to estimate more accurately the impact of offshore dynamic loading on offshore wind monopiles (Lin and Liao, 1999 [43]; Leblanc et al., 2010 [40]; Klinkvort and Hededal, 2013 [37]; Albiker et al., 2017 [4] ; Frick and Achmus, 2019 [25]).
The cyclic load ratio ζ_c, also called R_H in Figure 2.10, accounts for the changing direction of the loading within one cycle (Leblanc et al., 2010 [40]):

$$\zeta_c = \frac{M_{min}}{M_{max}} = \frac{H_{min}}{H_{max}} \tag{2.1}$$

Where M_{max} and M_{min} are the maximum and minimum moment in a loading cycle, H_{max} and H_{min} are the maximum and minimum applied force in a loading cycle.
The parameter ζ_c defines one-way and two-way loading. In one-way loading, $0 < \zeta_c < 1$ for asymmetric one-way loading and $\zeta_c = 0$ for symmetric one-way loading. In two-way loading, $-1 < \zeta_c < 0$ for asymmetric two-way loading and $\zeta_c = -1$ for symmetric two-way loading.

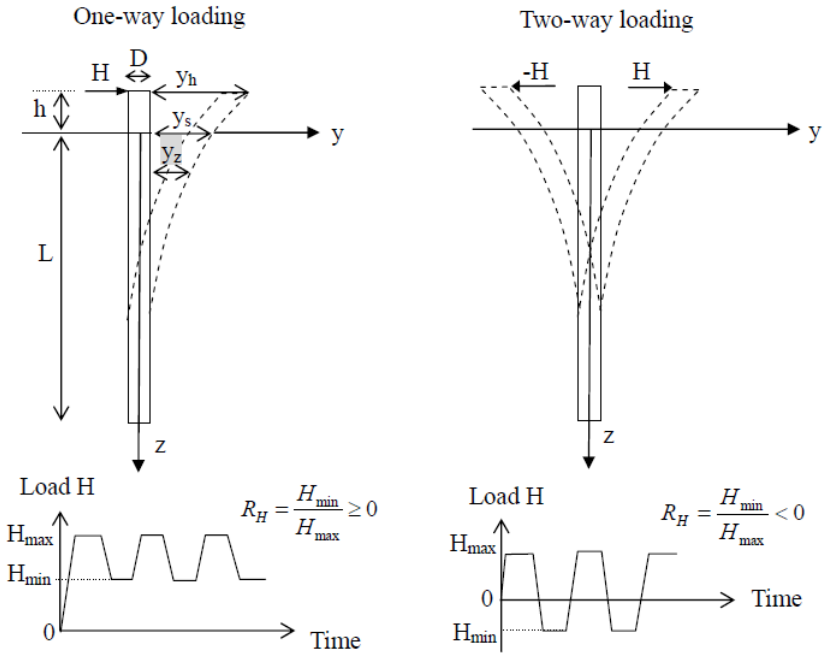

Figure 2.10: Classification of cyclic lateral loading conditions on single pile, after Kuo (2008) [39]

Researchers have not reached an agreement on the most detrimental loading between one-way and two-way loading for the soil (Jalbi et al. (2019) [33]).
In a scaled pile experiment, Leblanc et al. (2010) [40] observed that the highest accumulated rotation θ_{max} of the monopile at mudline was reached for asymmetric two-way loading (ζ_c = -0.6). Similar observations have been reported by Albiker et al. (2017) [4] and Frick and Achmus (2019) [25] during scaled pile experiment. They concluded that the highest accumulated rotation at mudline is reached for asymmetric two-way loading where ζ_c lies in the range $[-0.33; -0.6]$.
Long and Vanneste (1994) [47] and Lin and Liao (1999) [43] observed the opposite phenomenom during full scale experiments: one-way loading creates more accumulated displacement than two-way loading. Those observations were confirmed by the centrifuge model tests of Klinkvort and Hededal (2013) [37]. They observed that the highest accumulated rotation of the monopile was reached for symmetric one-way loading

$\zeta_c \approx 0$. Rudolph et al. (2014) [62] and Nanda et al. (2017) [50] observed higher accumulated displacement for multi-directional one-way loading.
Jalbi et al. (2019) [33] analyzed the loading of 15 OWTs from 12 wind farms in Northern Europe. In normal operational conditions, the cyclic load ratio ζ_c is positive, indicating one-way loading. The wind turbines are designed and oriented to benefit from the best production rate in one-way loading. For extreme events, the cyclic load ratio ζ_c becomes negative. Jalbi et al. (2019) [33] concluded that most windfarms in the Northern Europe experience mostly one-way loading during their lifetime.

2.3 Current design practice for offshore wind monopiles

As no generally accepted design procedure yet exists for the design of offshore wind monopiles under cyclic loading, the research community actively works toward this objective. This section aims to present an overview of the current design practice to assess the impact of cyclic loading on the soil and pile displacement.
In this section, the rigid behaviour of the offshore wind monopiles will be presented. Then, the strengths and limitations of the p-y curves will be discussed. As p-y curves for the offshore wind have been improved in the last years, the new developments will be presented. Finally, the design method of the power laws will be introduced.

2.3.1 Rigid behaviour of wind monopiles

The monopiles used in the offshore wind industry have a large diameter from 4 to 12m and have an embedded length between 20 to 40m (Wu et al., 2019 [73]). The offshore wind monopiles correspond to a ratio $\frac{L}{D}$ between 2 and 6. Because of their large diameters, offshore wind monopiles behave similarly to rigid bodies (Leblanc et al., 2010 [40]).
Poulos and Hull (1989) [57] used the stiffness parameter κ_s to characterise the stiffness of piles:

$$\kappa_s = \frac{E_p I_p}{E_{soil} L^4} \tag{2.2}$$

Where E_{soil} is the Young's modulus of the soil, L is the embedded pile length, E_p and I_p are the elastic modulus and moment of inertia respectively.
In Poulos and Hull (1989) [57], $\kappa_s > 0.208$ represents a rigid pile and $\kappa_s < 0.0025$ represents a flexible pile.

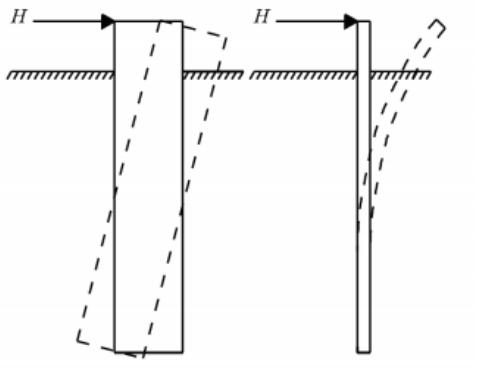

Figure 2.11: Rigid pile deformation about a pivot point (left) and a flexible pile deflection (right) demonstration from Sorensen et al. (2012) [65])

Figure 2.11 presents the difference of behaviour between a rigid pile and a flexible pile when a lateral load is applied at the top of the monopile with an eccentricity. Poulos and Hull (1989) [57] demonstrated that moving from a flexible to a rigid pile changes its response to the loading. Rigid piles tend to rotate in the soil instead of bending like a clamped slender beam (Jalbi et al., 2019 [33]). Thus, for identical loading and embedded length, a flexible pile has a higher displacement at mudline than a rigid pile.

2.3.2 P-y curves

To model the behaviour of monopiles, the traditional design procedure is the Winkler beam approach. At given depths, the lateral soil resistance (p) is expressed in function of the pile deflection (y). Those plots are called p-y curves (Murphy et al., 2018 [49]).
In the Winkler approach, the pile is modelled as an elastic beam, discretized into a number of structural elements, separated by nodal points. The soil is represented as a series of discrete, uncoupled, non-linear elastic springs varying with depth, positionned at the nodal points along the pile, acting normal to the beam element (Leblanc et al., 2010 [40]). Figure 2.12 presents the concept of the Winkler approach.

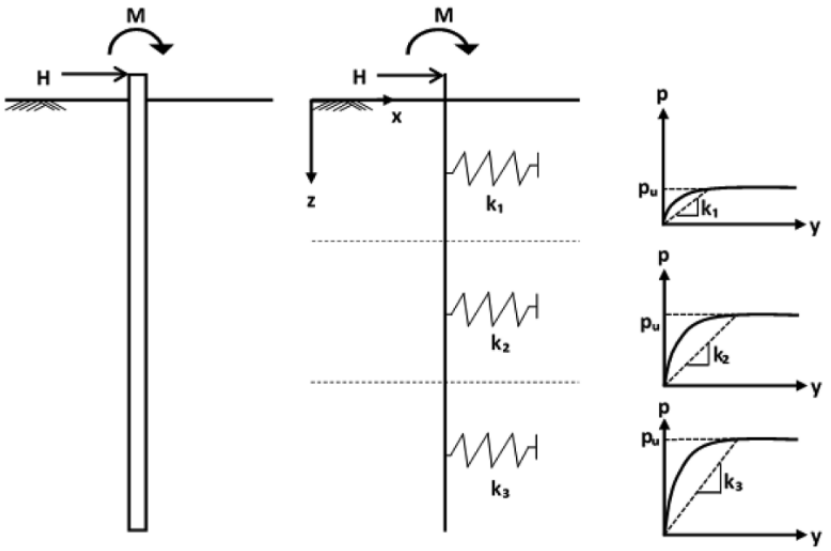

Figure 2.12: Beam on non-linear Winkler foundation, after Jalbi et al. (2019) [33]

The p-y curves are calibrated on field tests which are performed on slender piles in homegeneous soils (Reese et al., 1975 [60], Matlock, 1970 [48]). For monopiles in sand, the soil resistance p is:

$$p = A_{cycl} p_u tanh(\frac{B_D z}{A_{cycl} p_u} y) \tag{2.3}$$

Where B_D is a parameter accounting for the relative density of the sand, z is the depth, $A_{cycl} = 0.9$ for cyclic loading, p_u is the static ultimate lateral resitance, and y is the pile displacement (API, 2011 [8]).
In Equation 2.3, the p-y curves do not account for the number of loading cycles N, the loading amplitude and the pile dimensions. Because the offshore wind monopiles have a rigid behaviour and the p-y curves are designed for flexible piles, the p-y curves provide a conservative estimation of the pile lateral displacement.
However, the p-y curve remains a practical tool for the design of monopiles because of its simplicity, low computational cost and ability to model multi-layered soils (Bouzid et al., 2013 [13]). Design standards have adapted the design procedure of the p-y curves to the rigid behaviour of wind monopiles. New guidelines and tools have been investigated.

DNVGL-ST-0126 [24]

According to the new version of the DNVGL-ST-0126 [24], the use of p-y curves for piles with a diameter higher than 1m must be validated with FE analysis. The cyclic effect must also be accounted for. However, no agreement has been reached within the scientific community on the method to use for calculating the cyclic effect (Murphy et al., 2018 [49]).

PISA project

The Pile Soil Analysis (PISA) is a joint-industry project for the design improvement of the offshore wind foundations. The PISA project consists of developping a new design model based on the simplicity of the p-y

curves. Field tests on onshore sites were performed for validating the PISA numerical model (Burd et al., 2019 [16]).
The PISA design model consists of a 1D model where the pile is modelled as a Timoshenko beam. Figure 2.13 presents the 1D model. The pile dynamic behaviour depends on four elements: the lateral soil reaction along the shaft (p), the distributed reaction along the shaft (m), the base horizontal force (H_B) and the base moment (M_B) (Panagoulias et al., 2019 [55]). Compared to the original p-y curves, the PISA numerical model uses new soil reaction components that are calibrated on 3D FE analyses. The 3D FE software PLAXIS Monopile Designer (Panagoulias et al., 2018 [54]) can be used for calibrating the soil reaction components of the 1D model (Kaltekis et al., 2019 [35]).

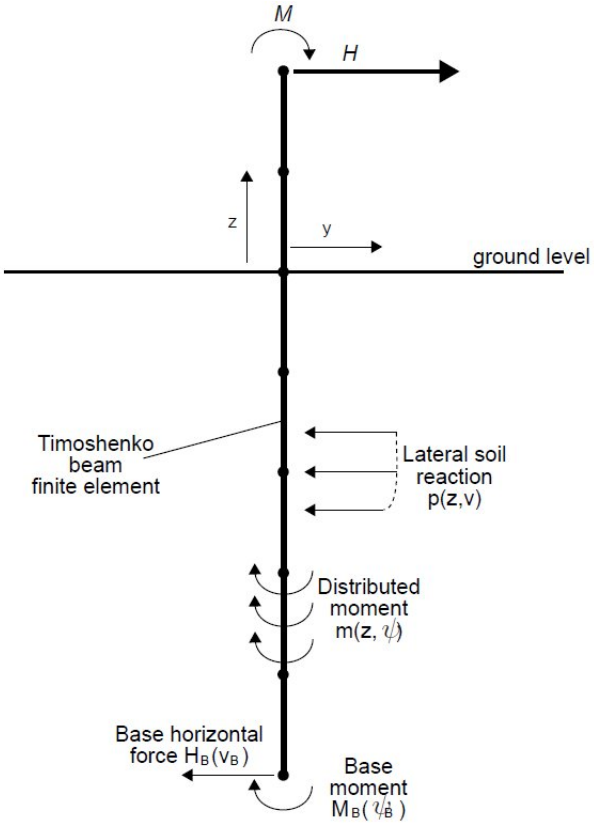

Figure 2.13: Soil reaction components applied to the 1D FE model, after Byrne et al., 2015 [17]

The use of a 1D model limits the computation times while the calibration of the soil reaction components on 3D FE models ensures the realism of the results (Burd et al., 2019 [16]).

2.3.3 Power laws

For determining the monopile displacement at mudline after cyclic loading, a practical approach consists of fitting lab or field results with power law curves taking into account the number of cycles (Li et al., 2015 [42]). Appendix A lists the main pile tests realised in the last years and on which the power laws were calibrated.
The monopile response (displacement or rotation) of the monopile after applying N loading cycles is:

$$y_N = f(N, y_1) \tag{2.4}$$

Where y_1 is the monopile response after 1 cycle.

Logarithmic function

For determining the pile displacement at mudline, a logarithmic function is used. According to Hettler (1981) [29], the accumulated pile head displacement after N load cycles is:

$$y_N = y_1(1 + b_y * ln(N)) \tag{2.5}$$

Where b_y is a model parameter. The model parameter b_y has been calculated with different methods:

- **Fit with lab results**
  For one-way loading, Hettler (1981) [29] estimated $b_y \approx 0.2$ (Frick and Achmus, 2019 [25]).
  In Li et al (2010) [41], b_y values were determined by fitting the Equation 2.5 with the test results.
  In Li et al (2015) [42], the logarithmic function is also applied for determining the accumulated rotation θ_N with the following formula:

$$\theta_N = \theta_1(1 + b_\theta * ln(N)) \tag{2.6}$$

  Thus, 2 values of b are determined: b_y is the model parameter for displacement (Equation 2.5) and b_θ is the model parameter for the accumulated rotation (Equation 2.6).

- **Parameters are dependent on the experimental conditions**
  In Lin and Liao (1999) [43], b_y depends on the soil conditions, the installation method, the cyclic load amplitude and the length of the pile:

$$b_y = 0.032 * \frac{L}{T} * \beta * \xi * \phi_{load} \tag{2.7}$$

  Where the coefficients β depends on soil type, ξ depends on the pile installation method, ϕ_{load} depends on the cyclic load ratio, L is the length of the pile (Lin and Liao, 1999 [43]).
  The pile/soil relative stiffness ratio is:

$$T = (\frac{E_p I_p}{n_b})^{1/5} \tag{2.8}$$

  With E_p the modulus of elasticity, I_p the moment of inertia of the pile and n_b the coefficient of soil reaction (Lin and Liao, 1999 [43]).
  In Lin and Liao (1999) [43], as the sand is dense, the pile is driven and the loading is one-way: $\beta = \xi = \phi_{load} = 1$ and $L/T = 1$. Thus, $b_y = 0.032$.
  In Rosquet et al. (2007) [61], b_y depends on the loading conditions only:

$$b_y = 0.08(\frac{H_{cycl}}{H_{max}})^{0.35} \tag{2.9}$$

  Where H_{cycl} is the load variation amplitude and H_{max} is the maximum applied load.

The logarithmic function gives a good approximation for estimating the displacement of slender elastic piles under a limited number of loads (<500) (Leblanc et al., 2010 [40]).

Exponential function

The accumulated pile displacement (y_N) or rotation (θ_N) after N load cycles can be estimated with an exponential function:

$$y_N = y_1 * N^{\alpha_y} \tag{2.10}$$

$$\theta_N = \theta_1 * N^{\alpha_\theta} \tag{2.11}$$

Where y_1 and θ_1 are respectively the displacement and the rotation after 1 cycle and α is the model parameter. The model parameter α has been calculated with different methods:

- **Fit with lab results**
  The exponential function was first introduced by Little and Briaud (1988) [44] to degrade the cyclic shear stiffness for slender piles:

$$\frac{K_S(N)}{K_S(1)} = N^{-\alpha} \tag{2.12}$$

  Where $K_S(N)$ and $K_S(1)$ are the secant shear stiffnesses after Nth cycles and 1 cycle respectively, α is the negative slope of the best fit line obtained from piles experiments.

- **Parameters are dependent on the experimental conditions**
  Long and Vanneste (1994) [47] determined the degradation parameter α as (Frick and Achmus, 2019 [25]):

$$\alpha = 0.17 * F_L * F_I * F_D \tag{2.13}$$

  Where F_L, F_I and F_D are factors considering the characteristics of the cyclic load, soil density and pile installation.
  Leblanc et al. (2010) [40] is the first study to focus on the cyclic loading on rigid and large diameter monopiles. By using the exponential law of Long and Vanneste (1994) [47] and Little and Briaud (1988) [44], Leblanc et al (2010) [40] determined the accumulated rotation due to cyclic loading with:

$$\frac{\Delta\theta(N)}{\theta_1} = \frac{\theta_N - \theta_1}{\theta_1} = T_b(\zeta_b, R_d) * T_c(\zeta_c) * N^{\alpha} \tag{2.14}$$

  Where $\alpha = 0.31$
  (2.14) fits the measured accumulated displacement for 10^4 cycles. The hypothesis is made that extrapolation until 10^7 (FLS) also holds.
  In (2.14), the accumulated rotation depends on the dimensionless functions T_b and T_c. The function T_b depends on the cyclic load magnitude ζ_b and on the relative density R_d. The function T_c depends on the cyclic load ratio ζ_c.
  The cyclic load magnitude ζ_b measures the size of the cyclic loading normalised with respect to the static moment capacity of the pile (M) in (2.15).
  The cyclic load ratio ζ_c characterizes the cyclic load in (2.16) where $\zeta_c = 1$ for static test, $\zeta_c = 0$ for one-way loading and $\zeta_c = -1$ for two-way loading.

$$\zeta_b = \frac{M_{max}}{M} = \frac{H_{max}}{H} \tag{2.15}$$

$$\zeta_c = \frac{M_{min}}{M_{max}} = \frac{H_{min}}{H_{max}} \tag{2.16}$$

  Here M_{max} and M_{min} are the maximum and minimum moment in a loading cycle, H_{max} and H_{min} are the maximum and minimum applied force in a loading cycle.

The exponential function provides a good agreement with the accumulated displacement and rotation for rigid and large monopiles for a high number of cycles (>500) (Leblanc et al., 2010 [40]). The method developped by Leblanc et al. (2010) [40] has been validated in Klinkvort et al. (2012) [36], Klinkvort and Hededal (2013) [37], Truong and Lehane (2015) [68], Albiker et al. (2017) [4], Frick and Achmus (2019) [25], Truong et al. (2019) [69], Frick and Achmus (2020) [26].

2.4 Conclusion

In this chapter, the results of the literature overview were presented.

- **Cyclic loading**
  Cyclic loading consists of the repetitive application of a load. For simplifying the loading during the design phase, cyclic loading is assumed to have a constant time period and loading amplitude. In offshore conditions, the wind and the waves are considered the most impactful for the structure.

- **Cyclic behaviour of sand**
  Whereas in drained conditions, shakedown and ratcheting are the most problematic events, cyclic liquefaction and cyclic mobility are the main failure modes in undrained conditions. The behaviour of sand is different in compression and extension: in extension, the sands cannot reach the same critical state as in compression. Thus, the impact of one-way loading was compared to the impact of two-way loading. No agreement has been reached on the most detrimental case between the two loading cases.

- **Current design practice**
  As the offshore wind monopiles have a rigid behaviour, their behaviour cannot be precisely represented by the standard p-y curves. Guidelines advise now to calibrate p-y curves on FE models. New tools like the PISA design model developped new soil reaction components that are calibrated on 3D FE model.

The power law is a practical tool for determining the pile lateral displacement at mudline after cyclic loading. Whereas the logarithmic function provides a good estimation of the pile lateral displacement until 500 cycles, the exponential law is more adapted from 500 cycles.

Chapter 3

Stiffness Degradation Method (SDM)

The Stiffness Degradation Method (SDM) is an explicit numerical procedure (subsection 1.1.5) that assesses the behaviour of a monopile in sand under cyclic loading. The stress-dependent stiffness of the soil is degraded according to a semi-empirical law that accounts for the stresses in the soil, the number of cycles and soil-dependent parameters. First introduced by Kuo (2008) [39] and Achmus et al. (2009) [2], the SDM has been widely verified against pile test data.
First, the stiffness degradation is depicted. Then, the FE implementation of the SDM is presented. Finally the parameters of the method are introduced.

3.1 Origin of the Stiffness Degradation Method

The SDM is based on two cyclic concepts: the stress-dependency of the cyclic strains and the cyclic degradation of the soil stiffness.

3.1.1 Permanent strains in sand under cyclic loading

Huurman (1996) [30] developped a model for calculating permanent axial and radial strains in granular soils based on cyclic triaxial tests in drained conditions. Up to one million loading cycles were applied on the soil samples. Huurman (1996) [30] predicts the permanent axial strains as follows:

$$\epsilon_{p,N} = A(\frac{N}{1000})^B + C(exp(D\frac{N}{1000}) - 1) \tag{3.1}$$

In Equation 3.1, the permanent strains are stress-dependent as the coefficents used in Equation 3.1 are:

$$A = a_1 * X^{a2} \tag{3.2}$$

$$B = b_1 * X^{b2} \tag{3.3}$$

$$C = c_1 * X^{c2} \tag{3.4}$$

$$D = d_1 * X^{d2} \tag{3.5}$$

Where $a1$, $a2$, $b1$, $b2$, $c1$, $c2$, $d1$ and $d2$ are model parameters determined by fitting Equation 3.1 with lab test data. For sand, Huurman (1996) [30] determined that $C = 0$ and $D = 0$. The cyclic stress ratio X is:

$$X = \frac{\sigma_1}{\sigma_{1,f}} \tag{3.6}$$

Where σ_1 is the major principal cyclic stress and $\sigma_{1,f}$ is the major principal stress at failure calculated with the Mohr-Coulomb failure criterion:

$$\sigma_{1,f} = \frac{\sigma_3(1 + sin\phi) + 2c * cos\phi}{1 - sin\phi} \tag{3.7}$$

Where σ_3 is the minor principal stress, ϕ is the friction angle and c is the cohesion.

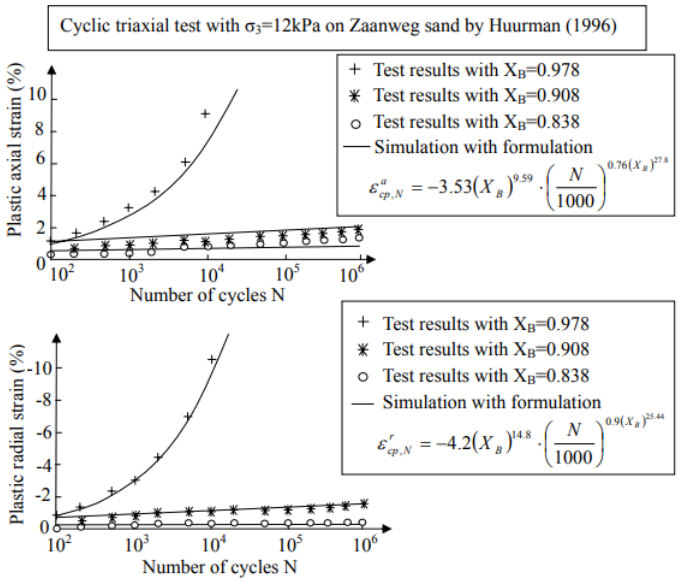

Figure 3.1: Formulation evaluation of Huurman (1996) [30] after Kuo (2008) [39]

On Figure 3.1, both shakedown and ratcheting are modelled with the stress-dependent empirical law of Huurman(1996) [30]. The Equation 3.1 of Huurman (1996) [30] is able to model the cyclic behaviour of sand in drained conditions.

3.1.2 Stiffness degradation concept

From Figure 3.2, the secant shear modulus G_s in a cyclic simple shear stress test is defined as follows:

$$G_s = \frac{\tau_N}{\gamma_N} \tag{3.8}$$

Where τ_N and γ_N are respectively the cyclic shear stress and the cyclic shear strains, defined in Figure 3.2.

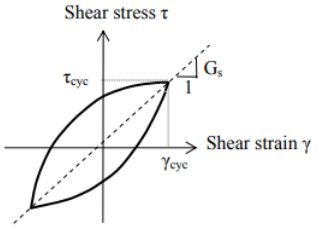

Figure 3.2: Definition of secant shear modulus from Kuo (2008) [39]

If the drained cyclic simple shear stess test is stress-controlled, a degradation of the secant shear modulus is observed in Figure 3.3.

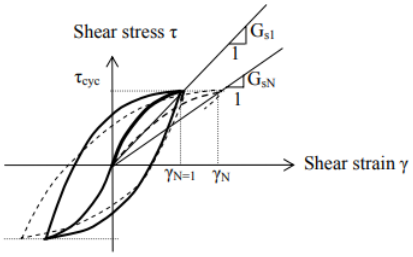

Figure 3.3: Shear modulus response of sand under stress-controlled drained cyclic test, from Kuo (2008) [39]

Idriss et al (1978) [31] adapted the concept of secant shear modulus degradation in a drained cyclic simple shear stress test with stress-controlled conditions to the cyclic drained triaxial test. Hence, the shear strains γ_N, the secant shear modulus G_s and the shear stress τ_N in a simple shear stress test correspond respectively to the axial strains ϵ_N, the secant stiffness modulus E_s and the stress σ_{cycl} of a triaxial test.
On Figure 3.4, during a stress-controlled cyclic triaxial test under drained conditions, the plastic strains increase with the number of cycles N.

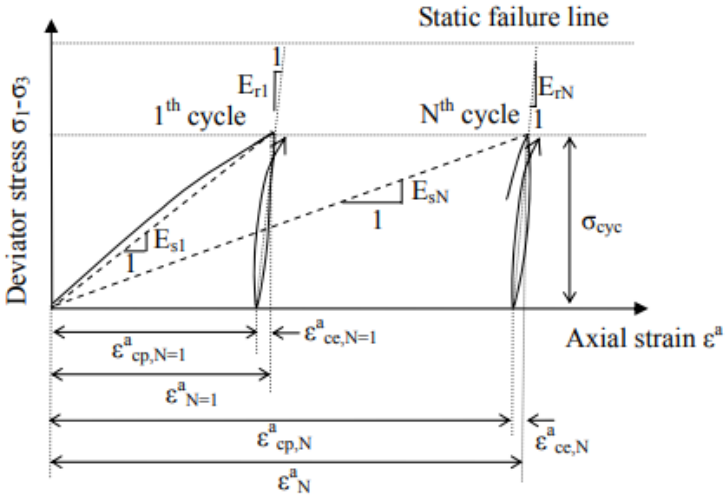

Figure 3.4: Schematic degradation of secant modulus under cyclic loading after Kuo (2008) [39]

The increase of the permanent axial strains is interpreted as a decrease of the secant stiffness modulus E_s:

$$\frac{E_{sN}}{E_{s1}} \approx \frac{\frac{\sigma_{cycl}}{\epsilon_N}}{\frac{\sigma_{cycl}}{\epsilon_{N=1}}} = \frac{\epsilon_{N=1}}{\epsilon_N} = \frac{\epsilon_{p,N=1}+\epsilon_{e,N=1}}{\epsilon_{p,N}+\epsilon_{e,N}} \approx \frac{\epsilon_{p,N=1}}{\epsilon_{p,N}} \tag{3.9}$$

Where E_{sN} and E_{s1} are the secant stiffness moduli after N and 1 cycle respectively, $\epsilon_{N=1}$ and ϵ_N are the total axial strains after 1 and N cycle respectively, $\epsilon_{p,N=1}$ and $\epsilon_{p,N}$ are the plastic strains after 1 and N cycle respectively, $\epsilon_{e,N=1}$ and $\epsilon_{e,N}$ are the elastic strains after 1 and N cycle respectively. In the SDM, the elastic strains are considered sufficiently small to be neglected.
In the SDM, the oedometric stress-dependent stiffness modulus is degraded (Kuo, 2008 [39]):

$$E_s = \kappa \sigma_{at} (\frac{\sigma_m}{\sigma_{at}})^{\lambda} \tag{3.10}$$

Where σ_{at} is the atmospheric pressure, σ_m is the mean principal stress, κ and λ are stiffness constants.
The increase of the axial strain is related to the decrease of the stiffness:

$$\frac{E_{sN}}{E_{s1}} = \frac{\epsilon_{p,N=1}}{\epsilon_{p,N}} = N^{-b_1(X)^{b_2}} \tag{3.11}$$

Where b_1 and b_2 are regression parameters. X is the cyclic stress ratio defined in Huurman (1996) [30] with Equation 3.6.

3.2 Implementation in a FE model

The SDM is implemented in the FE software ABAQUS (Smith, 2009 [64]). The soil is modelled as a linear elastic material with a Mohr-Coulomb failure criterion and a stress-dependent soil stiffness. The soil constitutive model of the SDM is implemented in ABAQUS with an user-defined material (UMAT). The SDM estimates the degraded stiffness based on the results of a static analysis. The method consists of 3 steps described in Figure 3.5:

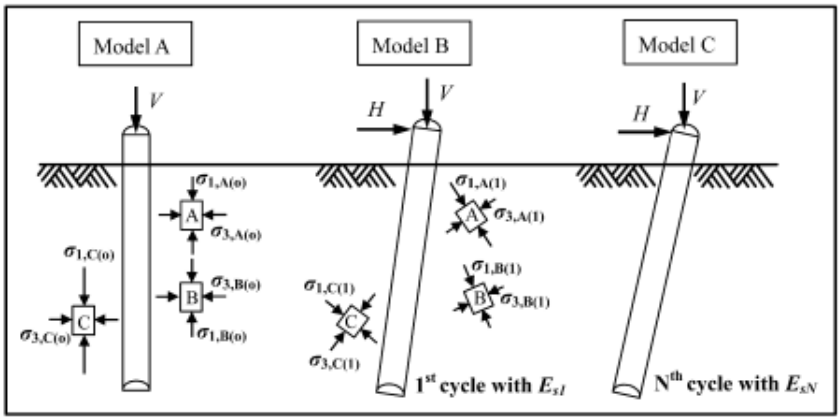

Figure 3.5: Schematic sketch of the determination of degradation stiffness in the pile-soil system after Achmus et al. (2009) [2]

1. **Initial phase (Model A):**
   An axial load is applied on top of the monopile to represent the weight of the OWT and support structure. The method does not assess the strains caused by the installation of the foundation. So, the monopile is wished into place. The initial stress state is represented by the initial principal stress at failure $\sigma_{1,f}^{(0)}$ and the initial cyclic stress ratio $X^{(0)}$. For every soil element:

$$\sigma_{1,f}^{(0)} = \frac{\sigma_3^{(0)}(1+sin(\phi))+2c*cos(\phi)}{1-sin\phi} \tag{3.12}$$

$$X^{(0)} = \frac{\sigma_1^{(0)}}{\sigma_{1,f}^{(0)}} \tag{3.13}$$

2. **Loading phase after 1 cycle (Model B)**:
   A lateral load is applied at the top of the monopile. This load represents the 1st cycle of the cyclic event. The stress state of this phase is represented by the corresponding principal stress at failure $\sigma_{1,f}^{(1)}$ and the cyclic stress ratio $X^{(1)}$. For every soil element:

$$\sigma_{1,f}^{(1)} = \frac{\sigma_3^{(1)}(1+sin(\phi))+2c*cos(\phi)}{1-sin\phi} \tag{3.14}$$

$$X^{(1)} = \frac{\sigma_1^{(1)}}{\sigma_{1,f}^{(1)}} \tag{3.15}$$

   To take into account the stress changes caused by phases 1 and 2, the final cyclic stress ratio for every soil element after phase 2 is:

$$X = \frac{X^{(1)}-X^{(0)}}{1-X^{(0)}} \text{ with } 0 \le X \le 1 \tag{3.16}$$

3. **Loading phase after N cycles (Model C):**
   The stiffness is degraded with Equation 3.11 to obtain the secant stiffness modulus after N cycles.

3.3 Parameters

Because the soil constitutive model is a linear elastic material with Mohr-Coulomb failure criterion, the number of parameters is limited. Thus, the SDM requires only nine parameters in total: seven soil parameters and two model parameters.

3.3.1 Soil parameters

The SDM requires standard soil parameters: the effective unit weight γ', the friction angle ϕ, the dilatancy angle ψ, the cohesion c and the Poisson's ratio ν (Achmus et al., 2009 [2]).
Two stiffness parameters are required to calibrate the soil stiffness that is stress-dependent: κ and λ. κ is a material constant that is sometimes called the "Janbu modulus" (Depina et al., 2015 [22]). λ is a stress index (Peralta and Achmus, 2010 [56]).

3.3.2 Model parameters

Model parameters b_1 and b_2 are calibrated from cyclic triaxial tests in compression. The method to determine parameters b_1 and b_2 from cyclic triaxial tests in compression is described in Appendix B.
Kuo (2008) [39] determined sets of parameters b_1 and b_2 from cyclic triaxial tests available in literature for different sand density. The parameter sets are presented in Table 3.1.
For dense sand, the values of b_1 are between 0.2869 and 0.07. The values of b_2 are between 22.20 and 0. By averaging the values in Table 3.1, Kuo (2008) [39] determined for dense sand: $b1 = 0.20$, $b_2 = 5.76$ and for medium dense sand: $b_1 = 0.16$ and $b_2 = 0.38$.
For cyclic pile tests, in case cyclic triaxial test data are not available for the soil, the parameters b_1 and b_2 can be calibrated directly on the pile test results (Kuo, 2008 [39]). The procedure consists of choosing a set of parameters available in literature that corresponds to the nature of the sand (medium dense sand or dense sand). The parameters are then adapted to fit the test results.

Researchers	Soil type	b1	b2
Morgan (1966)	Medium dense	0.094	0.71
Wichtman (2005)	Medium dense	0.235	0.05
Timmerman & Wu (1969)	Dense sand	0.1114	0
Gaskin et al. (1979)	Dense sand	0.1265	0.98
Lenz-Baladi (1980)	Dense sand	0.1484	0.42
Addo-Adebi (1980)	Dense sand	0.1607	1.56
McDonald & Raymond (1984)	Dense sand	0.16	21.4
Thiel (1988)	Dense sand	0.1010	0.05
Huurman (1996)	Dense sand	0.1010	0.05
Huurman (1996)	Dense sand	0.2872	16.20
Huurman (1996)	Dense sand	0.268	4.9
Huurman (1996)	Dense sand	0.07	0
Huurman (1996)	Dense sand	0.305	12.60
Huurman (1996)	Dense sand	0.735	22.20
Huurman (1996)	Dense sand	0.1399	0.95
Huurman (1996)	Dense sand	0.2869	4.60
Huurman (1996)	Dense sand	0.18	0.53
Gotschol (2002)	Dense sand	0.0605	0.05

Table 3.1: Model parameters b_1 and b_2 calibrated on existing cyclic triaxial tests after Kuo (2008) [39]

3.4 Conclusion

In the SDM, the soil stiffness is degraded with the semi-empirical formula of Huurman (1996) [30]. It can model the cyclic behaviour of drained sands. In the derived semi-empirical law of the SDM, the soil stiffness is dependent on the stresses in the soil, the number of cycles and two parameters b_1 and b_2. The SDM is implemented on the FE software ABAQUS. First, a static analysis is performed. Based on the stresses in the soil after the static analysis, the stiffness is degraded. Parameters b_1 and b_2 are calibrated on cyclic triaxial test in compression. For verifying pile test without cyclic triaxial test, b_1 and b_2 can be calibrated on the experiment data.

Chapter 4

FE implementation of the SDM

The Stiffness Degradation Method (SDM) is implemented into the FE software PLAXIS 3D (Brinkgreve, 2013 [15]) with an automatic routine coded in Python. The main steps of the FE implementation will be presented. There are seven steps: model parameters, soil constitutive model, monopile structure, clusters, construction phases, stiffness degradation procedure and update of the stiffness.

4.1 Step 1: Model parameters

In the first step, the model parameters are determined: soil, pile, loading and project parameters. Figure 4.1 presents the dimensions of the PLAXIS 3D model in function of the pile diameter D and the embedded length L.

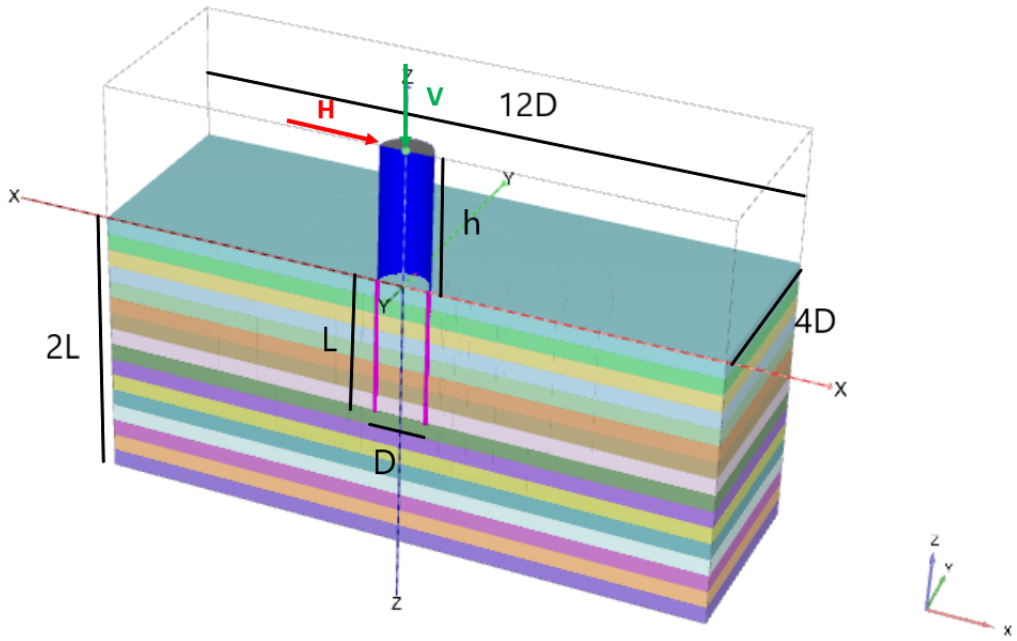

Figure 4.1: View of the PLAXIS 3D model presenting the model and pile dimensions

4.1.1 Soil parameters

In PLAXIS 3D, the soil is modelled with the constitutive model Mohr-Coulomb. Thus, the following soil parameters are required: the effective unit weight γ', the friction angle ϕ, the dilatancy ψ, the cohesion c, the Poisson's ratio ν and the SDM stiffness parameters κ and λ (section 3.3). The coefficient of earth pressure at rest $K0$ is defined as $1 - sin(\phi)$.

4.1.2 Monopile parameters

The monopile dimensions are the diameter D, the embedded length L and the eccentricity of the lateral load h (Figure 4.1). The monopile is made of steel with the following characteristics: the pile Young's modulus of

elasticity E_p, the Poisson's ratio ν_p, the wall thickness t_p, the shear modulus G_p and the unit weight w_p. The material is assumed isotropic.

4.1.3 Loading conditions

The loading conditions are simplified. The axial load V and the lateral load H are applied on top of the monopile with an eccentricity h (Figure 4.1). With the eccentricity, the bending moment created by the lateral load is also accounted for.

4.1.4 Project parameters

The model is in 3D and has tetrahedral elements (Brinkgreve, 2013 [15]). Because the pile-soil system is symmetric in geometry and loading, only half of the pile-soil system is modelled (Thieken et al., 2015 [66]). In Kuo (2008), the pile-soil system has a width of 12 times the pile diameter D. The model depth is the embedded length L plus 3 times the diameter D (Kuo, 2008). In the study model, the axis boundaries are defined to avoid the boundary condition effects. The length and the width of the model are respectively 12 and 4 times the diameter of the pile D. The depth of the model is 2 times the pile embedded length L.

4.2 Step 2: Soil constitutive model

In the SDM of Achmus et al. (2009) [2], the soil is linear elastic with a Mohr-Coulomb failure criterion and the stiffness is stress-dependent (Equation 3.10). The constitutive soil model is created with a user-defined material (UMAT) in the FE software ABAQUS (Smith, 2009 [64]).
In PLAXIS 3D, for representing the linear elastic material with Mohr-Coulomb failure criterion, the soil is modelled with the contitutive model Mohr-Coulomb of PLAXIS 3D (Brinkgreve, 2013 [15]).
Mohr-Coulomb is a linear elastic and perfectly plastic model. The linear elastic behaviour is modelled with the Hooke's law. The soil failure is reached at the Mohr-Coulomb failure criterion represented by the first principal stress at failure in Equation 3.7. Figure 4.2 presents the stress-strain behaviour of the soil with Mohr-Coulomb in comparison with the behaviour of a standard soil. As the behaviour of soil is non-linear, its behaviour below failure is not well captured by Mohr-Coulomb. However, the Mohr-Coulomb failure criterion is a good approximation of the drained failure state of soils. Mohr-Coulomb is not able to simulate the peak strength at failure and the softening behaviour that follows.

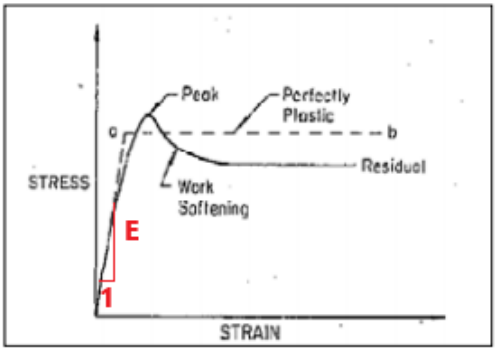

Figure 4.2: Elastic-perfectly plastic assumption of Mohr-Coulomb model, after Ti et al. (2009) [67]

In Mohr-Coulomb, the soil stiffness is represented by the Young's modulus E (Figure 4.2) and remains constant until failure is reached. To simulate the stress-dependency of the stiffness at initial stress conditions with Mohr-Coulomb in PLAXIS 3D, soil layers of constant layer depth a are created. Every soil layer is assigned a Mohr-Coulomb soil material which stiffness is calculated at the middle of the layer with Equation 3.10.
Figure 4.3 presents the stress-dependent stiffness of the SDM (Equation 3.10 for a = 2.5m, κ = 600 and λ = 0.55) and the resulting layer-dependent stiffness created with Mohr-Coulomb soil material on PLAXIS 3D. For an embedded length $L = 40m$, a layer-depth of $a = 2.5m$ provides a reasonable approximation of the SDM stress-dependent stiffness at initial stress conditions.

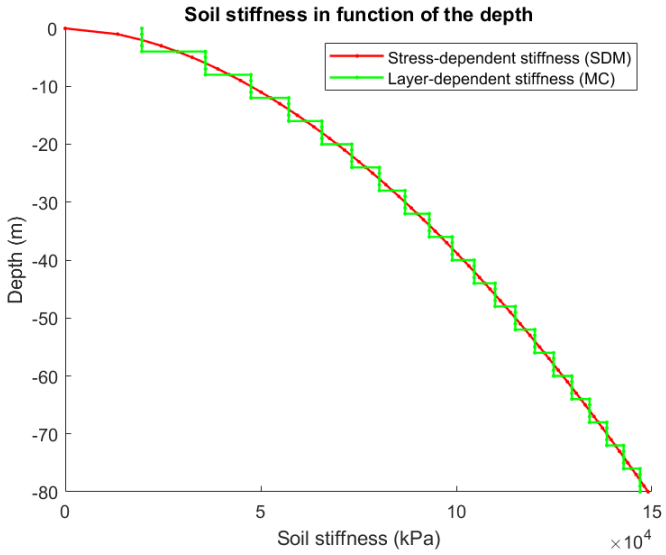

Figure 4.3: Layer-dependent stiffness (Mohr-Coulomb) and stress-dependent stiffness (SDM) in function of the depth at initial stress conditions for $\kappa = 600$ and $\lambda = 0.55$

4.3 Step 3: Monopile structure

For implementing the SDM on PLAXIS 3D, the pile was modelled differently than in Kuo (2008) [39]. In this section, the pile model of Kuo (2008) [39] is compared with the pile model in PLAXIS 3D. Figure 4.4 presents the pile structure and dimensions of the model in PLAXIS 3D.

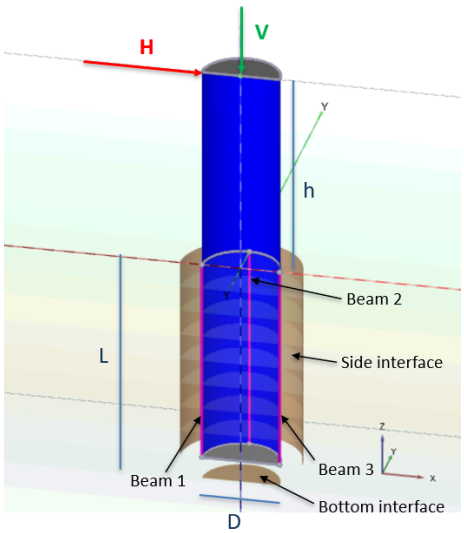

Figure 4.4: Monopile structure of the study model - View of the PLAXIS 3D pile model

4.3.1 Monopile model

The monopile model is different in Kuo (2008) [39] and in the study model. In both models, only half of the monopile is modelled because of the pile symmetry in geometry and loading. Besides, modelling half of the monopile saves computation time (Kuo, 2008) [39]. The pile has a diameter D and an embedded length L. As the lateral loading H is applied with an excentricity h to account for the bending moment, the monopile is extended above mudline at a height h (Figure 4.4).

Kuo (2008)

To focus on the cyclic lateral behaviour of the monopile, Kuo (2008) [39] neglects the effect of the soil plug in the pile. Thus, an equivalent solid pile with same diameter D and embedded length L is used. The pile unit weight w_p is determined as the volume weight average of the tubular pile and the plug soil. The pile elastic modulus E_p is the equivalent bending stiffness of the tubular pile.

Study model

In PLAXIS 3D, the monopile is constructed as half of a cylinder by using plates which are assigned a material with steel properties (subsection 4.1.2). As the loading is applied on top of the structure, the top of the pile is a rigid body in order to avoid the steel deformations due to the loading application. In contrary to Kuo (2008) [39], the effects of the soil plug are not neglected: the soil plug remains in the tubular pile. This pile model is more realistic.

4.3.2 Interfaces

In both models, interfaces are set between the soil and the outer side of the pile, respectively along the embedded pile and at the pile tip. The interfaces enable relative displacement between the soil and the monopile. The relative displacement between the monopile and the soil is controlled by the contact friction angle and the strength properties of the materials. Because of the difference of pile model between Kuo (2008) [39] and the study model, the contact friction angles of the interfaces are different.

Kuo (2008)

In Kuo (2008) [39], the side interface along the embedded pile has a contact friction angle that corresponds to $\frac{2}{3}$ of the soil friction angle ϕ. Because the pile is modelled as an equivalent solid pile, the bottom interface at the pile tip has an equivalent contact friction angle that is determined from the weight average area of the tubular pile and the soil plug (Kuo, 2008) [39].

Study model

In PLAXIS 3D, the contact friction angle is obtained by multiplying the coefficient R_{inter} with the soil friction angle ϕ. In the study model, two interfaces are set between the soil and the outer side of the pile, respectively along the embedded pile and at the pile tip, with the same coefficient $R_{inter} = \frac{2}{3}$. The friction between the soil plug and the inner side of the pile is consided negligible for studying the lateral displacement of the monopile under cyclic loading. Thus, no interface is set inside the monopile.

4.3.3 Lateral displacement

In Kuo (2008) [39], the method to calculate the pile lateral displacement is not described.
In PLAXIS 3D, the pile lateral displacement is extracted from three beams attached to the monopile structure. Three soft beams are created along the embedded section of the monopile (Figure 4.4). The three soft beams are located at the back of the pile and at the pile endpoints on the x-axis. The beam material is identical to the pile material except that the beam Young's modulus is the pile Young's modulus divided by 10. The impact of the beam stiffness on the lateral displacement will be studied in subsection 5.3.3.

4.4 Step 4: Soil clusters

In the SDM (subsection 3.1.2), the soil stiffness after the first loading cycle is degraded to obtain the soil stiffness after N loading cycles. In Kuo (2008) [39], the soil stiffness is updated at every node. In PLAXIS 3D, this procedure could be possible with a user-defined soil model (Brinkgreve, 2013 [15]). However, creating a user-defined soil model in PLAXIS 3D is complex and not adapted to the objective of this research. Thus, a clustering method similar to the Soil Cluster Degradation method of Zorzi et al. (2018) [75] was implemented. With this procedure, soil clusters are created around the monopile. As their soil material can be changed, the stiffness can be updated in the clusters.
In PLAXIS 3D, Figure 4.5 presents the dimensions of the cluster layout that can be changed by the user.

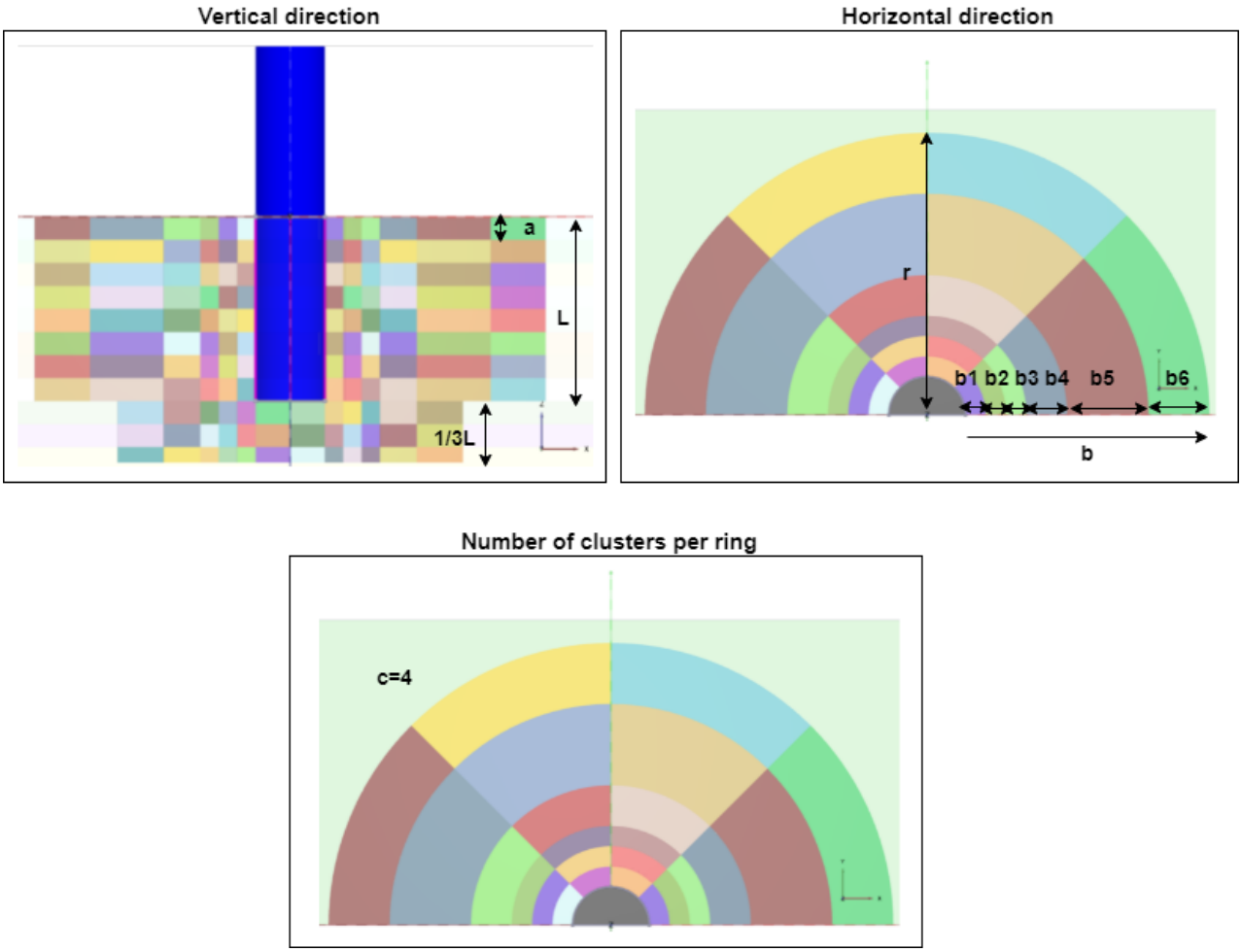

Figure 4.5: Definition of the soil clusters layout. Top and bottom pictures are respectively front and top view of the pile

The clusters layout is defined accordingly to the stiffness degradation pattern. The clusters layout is created according to the vertical and horizontal directions and the number of clusters per ring:

- **Vertical direction**
  The length of the clusters in the vertical direction is controlled by the constant layer depth a of the soil layering created in section 4.2. The clusters are created from mudline to $\frac{4}{3}$ of the pile embedded length L (Figure 4.5). The impact of the constant layer depth a will be studied in section 5.3.5.

- **Horizontal direction**
  The user can define the dimension b of every cluster in the horizontal direction. As the stiffness degradation is more severe close to the pile, the horizontal length b of the clusters should be smaller in this area. On Figure 4.5, the dimension b progressively increases with the distance to the pile.
  Because the SDM assesses the cyclic degradation around the pile, the stiffness degradation of the soil plug is neglected. From mudline to the pile embedded length L, there is no cluster in the pile. Clusters are created from the pile outer surface to the cluster layout radius r.
  From the pile embedded length L to $\frac{4}{3}L$, clusters are created below the pile. The impact of the cluster width b will be studied in section 5.3.5.

- **Number of clusters per ring**
  The number of clusters per ring c is chosen by the user. The number of clusters per ring should be sufficient to reasonably cover the area. The impact of the number of cluster per ring c will be studied in section 5.3.5.

Once the clusters are created, a mesh is generated. The coarseness is set to 0.075 which corresponds to a coarse mesh. A coarse mesh limits the computation times as there are less elements in the clusters. The im-

pact of the coarseness factor on the number of elements in the FE model and on the pile lateral displacement is studied in subsection 5.3.4.

4.5 Step 5: Phases

In PLAXIS 3D, construction phases are staged. Figure 4.6 presents the model stages of the SDM static analysis.

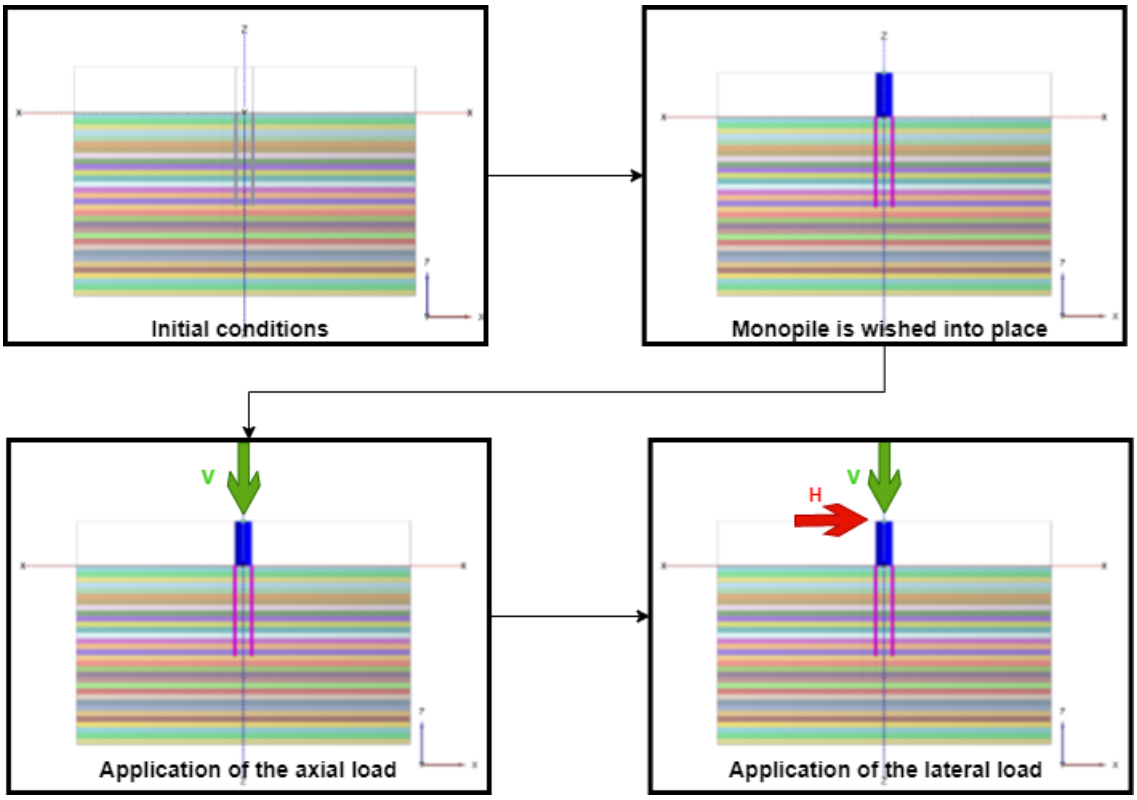

Figure 4.6: Static analysis: Construction stages of the SDM static analysis

The phases are defined as followed:

- **Initial conditions**
  The initial stress conditions in the soil are calculated with the K0 procedure.

- **Installation of the monopile**
  The plates and the rigid body that constitute the monopile are activated. The pile-soil interfaces and the three beams are also switched on.

- **Application of the axial load - Phase 0 of the SDM**
  As the SDM focuses on cyclic loading, the displacements created by the monopile intallation are not considered. Thus, the displacement in the soil is reset to 0.
  The axial load that represents the weight of the OWT and its support structure is applied on top of the structure. The impact of the vertical load V on the pile lateral displacement is studied in Appendix C.

- **Application of the lateral load - Phase 1 of the SDM**
  The lateral load H is applied on top of the monopile with an excentricity h.

Once the stages are defined and the corresponding items are activated, the calculation procedure is realized. The output data from the static analysis are used for the stiffness degradation procedure.

4.6 Step 6: Stiffness degradation procedure

In the stiffness degradation procedure, phase 0 and phase 1 correspond respectively to the application of the axial load and the application of the lateral load in the static analysis (section 4.5). The method to calculate the cyclic stress ratio and the degraded stiffness are explained in this section.

4.6.1 Cyclic stress ratio

First, the cyclic stress ratio is calculated. The cyclic stress ratio represents the load level in the soil, at every stress point. Figure 4.7 presents the steps for determining the cyclic stress ratio X in a cluster.

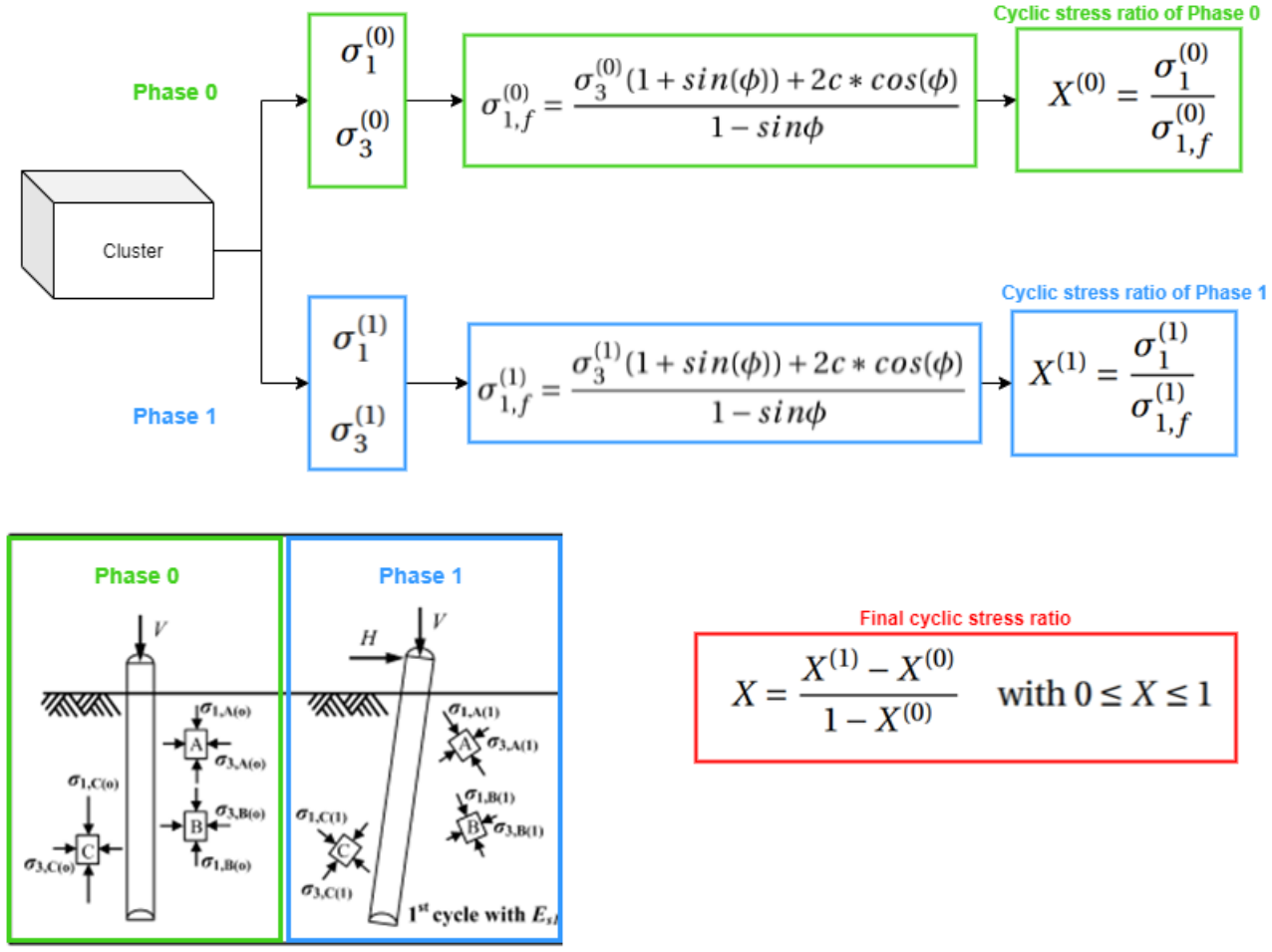

Figure 4.7: Schematic representation of the procedure for calculating the cyclic stress ratio in a cluster

In every soil cluster, at every stress point, the major principal effective stresses $\sigma_1^{(0)}$ and $\sigma_1^{(1)}$ and the minor principal effective stresses $\sigma_3^{(0)}$ and $\sigma_3^{(1)}$ at phase 0 and phase 1 are extracted from PLAXIS Output. Then, for every cluster, at every stress point, the major principal effective stresses at failure $\sigma_{1,f}^{(0)}$ and $\sigma_{1,f}^{(1)}$ for phase 0 and phase 1 are calculated with Equation 3.7. The cyclic stress ratios at phase 0 and phase 1 are calculated respectively with Equation 3.13 and Equation 3.15.
In the model, the soil elements do not necessarily encounter isotropic stress conditions like in a triaxial test. Thus, between phase 0 and phase 1, the principal stress might change. In the SDM, the cyclic stress ratio represents the stress level at a specific location. To ensure the increase of the cyclic stress ratio while the principal stress changes, the final cyclic stress ratio is used with Equation 3.16 (Kuo, 2008 [39]).
In the case where a stress point experiences a decrease of stress between phase0 and phase1, no change of the soil stiffness is expected. Thus, $X = 0$ (Kuo, 2008).

Once the stress ratios of all the stress points in a cluster are calculated, the final stress ratio X is averaged over the cluster. This procedure assigns a single cyclic stress ratio per cluster.

4.6.2 Stiffness degradation

Once the cyclic stress ratio is calculated in the cluster, the soil stiffness can be degraded. Figure 4.8 presents the procedure for degrading the soil stiffness. The soil stiffness is averaged over every cluster. For every soil cluster, the stiffness is degraded with Equation 3.11:

$$E_{s,N} = E_{s,1} N^{-b_1 X^{b_2}} \tag{4.1}$$

Where $E_{s,1}$ is the soil stiffness after the phase 1, N is the number of cycles, X is the final cyclic stress ratio, b_1 and b_2 are the SDM parameters.
At the end of the procedure, every cluster is assigned a single degraded soil stiffness $E_{s,N}$.

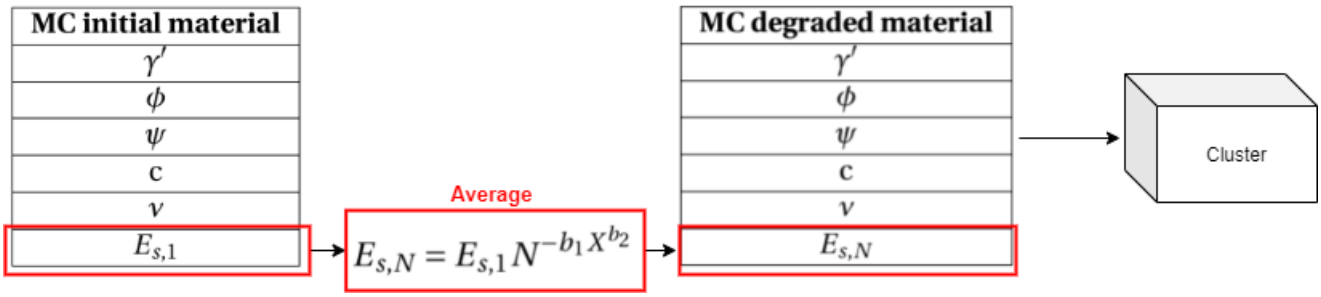

Figure 4.8: Schematic representation of the procedure for degrading the soil stiffness

4.7 Step 7: Update of the stiffness

The simulation is re-run with the same construction phases as in section 4.5.
The horizontal displacement in the x direction u_x of the three soft beams is extracted from Output PLAXIS.

4.8 Conclusion

The SDM was implemented in PLAXIS 3D with an automated routine. In this chapter, the main steps of the Python routine were presented. The procedure is divided into seven steps. First, the static analysis is carried out. It consists of steps 1 to 5: defining the model parameters, choosing the soil constitutive model, creating the monopile and clusters and running the construction phases. Afterwards, the cyclic analysis consists of degrading the soil stiffness in the clusters and re-running the static analysis with the updated clusters. As a conclusion, the SDM can be implemented on PLAXIS 3D.

Chapter 5

Verification of the study model

The verification of the study model is performed by comparing results with the reference system of Kuo (2008) [39]. The soil, pile and loading input parameters of section 4.1 are presented in Table 5.1. Two versions of the reference systems are presented here: a model with an embedded length L = 20m and a model with an embedded length L = 40m.

Reference system parameters					
Soil		**Pile**		**Loading**	
γ' (kN/m^3)	11	D (m)	7.5	V (MN)	10
ϕ (°)	37.5	L (m)	20 or 40	H (MN)	15
ψ (°)	7.5	h (m)	20		
c	0.1	t_p (m)	0.09		
ν	0.25	E_p (kPa)	2.1E8		
κ	600	ν_p	0.2		
λ	0.55	w_p (kN/m^3)	68		
b_1	0.20				
b_2	5.76				

Table 5.1: Input parameters of the reference system (Kuo, 2008 [39])

For verifying the study model, the same cluster layout is used for the short (L = 20m) and long pile (L = 40m). The clusters layout parameters are presented in Table 5.2.

Clusters layout	
a (m)	2.5
b (m)	[2;2;2;4;8;6]
c (-)	4

Table 5.2: Clusters layout parameters for verifying the study model on the reference system of Kuo (2008) [39]

5.1 Reference system with L=20m

In this section, the results of the reference system of Kuo (2008) [39] for the short pile will be compared with the results of the study model. The short pile has an embbedde length L = 20m which corresponds to the ratio $\frac{L}{D}$ = 2.67.

5.1.1 Stiffness degradation

Figure 5.1 presents the stiffness after N=1, 100 and 10 000 loading cycles between the study model and the reference system of Kuo (2008) [39]. At N=1 cycle, the stiffness of the study model is identical to the stiffness at initial stress conditions: the stiffness is not degraded at N=1 cycle. The stiffness at N=1 cycle is thus depth-dependent: the stiffness increases with depth. The soil stiffness in Kuo (2008) [39] is also depth-dependent. However, the soil stiffness of the study model at depth $\frac{4}{3}L$ is equivalent to the stiffness of Kuo (2008) [39] at 2.5L. Thus, at N=1 cycle, the soil stiffness of the study model is higher than in Kuo (2008) [39].
At N=100 loading cycles, the stiffness is degraded in every cluster based on the stress level in the soil at N=1 loading cycle. The stiffness degradation pattern has a conical shape and is more extended in the passive zone than in the active zone.

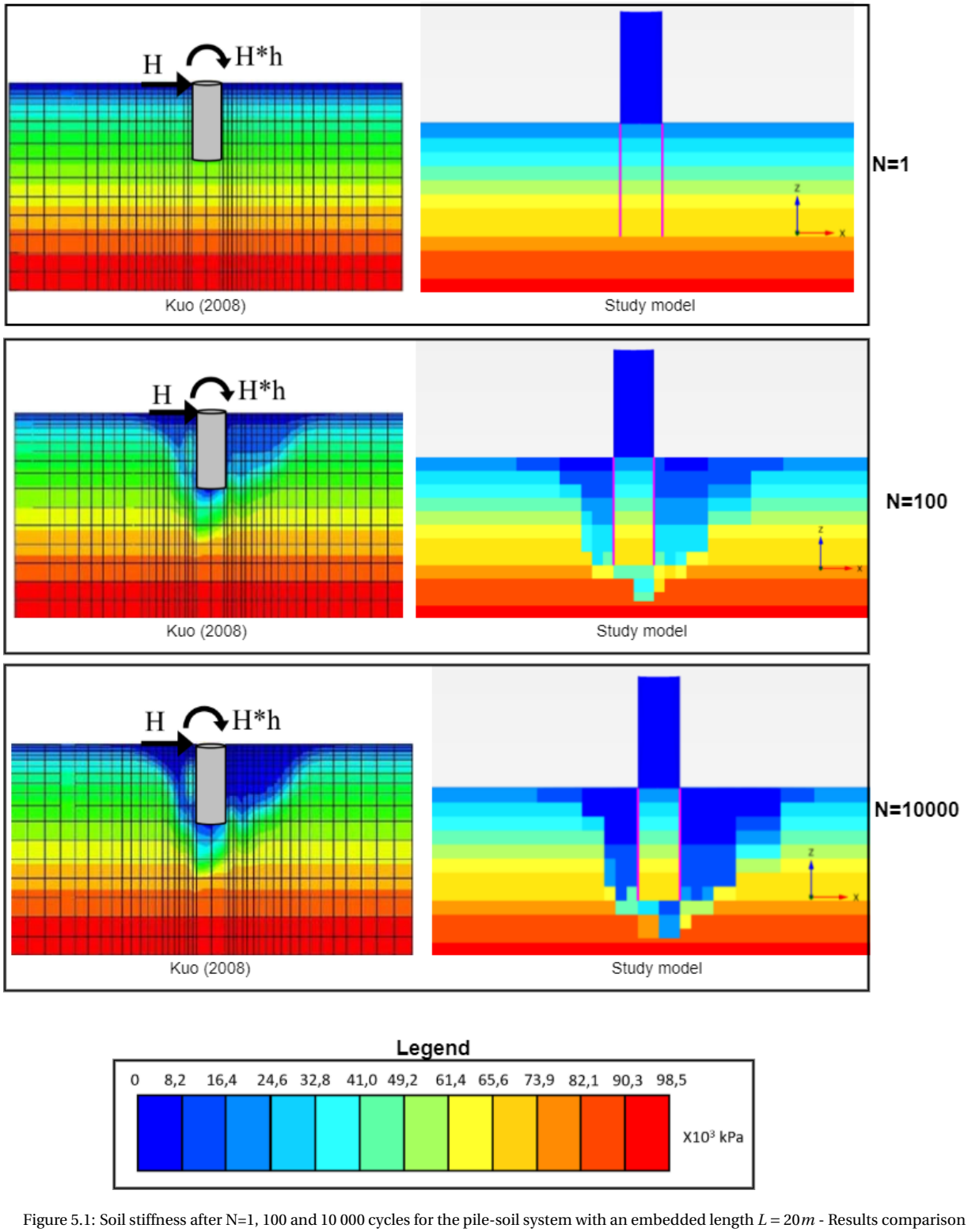

Figure 5.1: Soil stiffness after N=1, 100 and 10 000 cycles for the pile-soil system with an embedded length $L = 20m$ - Results comparison between the reference system of Kuo (2008) [39] and the study model

The degradation pattern around the pile between the study model and the reference model of Kuo (2008) [39] at N=100 cycles is similar. Similar to the observation at N=1 cycle, the soil stiffness of the study model is higher than in Kuo (2008).
At N=10 000 cycles, the degradation pattern around the pile is enhanced compared to the pattern at N=100 cycles. As observed at N=100 cycles, the degradation pattern at N=10 000 cycles has an asymmetrical conical shape as the degradation is more extended in the passive zone than in the active zone. The study model and

the reference model of Kuo (2008) [39] at N=10 000 cycles have a similar stiffness degradation pattern. The soil stiffness of the study model is higher than in Kuo (2008).
For a pile embedded length L = 20m ($\frac{L}{D}$ = 2.67), the study model provides the same stiffness degradation pattern as in the reference system of Kuo (2008) [39]. However, the soil stiffness in the reference model of Kuo (2008) is smaller than in the study model.

5.1.2 Pile deflection

In this section, the pile lateral diplacement in function of depth obtained with the study model is compared with the results of the reference system of Kuo (2008) [39] with an embedded length L=20m. Figure 5.2, Figure 5.3 and Figure 5.4 compare the pile lateral displacement in function of the depth obtained with the study model and with the reference model of Kuo (2008) [39] for respectively 1, 100 and 10 000 loading cycles.

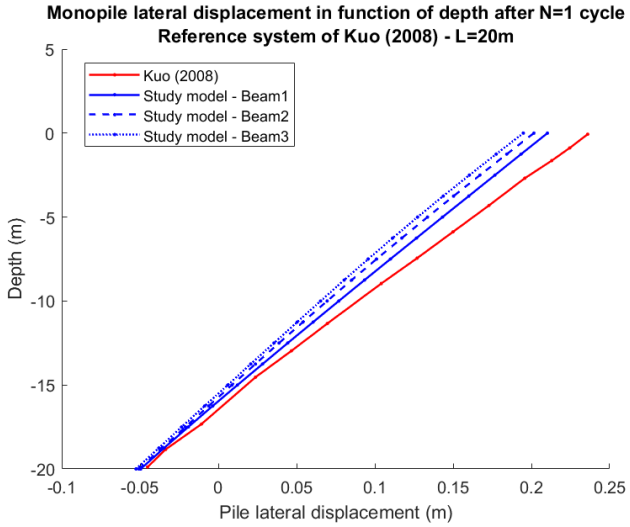

Figure 5.2: Lateral displacement of a monopile after N=1 cycle for L=20m - Results comparison between the reference system of Kuo (2008) [39] and the study model

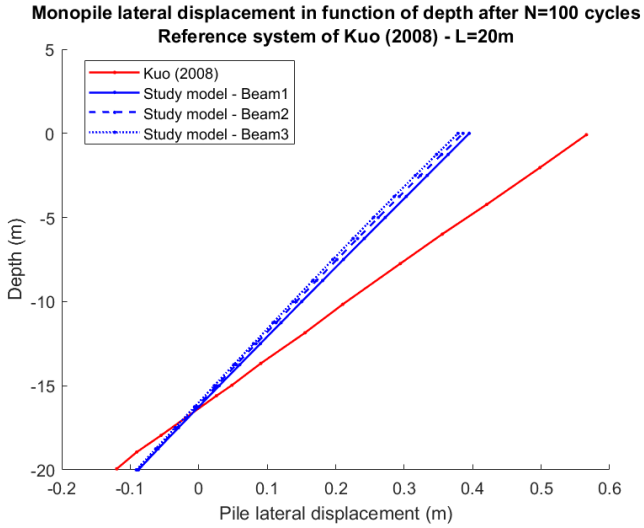

Figure 5.3: Lateral displacement of a monopile after N=100 cycle for L=20m - Results comparison between the reference system of Kuo (2008) [39] and the study model

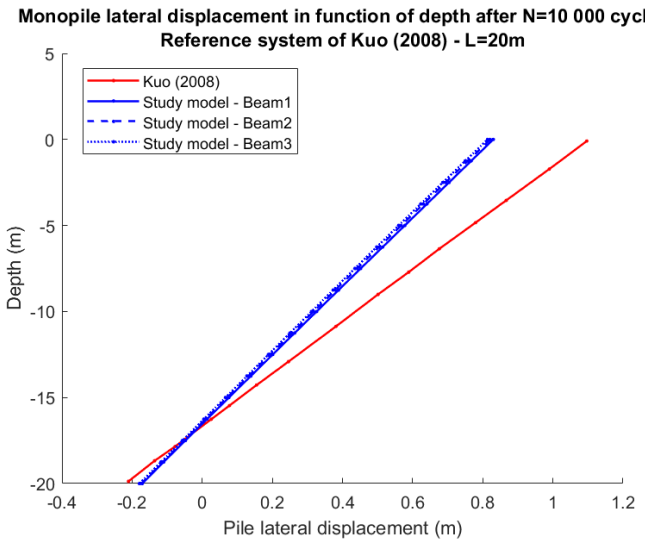

Figure 5.4: Lateral displacement of a monopile after N=10 000 cycle for L=20m - Results comparison between the reference system of Kuo (2008) [39] and the study model

The pile-soil model with an embedded length $L = 20$m is expected to have a rigid behaviour because of the pile dimensions and the small ratio $\frac{L}{D} = 2.67$.
For the study model, the lateral displacement of the three beams is plotted. The three beams are located at the sides and middle of the pile, along the pile plate. They represent the displacement of the pile at different location along its diameter. Thus, the displacement of the pile is not the same around the diameter. This phenomenom is caused by the pile model that uses curved plates and allows more motion of the structure. This pile setting corresponds to a more realistic pile behaviour compared to the equivalent solid pile of Kuo (2008) [39].
For N=1, N=100 and N=10 000 cycles, the study model underestimates the pile lateral displacement compared to the results of Kuo (2008) [39]. This observation is coherent with the overestimation of the stiffness observed in subsection 5.1.1. The displacement offset between the study model and Kuo (2008) [39] is higher at mudline than at the pile tip. The offset increases between the static results (N=1 cycle) and the cyclic results (N=100 and 10 000 cycles).
The results of the study model are in overall agreement with the results of the reference model of Kuo (2008) [39] for an embedded lenght $L = 20$m. The study model is able to capture the behaviour of a rigid pile.

5.2 Reference system with L=40m

In this section, the study model will be compared with the reference system of Kuo (2008) [39] with the long pile. The long pile has an embedded length $L = 40$m which corresponds to the ratio $\frac{L}{D} = 5.3$.

5.2.1 Principal stresses

Figure 5.5 compares the major and minor principal stresses at phase 0 between the study model and the reference system of Kuo (2008) [39]. At phase 0, the principal stresses in the study model corresponds to the stresses at initial stress conditions: the principal stresses are depth-dependent. At phase 0, the principal stresses in the study model are identical to the stresses in Kuo (2008) [39].
Figure 5.6 compares the major and minor principal stresses at phase 1 between the study model and the reference system of Kuo (2008) [39]. From mudline to one third of the embedded length L, the stresses in the active zone decrease close to the pile whereas they increase in the passive zone close to the pile. This result was expected as the pile is pushed toward the right and thus applies compression on the passive zone (increase of the negative principal stresses). The principal stresses of the study model are identical to the principal stresses of Kuo (2008) [39].

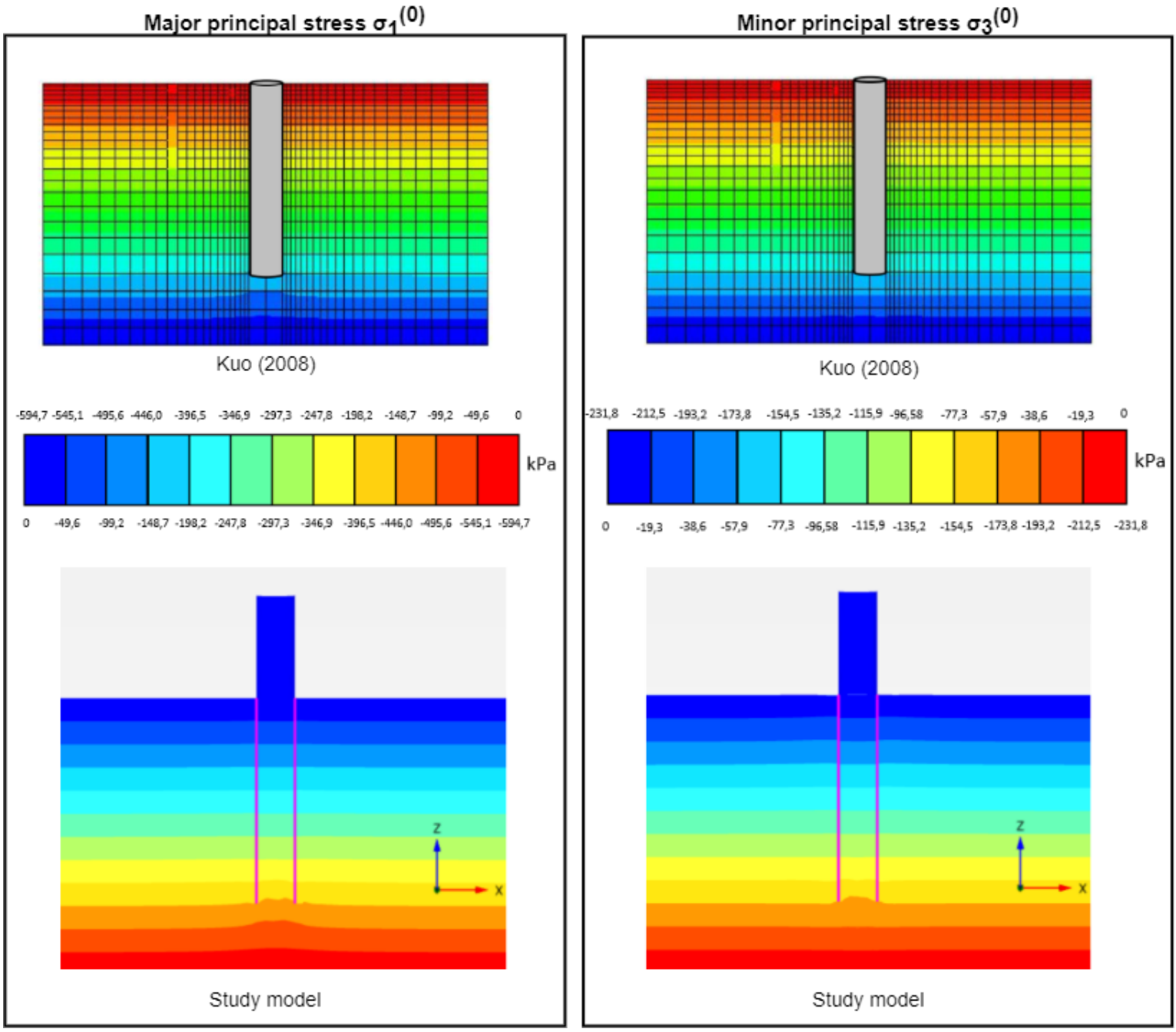

Figure 5.5: Major principal stress $\sigma_1^{(0)}$ and minor principal stress $\sigma_3^{(0)}$ at phase 0 for L=40m - Results comparison between the reference system of Kuo (2008) [39] and the study model

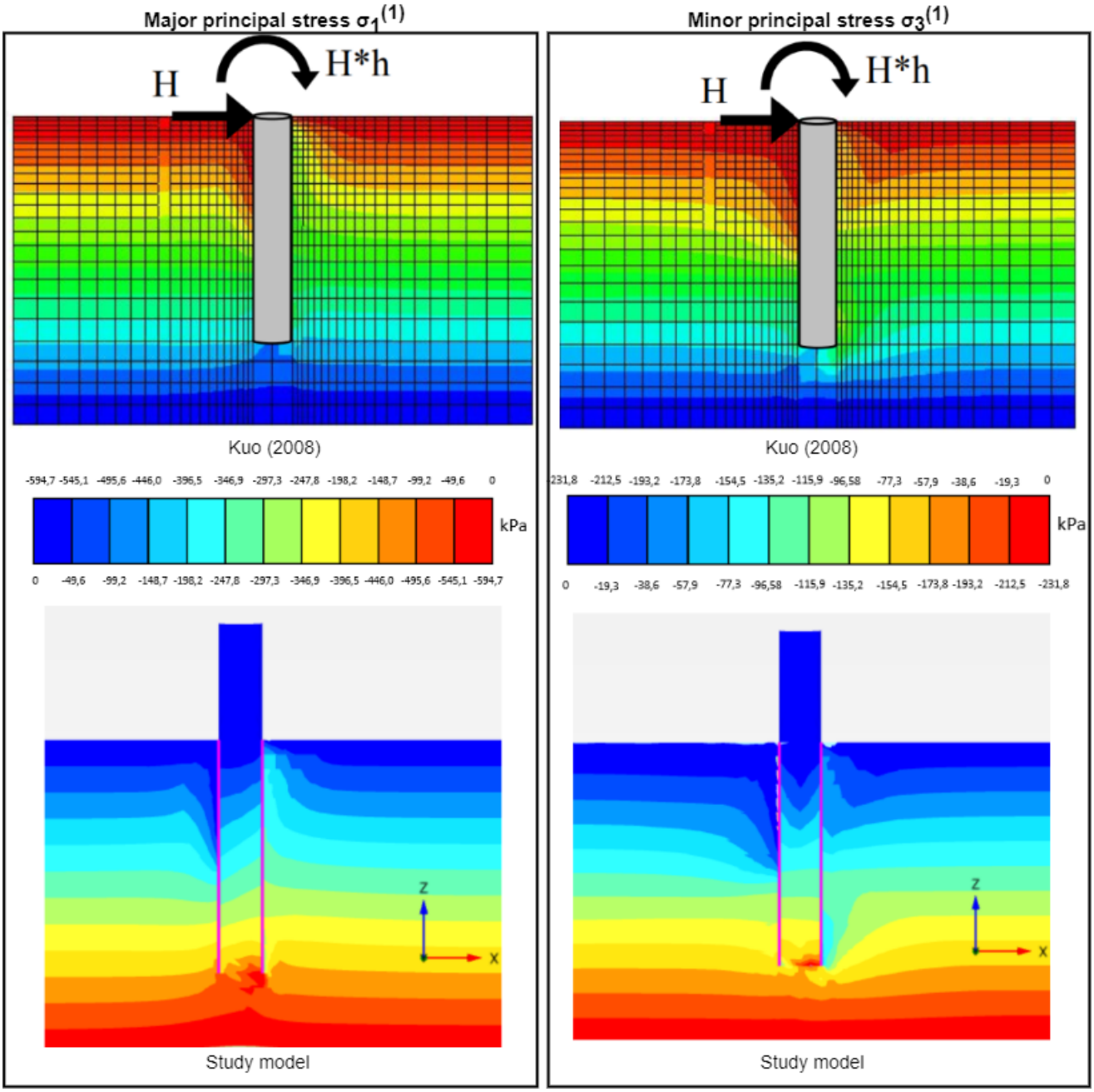

Figure 5.6: Major principal stress $\sigma_1^{(1)}$ and minor principal stress $\sigma_3^{(1)}$ at phase 1 for L=40m - Results comparison between the reference system of Kuo (2008) [39] and the study model

5.2.2 Stiffness degradation

Figure 5.7 presents the stiffness after N=1, 100 and 10 000 loading cycles between the study model and the reference model of Kuo (2008) [39]. At N=1 cycle, the stiffness is identical to the stiffness at initial stress-conditions: the stiffness is not degraded at N=1 cycle. The stiffness at N=1 cycle is thus depth-dependent and increases with depth. At the pile tip, the soil stiffness in the study model reaches 119200kPa whereas it reaches 83700 kPa in Kuo (2008). The soil stiffness in the study model is higher than in Kuo (2008).

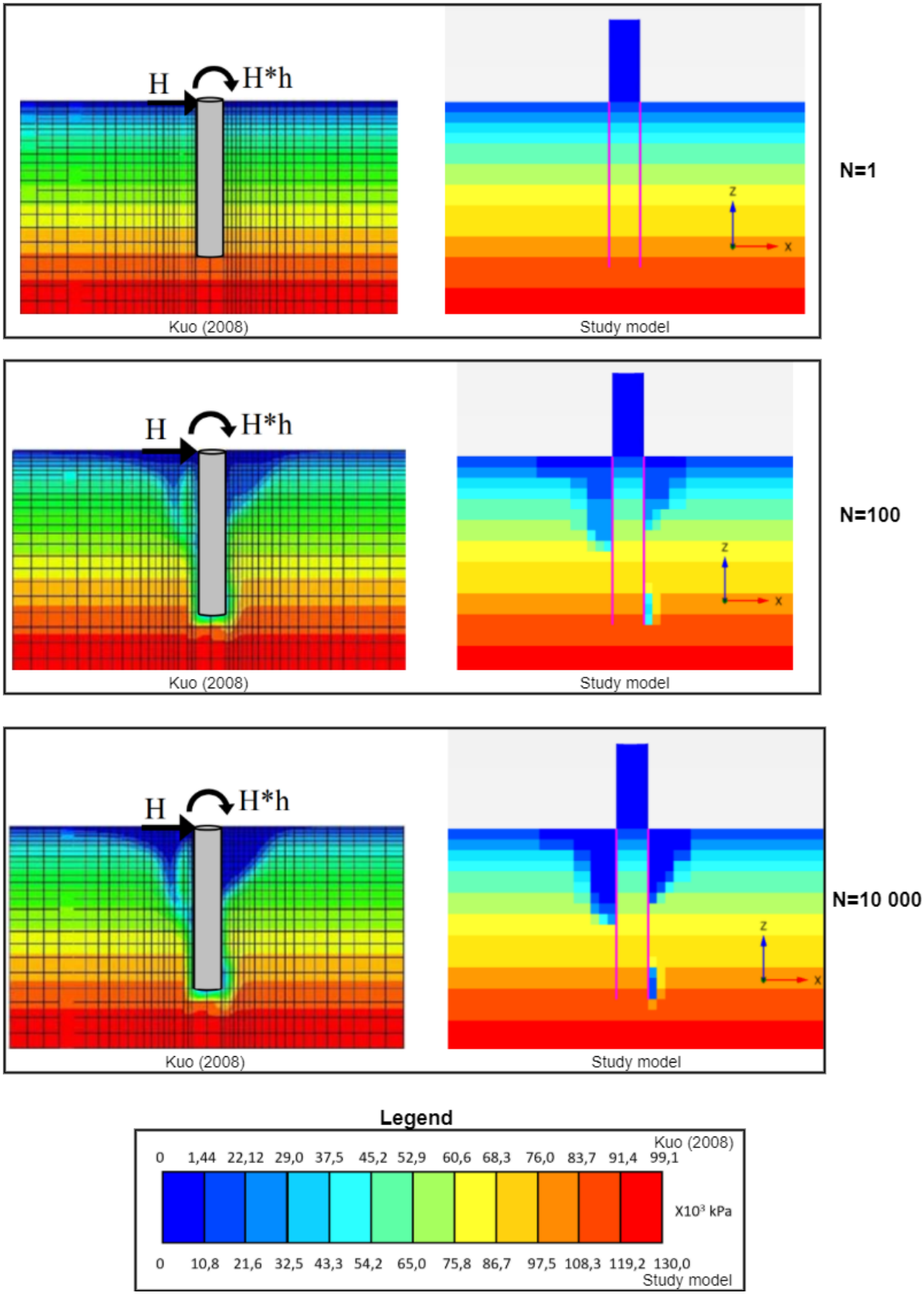

Figure 5.7: Soil stiffness after N=1, 100 and 10 000 cycles for the pile-soil system with an embedded length $L = 40m$ - Results comparison between the reference system of Kuo (2008) [39] and the study model

At N=100 loading cycles, the stiffness is degraded in every cluster based on the stress level in the soil at N=1 loading cycle. The degradation pattern around the pile from mudline to half the embedded length has a conical asymmetric shape. The asymmetry of the stiffness degradation was expected as the principal stresses are higher in the passive zone than in the active zone (subsection 5.2.1). From half of the embedded length to the pile tip, the study model does not capture fully the thin degradation pattern along the pile that is observed on the reference model of Kuo (2008) [39]. The study model is not able to capture this pattern because the clusters width along the pile is probably too large. As the degraded stiffness is averaged over the clusters, the stiffness is smoothed and some accuracy is lost. As observed previously, the soil stiffness in the study model is higher than in Kuo (2008).
At N=10 000 cycles, the degradation pattern around the pile is enhanced compared to the pattern at N=100 cycles. The degradation pattern at the pile tip is enhanced aswell. However, the degradation pattern along the pile from half the embedded length to the pile tip is not visible. As observed previously, the soil stiffness in the study model is higher than in Kuo (2008).
The study model provides similar stiffness degradation pattern compared to the reference model of Kuo (2008) [39]. However, as also observed in subsection 5.1.1, the study model overestimates the stiffness compared to the model of Kuo (2008) [39].

5.2.3 Pile deflection

In this section, the pile lateral diplacement in function of depth obtained with the study model is compared with the results of the reference system of Kuo (2008) [39].
Figure 5.8, Figure 5.9 and Figure 5.10 compare the pile lateral displacement in function of depth obtained with the study model and with the reference model of Kuo (2008) [39] for respectively 1, 100 and 10 000 loading cycles. The lateral displacement of the three beams is plotted. Because of the high embedded length ($\frac{L}{D} = 5.3$), the pile is expected to have a more flexible behaviour compared to the small pile ($\frac{L}{D} = 2.67$) of section 5.1.
At N=1, N=100 and N=10 000 cycles, the study model underestimates the pile lateral displacement. The underestimation of the displacement is coherent with the overestimation of the soil stiffness observed between the study model and Kuo (2008) [39] in subsection 5.2.2. As observed for the short pile, the displacement offset between the study model and Kuo (2008) is higher at mudline than at the pile tip. An increase of the offset is observed between the static phase ($N = 1$ cycle) and the cyclic results ($N = 100$ and $N = 10000$ cycles).
In overall, the results of the study model are in agreement with the results of the reference model of Kuo (2008) [39] for $L = 40$m. The study model is able to capture the behaviour of a more flexible pile.

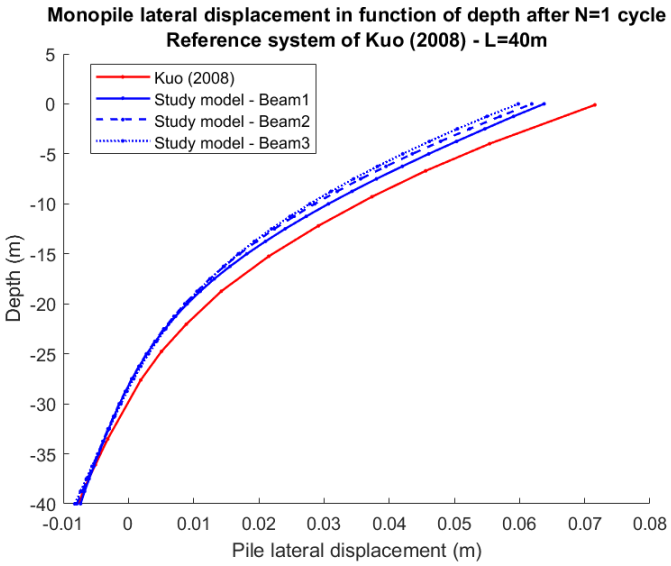

Figure 5.8: Lateral displacement of a monopile after N=1 cycle for L=40m - Results comparison between the reference system of Kuo (2008) [39] and the study model

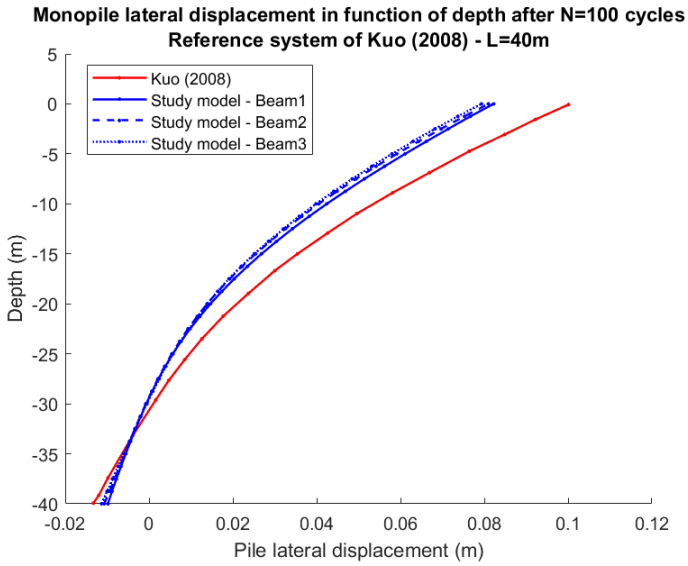

Figure 5.9: Lateral displacement of a monopile after N=100 cycles for L=40m - Results comparison between the reference system of Kuo (2008) [39] and the study model

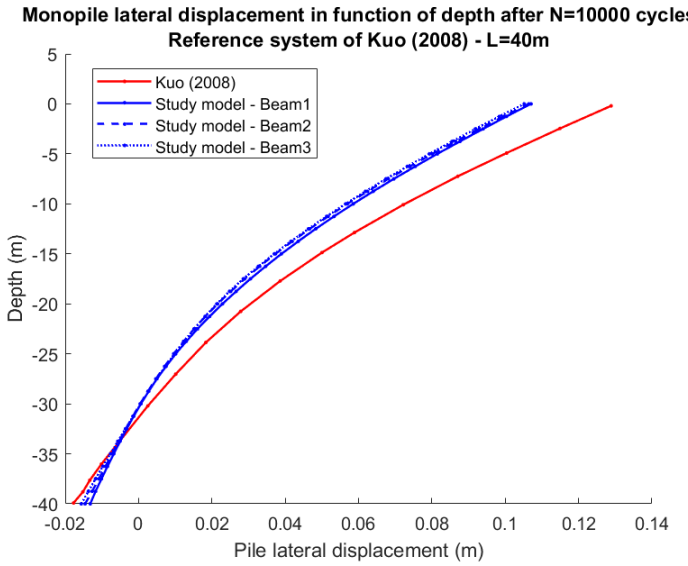

Figure 5.10: Lateral displacement of a monopile after N=10 000 cycles for L=40m - Results comparison between the reference system of Kuo (2008) [39] and the study model

5.3 Interpretation

The observations of section 5.1 and section 5.2 have been summarized. Possible causes are presented:

1. **The stresses at phase 0 and phase 1 are identical in the study model and Kuo (2008) [39]. However, the stiffness of the study model is higher than in the reference model of Kuo (2008) [39].**
   The difference of stiffness between Kuo (2008) [39] and the study model can be explained by differences in the method to calculate the stiffness and in the soil constitutive model. This topic will be discussed in subsection 5.3.1.

2. **The study model underestimates the pile lateral displacement compared to Kuo (2008) [39].**
   The underestimation of the pile displacement is coherent with the overestimation of the soil stiffness. The difference of the pile models between Kuo (2008) and the study model (subsection 4.3.1) could

be responsible for differences in the pile lateral displacement. This topic will be discussed in subsection 5.3.2. Moreover, using stiff beams for measuring the pile lateral displacement could also be responsible for the stiffer response of the pile-soil system. Thus, the impact of the beam stiffness on the pile deflection shape will be investigated in subsection 5.3.3. The study model uses a coarse mesh (section 4.4). The mesh coarseness factor could be responsible for the difference of results between the two models. Thus, the impact of the mesh refinement will be investigated in subsection 5.3.4.

3. **The offset between the lateral displacement of the study model and Kuo (2008) [39] is higher at mudline than at the pile tip. The offset increases between the static phase and the cyclic phase.**
   The stiffness degradation is more extended at mudline than at the pile tip (subsection 5.1.1, subsection 5.2.2). In the study model, the stiffness is averaged over the clusters. This procedure is not as precise as the original SDM which degrades the stiffness at every stress point. Thus, the cluster layout could be responsible for the difference of offset. As stated previously, the study model overestimates the stiffness during the static phase (N=1 cycle). The stiffness overestimation from the static phase adds up with the smoothing effect of the stiffness degradation in the clusters. This effect could explain the increase of the offset between the static and the cyclic phases.
   The difference of contact friction angle at the bottom interface (subsection 4.3.2) between Kuo (2008) and the study model could also explain the difference of offset between mudline and the pile tip. The impact of the bottom interface on the pile lateral displacement will be investigated in subsection 5.3.6.

4. **In overall, the results of the study model for the long pile ($L = 40$m) are closer to the results of Kuo (2008) [39] than for the short pile ($L = 20$m).**
   The same clusters layout was used for the two reference systems. For the same applied loads V and H, the stress level close to the pile for a pile-system with an embedded length $L = 20$m is higher than for $L = 40$m as the pile with $L = 20$m opposes less resistance to the soil than the pile with $L = 40$m. Averaging the degraded stiffness over the clusters causes a loss in accuracy. Thus, for $L = 20$m, the clusters would require more refinement close to the pile. The impact of the cluster layout refinement will be investigated in subsection 5.3.5.

In the next sections, the possible causes for the above observations will be investigated and discussed. The studies are performed on the reference system with the short pile ($L = 20$m) as this system needs more refinement and requires less computation times. Only the lateral displacement of the beam1 (Figure 4.4) will be plotted as it provides the closest results to Kuo (2008) [39].

5.3.1 Soil model

The method for modelling the linear elastic material with Mohr-Coulomb failure criterion and stress-dependent stiffness of the SDM is different in the study model and Kuo (2008) [39]. Whereas the study model uses the Mohr-Coulomb constitutive model with soil layers, the SDM of Kuo (2008) [39] uses a user-defined material (UMAT) (section 4.2).
subsection 5.2.1 proves that the two models have the same stresses at phase 0 and phase 1. However, the resulting stress-dependent stiffness (Equation 3.10) is different between the two models. Thus, the model of Kuo (2008) [39] calculate the stiffness differently than in the study model. There are several hypothesis for the model of Kuo (2008) [39]: different calculation of the mean principal stress σ_{mean} (Equation 3.10) and update of the stiffness between the SDM phases.
To the author's knowledge, the details of the user-defined constitutive soil model of the original SDM are not available. Thus, a thorough comparison of the constitutive models is not possible in this research and only assumptions can be made about the possible causes of difference in the stiffness calculation.

5.3.2 Pile model

As presented in subsection 4.3.1, the study model and the SDM of Kuo (2008) [39] do not use the same pile model. Whereas the study model has a hollow pile created with plates and filled with a soil plug, the pile of Kuo (2008) [39] is an equivalent solid pile which unit weight is the average of the unit weight of the plates and the soil plug and which stiffness is the equivalent stiffness of the hollow pile.
In the study model, three beams are attached to the pile and measure the lateral displacement at different locations along the pile diameter. By applying lateral loading at a specific location on the pile, the lateral

displacement will not be the same everywhere along the pile. This effects is called the ovalisation. With the beams, the study model accounts for ovalisation effects. Because the pile of Kuo (2008) [39] is an equivalent solid pile, it probably does not account for this effect.
The behaviour of the two piles is expected to be similar. However, the pile of the study model is more detailed compared to the pile of Kuo (2008) [39]. Those characteristics could cause some small differences in the pile lateral displacement.

5.3.3 Beam stiffness

In the study model, three beams measure the lateral displacement of the pile. The impact of the beam stiffness on the pile deflection shape has been investigated on the reference system with the short pile ($L = 20$m). Two types of beams are studied: a stiff beam with stiffness $E_{stiff,beam} = \frac{E_p}{10}$ and a flexible beam with stiffness $E_{flex,beam} = \frac{E_p}{10^6}$.
Figure 5.11 and Figure 5.12 present the pile lateral displacement in function of depth for N=1, N=100 and N=10 000 cycles.
The flexible beam provides a softer pile response compared to the stiff beam which is coherent with their respective stiffness. However, as the pile deflection shapes of the soft and flexible beams overlap, the impact of the beam stiffness is not consired significant.

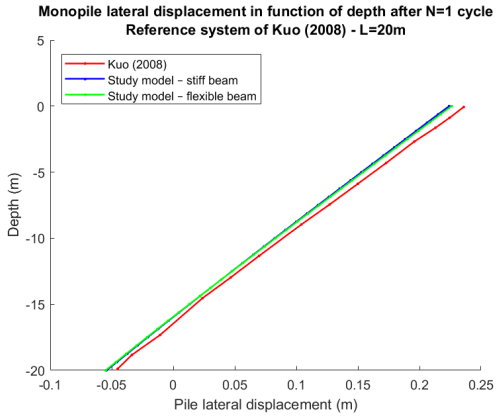

Figure 5.11: Lateral displacement of a monopile after N=1 cycle for L=20m - Results comparison between the reference system of Kuo (2008) [39] and the study model with stiff and flexible beams.

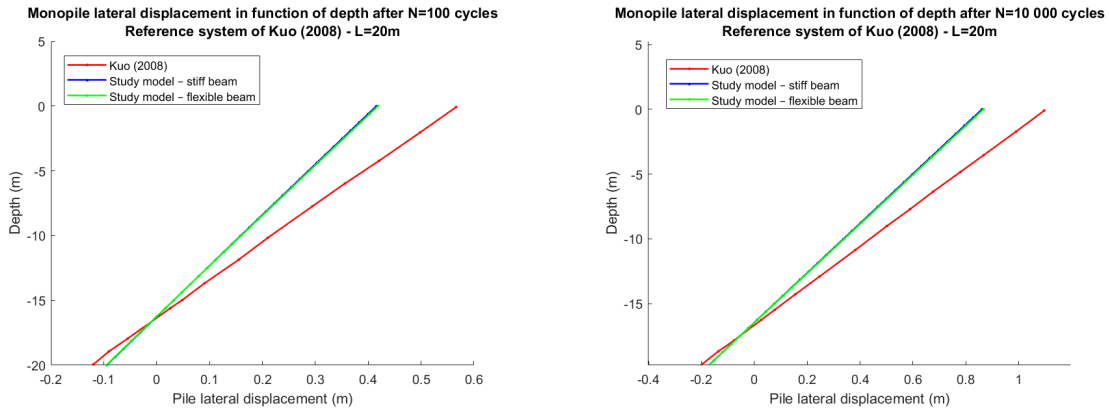

(a) N=100 cycles

(b) N=10 000 cycles

Figure 5.12: Lateral displacement of a monopile after N cycles for L=20m - Results comparison between the reference system of Kuo (2008) [39] and the study model with stiff and flexible beams.

5.3.4 Mesh refinement

In this section, the impact of the mesh refinement is studied. Figure 5.13 and Figure 5.14 present the pile lateral displacement after N=1, N=100 and N=10 000 cycles for two coarseness factors: coarse (0.075) and medium (0.050). Table 5.3 presents the number of elements in each model. Decreasing the coarseness factor increases the number of elements in the model which improves the accuracy of the results.

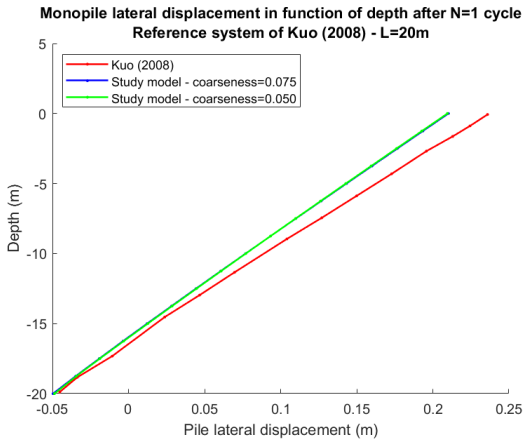

Figure 5.13: Lateral displacement of a monopile after N=1 cycle for L=20m - Results comparison between the reference system of Kuo (2008) [39] and the study model with two coarseness factors: 0.075 and 0.050

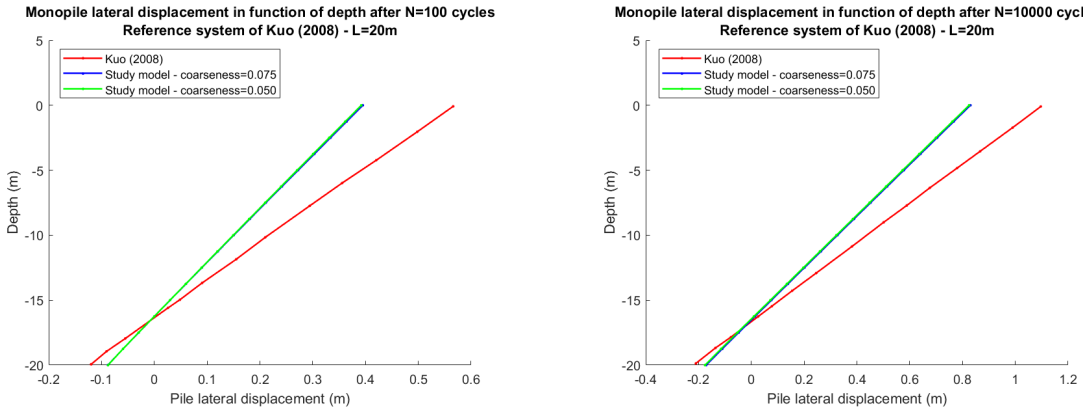

(a) N=100 cycles

(b) N=10 000 cycles

Figure 5.14: Lateral displacement of a monopile after N cycles for L=20m - Results comparison between the reference system of Kuo (2008) [39] and the study model with two coarseness factors: 0.075 and 0.05

Coarseness factor	Description	Number of elements	Number of nodes
0.075	Coarse	16258	24148
0.050	Medium	18212	27300

Table 5.3: Number of elements and nodes of the FE models for different coarseness factors

The pile deflection shapes of the medium and coarse factors (respectively 0.050 and 0.075) are very similar. The study model with the medium coarse mesh provides a slightly stiffer pile-soil response. Because the coarse mesh has less elements than the medium mesh, the computation times are smaller. Thus, the coarse mesh is recommended.

5.3.5 Cluster layout

In this section, the refinement of the cluster layout is investigated. First, the constant layer depth a, the cluster width b close to the pile and the number of clusters c per ring will be invidually refined. Finally, final recommendations about the cluster layout will be presented.

Constant layer depth a

The reference system with the short pile ($L = 20$m) had its contant layer depth a refined from 2.5 to 1.5m. Figure 5.15 and Figure 5.16 present the pile lateral displacement in function of depth for N=1, N=100 and N=10 000 cycles.
At N=1 cycle, refining the constant layer depth a provides results closer to Kuo (2008) [39]. The study model with the refined layer depth $a = 1.5$m has a pile deflection that is parallel to the pile deflection of Kuo (2008) [39]. Thus, the offset at mudline is the same as the offset at the pile tip. The lack of refinement of the constant layer depth a is thus responsible for the difference of offset between mudline and the pile tip at N=1 cycle.
At N=100 and N=10 000 cycles, refining the constant layer depth a provides results closer to Kuo (2008). However, there is still a significant difference of offset between the mudline and the pile tip.

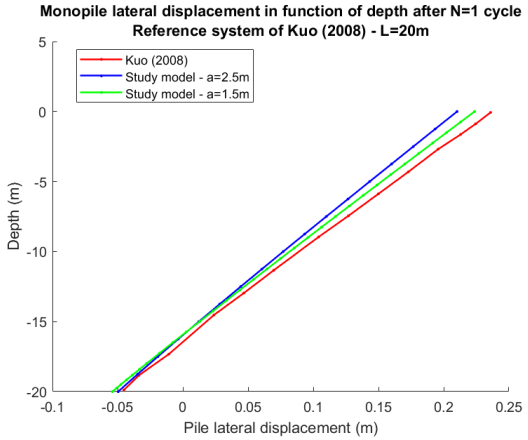

Figure 5.15: Lateral displacement of a monopile after N=1 cycle for L=20m - Results comparison between the reference system of Kuo (2008) [39] and the study model for two constant layer depths: $a = 2.5$m and $a = 1.5$m.

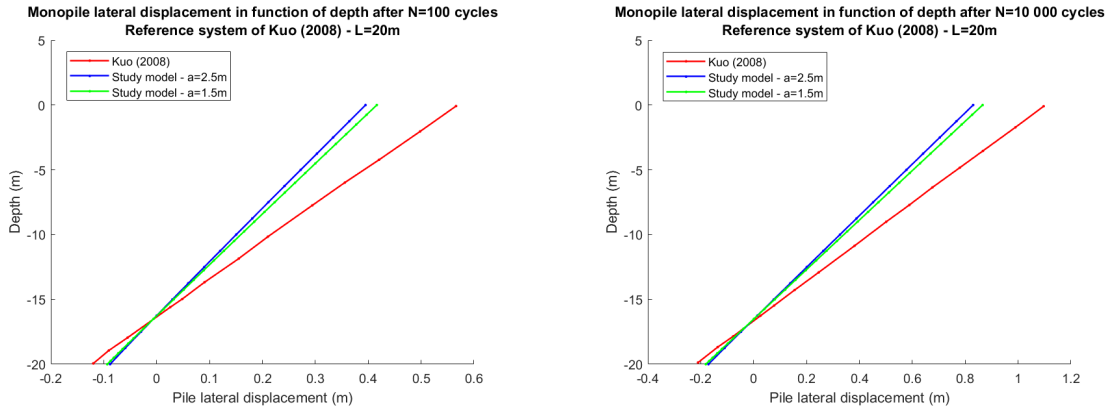

(a) N=100 cycles

(b) N=10 000 cycles

Figure 5.16: Lateral displacement of a monopile after N cycles for L=20m - Results comparison between the reference system of Kuo (2008) [39] and the study model for two constant layer depths: $a = 2.5$m and $a = 1.5$m.

Clusters width b close to the pile

The reference system with the short pile (L = 20m) had its cluster width b refined close to the pile from 2m to 1m for a distance of 6m around the pile.

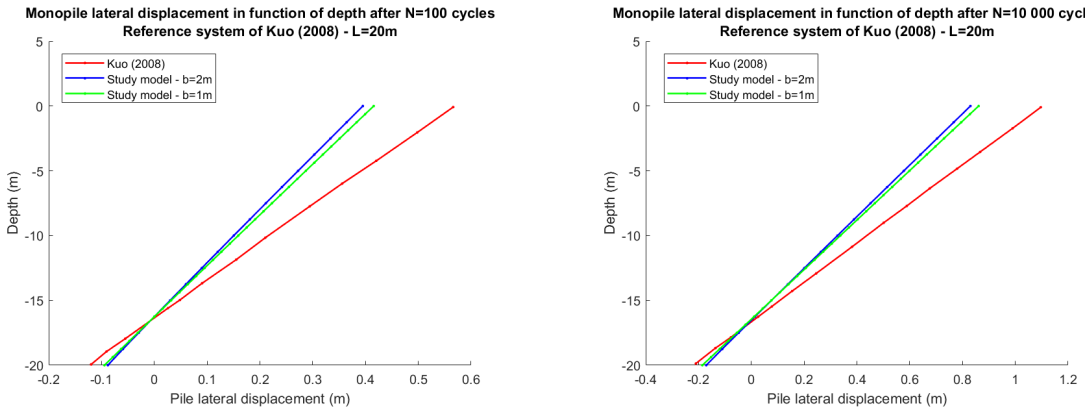

(a) N=100 cycles (b) N=10 000 cycles

Figure 5.17: Lateral displacement of a monopile after N cycles for L=20m - Results comparison between the reference system of Kuo (2008) [39] and the study model for two cluster width b close to the pile: b = 2m and b = 1m.

Figure 5.17 presents the pile lateral displacement in function of depth for two different cluster width b at N=100 cycles and N=10 000 cycles. Refining the clusters width b close to the pile decreases the displacement offset between the study model and the reference model of Kuo (2008) [39].

Number of clusters per ring c

The reference system with the short pile (L = 20m) had its number of clusters per ring c varied from 3 to 5. Figure 5.18 presents the pile lateral displacement in function of depth for three numbers of clusters per ring c at N=100 and N=10 000 cycles.
The study model with the highest number of clusters per ring c provides the closest results to Kuo (2008) [39]. Thus, increasing the numbers of clusters per ring c provides closer results to Kuo (2008) [39]. However, as the pile deflection shapes for the three numbers of clusters per ring c overlap each other, it can be concluded that varying c from 3 to 5 does not impact significantly the pile lateral displacement. Thus, the default value of c = 4 will be kept as recommendation.

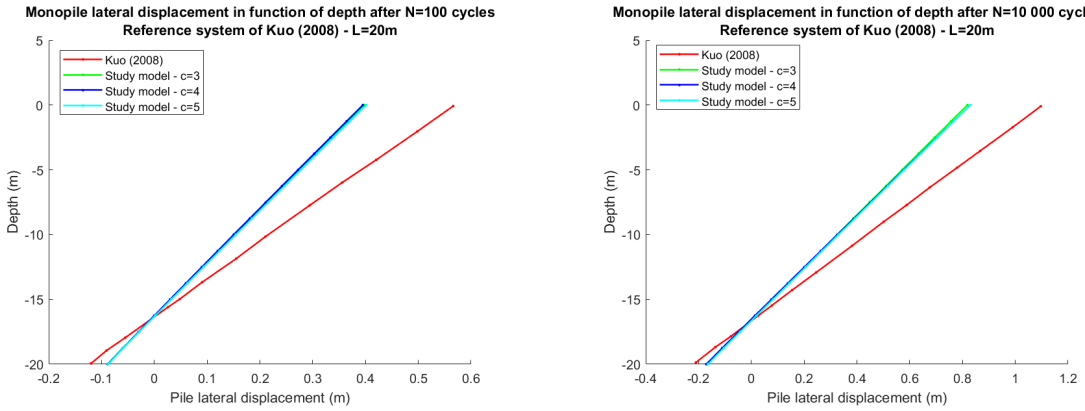

(a) N=100 cycles (b) N=10 000 cycles

Figure 5.18: Lateral displacement of a monopile after N cycles for L=20m - Results comparison between the reference system of Kuo (2008) [39] and the study model for three numbers of clusters per ring c: c = 3, c = 4 and c = 5.

Cluster layout recommendations

Table 5.4 summarizes the revised cluster layout for the two reference systems of Kuo (2008) [39]. Recommendations for the clusters layout have been created from Table 5.4. Table 5.5 presents the cluster layout recommendations for the study model.

	Revised cluster layout		
System	a (m)	b (m)	c (-)
L=20m	1.5	1	4
L=40m	2.5	2	4

Table 5.4: Revised cluster layout for the two reference systems of Kuo (2008) [39]

For two identical pile-soil systems with different embedded lengths L = 20m and L = 40m, the same cluster layout was used. The system with the highest embedded lenght L = 40m has the closest fit with Kuo (2008). Thus, the cluster layout of the short pile L = 20m was refined. Refining parameters a and b improved the results. Thus, parameters a and b are dependent on the pile embedded length L and they are normalized in function of L. However, as refining parameter c did not impact significantly the pile lateral displacement, parameter c is not sensitive to the variations of the embedded length L. It is advised to keep parameter $c = 4$ as it provides a reasonable coverage of the soil around the structure.

Cluster layout recommendation		
$\frac{a}{L} = 0.05$	$\frac{b}{L} = 0.05$	$c = 4$

Table 5.5: Recommendations for the cluster layout of the study model

5.3.6 Bottom interface

The impact of the interface located at the pile tip has been investigated on the reference system of the short pile (L = 20m). Figure 5.19 and Figure 5.20 present the pile lateral displacement in function of depth for the study model with and without the interface at the pile tip for N=1, N=100 and N=10 000 cycles.
The study model without bottom interface provides a significantly stiffer pile response compared to the study model with the bottom interface. Without bottom interface, there are no relative displacement between the monopile and the soil. The study model provides closer results to Kuo (2008) [39] if there is an interface at the pile tip.

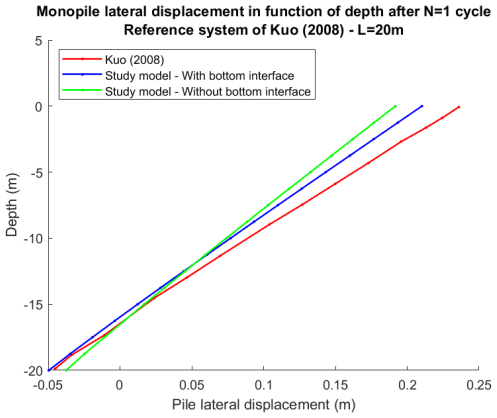

Figure 5.19: Lateral displacement of a monopile after N=1 cycle for L=20m - Results comparison between the reference system of Kuo (2008) [39] and the study model with and without interface at the pile tip

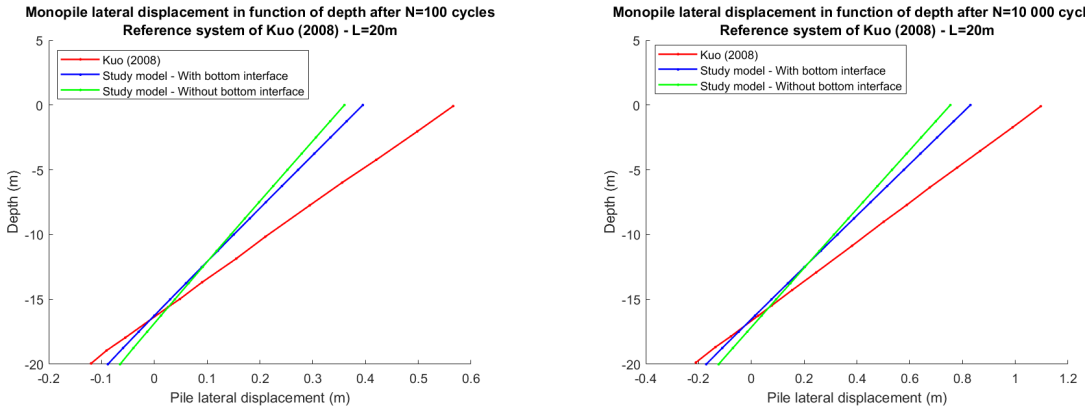

(a) N=100 cycles

(b) N=10 000 cycles

Figure 5.20: Lateral displacement of a monopile after N cycles for L=20m - Results comparison between the reference system of Kuo (2008) [39] and the study model with and without interface at the pile tip

5.4 Conclusion

In this chapter, the study model was verified by comparing results with the reference system of Kuo (2008) [39]. First, the stiffness degradation pattern of the study model was compared with the reference system of Kuo (2008) [39]. Afterwards, the pile lateral displacement after N loading cycles of the two models was compared. The study model and the reference system of Kuo (2008) [39] provide similar results for both short and long piles.
Based on the discussions and studies investigated in this chapter, the following interpretations were drawn:

1. **The stiffness of the study model is higher than in the reference model of Kuo (2008) [39]**.
   As the principal stresses at phase 0 and phase 1 are identical in the study model and in Kuo (2008) [39], the difference of stress-dependent stiffness should be caused by the stiffness calculation. More details about the user-defined material of the SDM are needed to conclude decisively on this interpretation.

2. **The study model underestimates the pile lateral displacement compared to Kuo (2008) [39].**
   The underestimation of the pile displacement is mainly caused by the overestimation of the soil stiffness. The difference of pile model and interfaces could have an impact on the pile-soil response, however it is expected to remain small. The impact of the beam stiffness on the pile lateral displacement can be neglected. A coarse mesh provides reasonable accuracy of the results and limited computation times.

3. **The offset between the lateral displacement of the study model and Kuo (2008) [39] is higher at mudline than at the pile tip. The offset increases between the static phase and the cyclic phase.**
   Because the stiffness is stress-dependent, it is smaller at mudline than at the pile tip. Thus, the stiffness overestimation has more impact at mudline than at the pile. Because of the stiffness overestimation, the displacement offset between the study model and Kuo (2008) [39] is higher at mudline than at the pile tip.
   The difference of offset between mudline and pile tip can be partly mitigated by refining the cluster layout. Refining the constant layer depth a and the cluster width b decreases the difference of offset between mudline and pile tip. However, this procedure cannot compensate for the effects of the stiffness overestimation. Refining the number of clusters per ring has a negligible impact.
   By averaging the degraded stiffness within the clusters, the stiffness is smoothed. The loss of accuracy created by the clustering adds up to the stiffness overestimation from the initial conditions. Thus, the offset difference increases from the static to the cyclic results.

4. **In overall, the results of the study model for the long pile ($L = 40$m) are closer to the results of Kuo (2008) [39] than for the short pile ($L = 20$m).**
   The overestimation of the soil stiffness plays a role in the difference of offsets between the short and the long pile. Because of its embedded length, the short pile opposes less resistance to the loading

compared to the long pile. Thus, the soil stiffness overestimation has more impact on the small pile ($\frac{L}{D} = 2.7$) than on the long pile ($\frac{L}{D} = 5.3$). The results of the study model will be closer to the SDM of Kuo (2008) [39] if the pile is long.
Refining the cluster layout of the short pile system ($L = 20$m) provides closer results to Kuo (2008) [39]. Cluster layout dimensions were recommended in this chapter.

Chapter 6

Validation of the study model

In this chapter, the study model is validated against three pile tests: Hettler (1981) [29], Achmus et al. (2007) [1] and Li et al. (2015) [42].
Kuo (2008) [39] validated the SDM against the pile tests of Hettler (1981) [29] and Achmus et al. (2007) [1]. Thus, the results of the study model will also be compared with the numerical results of Kuo (2008) [39]. Then, the impact of parameters b_1 and b_2 will be studied based on the pile test of Achmus et al. (2007) [1]. Finally, the pile test of Li et al. (2015) [42] will be verified with the study model.

6.1 Pile test of Hettler (1981)

For validating the SDM, Kuo (2008) [39] verified the numerical model with the pile test of Hettler (1981) [29]. In this section, the pile test settings are presented. Then, the results of the study model are compared with the pile test data of Hettler (1981) [29] and the numerical results of Kuo (2008) [39].

6.1.1 Pile test settings

The 1-g experiment of Hettler (1981) [29] consists of a slender pile in a cylindrical soil sample of 0.5m depth and 0.85m width. The slender pile is embedded in the soil with a length $L = 0.185$m and has a diameter $D = 0.0259$m ($\frac{L}{D} = 7.1$). The soil consists of dry Karlsruhe dense sand. The load is applied at mudline on the pile head. Thus, the experiment does not account for any load eccentricity. Up to 10^4 loading cycles were applied on the pile head with a constant force amplitude. The three loading cases H/H_u of Hettler (1981) [29] were defined based on test results. Figure 6.1 and Table 6.1 present the test settings and model parameters. The numerical FE model is described in Appendix D.
Kuo (2008) [39] back-calculated the pile test of Hettler (1981) [29] and determined the SDM model parameters that would provide the best fit with the cumulated lateral displacement of the pile measured during the experiment: $b1 = 0.12$ and $b2 = 0.32$ (subsection 3.3.2).

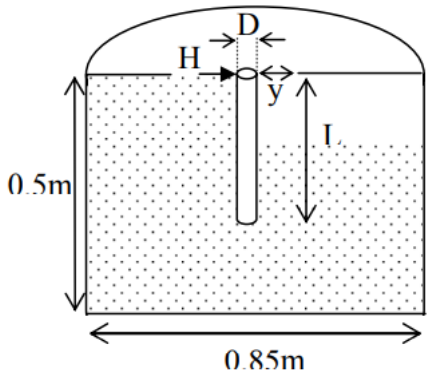

Figure 6.1: Pile test settings of Hettler (1981) [29], after Kuo (2008) [39]

Numerical model parameters of the pile test of Hettler (1981)					
Soil		Pile		Loading	
γ (kN/m^3)	16.9	D (m)	0.0259	H (N)	66%H_u,36%H_u, 24%H_u
ϕ (°)	42	L (m)	0.185		
ψ (°)	12.5	h (m)	0		
c	0.1	t_p (m)	0.003		
ν	0.16	E_p (kPa)	1.5E8		
κ	350	ν_p	0.16		
λ	0.65	w_p (kN/m^3)	68		
b_1	0.12				
b_2	0.32				

Table 6.1: Input parameters of the numerical model Hettler (1981) [29], after Kuo (2008) [39]

6.1.2 Results comparison

The pile test of Hettler (1981) [29] was back-calculated with the study model. The numerical and experimental results are then compared in Figure 6.2. The study model provides good agreement with the results of Hettler (1981) [29] and Kuo (2008) [39].
The study model slightly underestimates the pile head lateral displacement compared to Kuo (2008) [39]. Those observations are coherent with the results of chapter 5.
For the loads $H = 36\%H_u$ and $H = 24\%H_u$, the study model provides a better fit with the test results than Kuo (2008) [39]. For the loads $H = 36\%H_u$ and $H = 24\%H_u$, the numerical results of Kuo (2008) [39] overestimate the pile head displacement. As the study model underestimates slightly the pile lateral displacement compared to the SDM of Kuo (2008), the study model is closer to the test results.

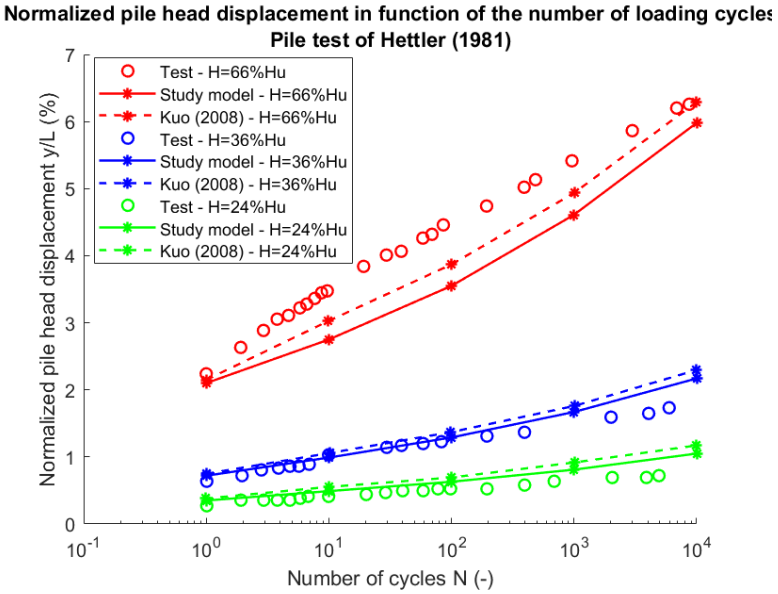

Figure 6.2: Normalized pile head displacement of a monopile after N loading cycles under constant cyclic lateral loading: $H = 66\%H_u$, $H = 36\%H_u$ and $H = 24\%H_u$ - Comparison of the results of Hettler (1981) [29], study model and Kuo (2008) [39]

6.2 Pile test of Achmus et al. (2007)

The SDM of Kuo (2008) [39] was verified against the pile test data of Achmus et al. (2007) [1]. In this section, the pile test settings are presented. Then, the results of the study model are compared with the pile tests data of Achmus et al. (2007) [1] and the numerical results of Kuo (2008) [39]. Finally, the impact of parameters b_1 and b_2 on the pile lateral displacement is investigated with the pile test settings of Achmus et al. (2007) [1].

6.2.1 Pile test settings

The 1-g experiment of Achmus et al. (2007) [1] consists of a rigid pile in a cylindrical soil sample of 0.78m depth and 0.6m width. The rigid pile is embedded in the soil with a length L = 0.2m and has a diameter D = 0.06m ($\frac{L}{D}$ = 3.3). The soil consists of dense sand. The load is applied with a load eccentricity h = 0.24m. The lateral diplacement is measured at the pile head at 0.33m above mudline. Up to 10^4 loading cycles were applied on the pile head with a constant force amplitude. The ultimate resistance H_u is determined from lab tests. $H_u = 40N$ is defined as the lateral loading that creates a lateral displacement above 10% of the embedded length. Figure 6.3 and Table 6.2 present the test settings and model parameters. Appendix D presents the numerical FE model.

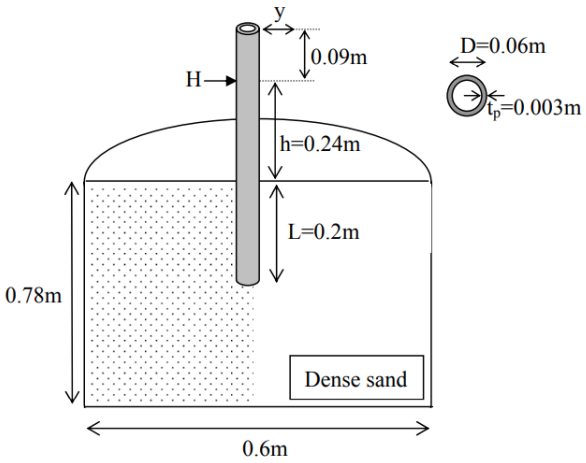

Figure 6.3: Pile test settings of Achmus et al. (2007) [1], after Kuo (2008) [39]

Numerical model parameters of the pile test of Achmus et al. (2007)					
Soil		Pile		Loading	
γ (kN/m^3)	19	D (m)	0.06	H (N)	40%H_u,10%H_u
ϕ (°)	37.5	L (m)	0.2		
ψ (°)	7.5	h (m)	0.24		
c	0.1	t_p (m)	0.003		
ν	0.25	E_p (kPa)	2.1E8		
κ	300	ν_p	0.25		
λ	0.65	w_p (kN/m^3)	78		
b_1	0.12				
b_2	0.5				

Table 6.2: Input parameters of the numerical model of Achmus et al. (2007) [1], after Kuo, 2008 [39]

6.2.2 Results comparison

The numerical and experimental results are compared in Figure 6.4. The study model provides good agreement with the results of Achmus et al. (2007) [1] and Kuo (2008) [39].
The study model slightly underestimates the pile head lateral displacement compared to Kuo (2008) [39]. Those observations are coherent with the observations of chapter 5.
For the loads $H = 40\%H_u$ and $H = 10\%H_u$, the study model provides a closer fit with the test results than Kuo (2008) [39]. As explained in subsection 6.1.2, this observation is caused by the slight overestimation of lateral displacement that Kuo (2008) provides with the SDM. As the study model slightly underestimates the lateral displacement compared to Kuo (2008), the study model is closer to the test results.

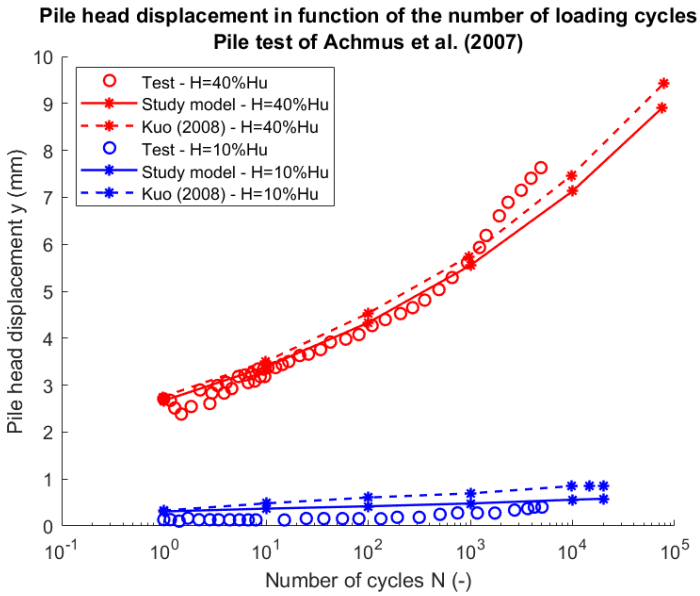

Figure 6.4: Pile head displacement of a monopile after N loading cycles under constant cyclic lateral loading $H = 40\%H_u$ and $H = 10\%H_u$- Comparison of the results of Achmus et al. (2007) [1], study model and Kuo (2008) [39]

6.2.3 Impact of parameters b_1 and b_2

The impact of parameters b_1 and b_2 on the pile head lateral displacement is assessed on the pile test of Achmus et al. (2007) [1] for the load case $H = 40\%H_u$. Table 6.3 presents the variability of b_1 and b_2.

Parameter study on b_1 and b_2		
Case	b_2	b_1
Case 1	0.5	0.08, 0.12, 0.16
Case 2	0.05, 0.5, 5	0.12

Table 6.3: Model parameters b_1 and b_2 of the sensitivity study

Figure 6.5 presents the pile head displacement in function of the number of cycles for varying b_1 values. Increasing b_1 has an important impact of the pile head lateral displacement. At N=10000 cycles, the lateral displacement doubles from $b_1 = 0.08$ to $b_1 = 0.16$.

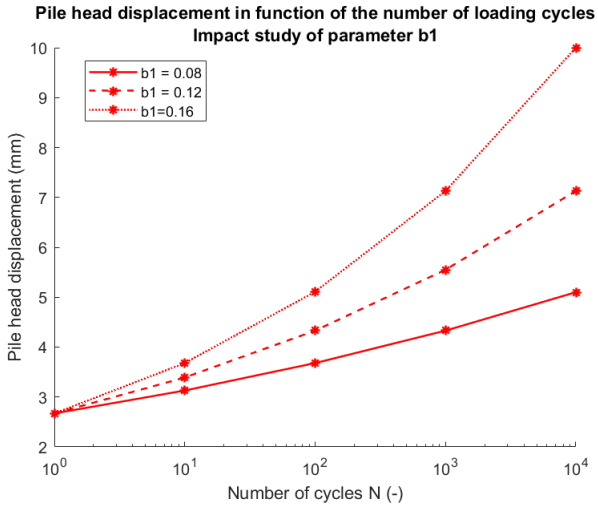

Figure 6.5: Pile head displacement of a monopile after N loading cycles under constant cyclic lateral loading $H = 40\%H_u$- b_2 is kept constant and b_1 is set to respectively 0.08, 0.12 and 0.16

Figure 6.6 presents the pile head displacement in function of the number of cycles for varying b_2 values. Increasing b_2 decreases the pile head lateral displacement. However, the decrease of displacement is very small.

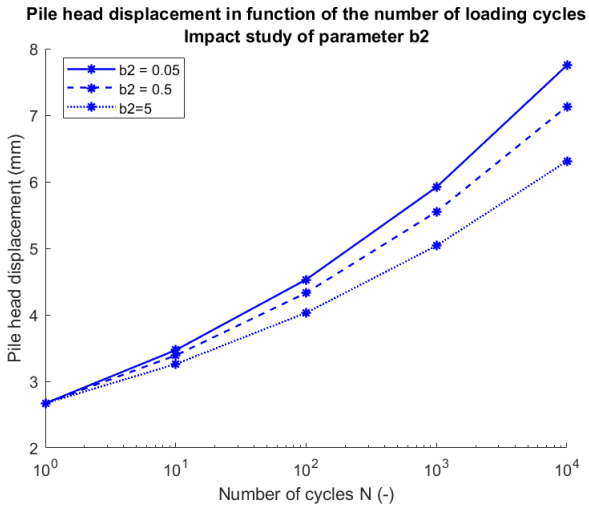

Figure 6.6: Pile head displacement of a monopile after N loading cycles under constant cyclic lateral loading $H = 40\%H_u$- b_1 is kept constant and b_2 is set to respectively 0.05, 0.5 and 5

The parameter study shows that for an identical system, parameters b_1 and b_2 have an important impact on the pile lateral displacement, especially parameter b_1.
According to Kuo (2008) [39], b_1 depends on high cyclic stress level whereas b_2 depends on low cyclic stress level. As high cyclic stress levels are more likely to create cumulated displacement, b_1 has a higher impact on the cumulated displacement at mudline than b_2.
The sensitivity study confirms the decisive impact of parameters b_1 and b_2 on the estimation of the pile lateral displacement.

6.3 Pile test of Li et. al (2015)

The pile test of Li et al. (2015) [42] was back-calculated with the study model. In this section, the pile test settings are presented. Then, the results of the study model are compared with the test results of Li et al. (2015) [42].

6.3.1 Pile test settings

The 1-g experiment of Li et al. (2015) [42] consists of a pile in over-consolidated dense uniform sands that are considered similar to dense sands in the North Sea. The site is located in Ireland, at Blessington, Co. Wicklow (Li et al., 2015 [42]). In contrary to the pile tests of Hettler (1981) [29] and Achmus et al. (2007) [1], the pile test of Li et al. (2015) [42] is carried out on non-disturbed sands and is thus more representative of real soil conditions.
The pile is embedded in the soil with a length $L = 2.2$m and has a diameter $D = 0.34$m ($\frac{L}{D} = 6.47$). The load is applied with a load eccentricity $h = 0.40$m. The lateral pile displacement is measured at mudline. Up to 1000 cycles were applied on the pile head with a constant loading amplitude. The ultimate resistance H_u is determined with monotonic pile tests presented in section 6.3.2. Figure 6.7 presents the test settings. Table 6.4 and Table 6.5 present the soil, pile and loading conditions. The numerical FE model is described in Appendix D.
The soil input parameters of the study model have been determined by Yang et al. (2018) [74] based on CPT tests and correlations. The soil consists of multi-layered dense sands with homogeneous parameters over depth.

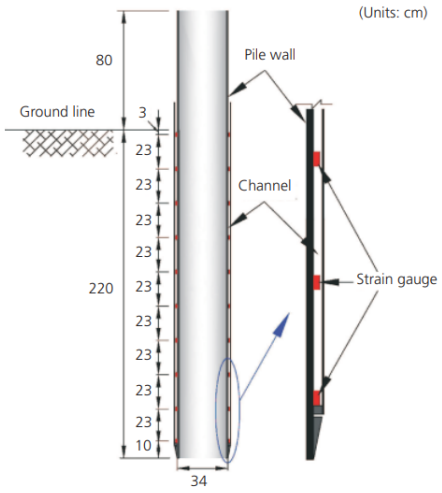

Figure 6.7: Pile test settings of Li et al. (2015) [42]

Numerical model parameters of the pile test of Li et al. (2015) [42]						
Soil						
Layer No.	γ (kN/m^3)	ϕ (°)	ψ (°)	c	ν	E_s (kPa)
1	20	55,5	23,1	1	0,2	26500
2	20	52,5	19,4	1	0,2	39800
3	20	49,5	15,6	1	0,2	45000
4	20	47,3	12,8	1	0,2	47000

Table 6.4: Input parameters of the numerical model of Li et al. (2015) [42], after Yang et al. (2018) [74] - Soil parameters

Numerical model parameters of the pile test of Li et al. (2015) [42]			
Pile		**Loading**	
D (m)	0.34	H (kN)	30% Hu
L (m)	2.2		
h (m)	0.4		
t_p (m)	0.08		
E_p (kPa)	2,10E+08		
ν_p	0.3		
w_p (kN/m^3)	68.5		

Table 6.5: Input parameters of the numerical model of Li et al. (2015) [42], after Yang et al. (2018) [74] - Pile and loading parameters

6.3.2 Results comparison

First, the monotonic test PC2 for different loading amplitude was calculated with the study model. Then, the cyclic test PC2 - LA1 was verified.

Monotonic pile test

Figure 6.8 presents the results of the monotonic pile test PC2 and the numerical results of the study model. In overall, the study model provides results in agreement with the monotonic results of Li et al. (2015) [42]. However, from 60kN to 100kN, the study model overestimates the pile lateral displacement. As the cyclic pile test PC2 - LA1 has a loading amplitude of 33 kN and the numerical results of the study model match with the test result at this amplitude, the cyclic analysis can be realised.

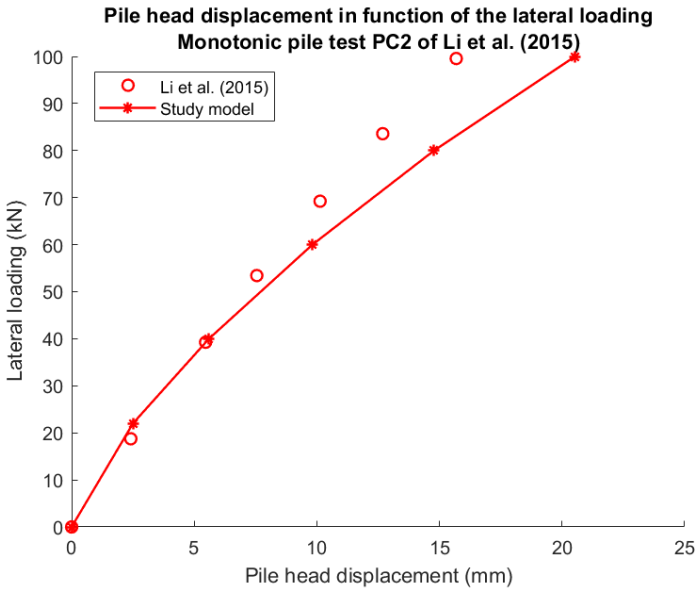

Figure 6.8: Pile head displacement of a monopile in function of the monotonic lateral loading - Comparison of the results of Li et al. (2015) [42] and the study model

Cyclic pile test

The pile test PC2 LA1 was back-calculated with the study model. Figure 6.9 presents the results of the pile tests and the numerical results of the study model.

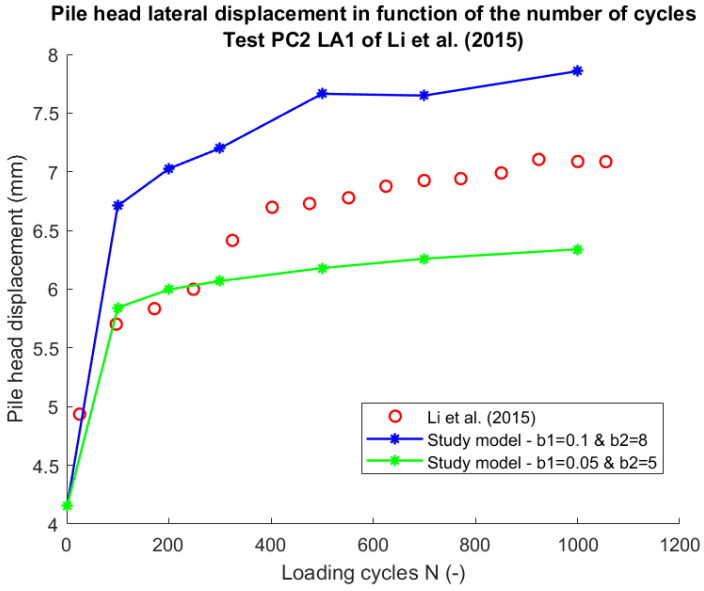

Figure 6.9: Pile head displacement of a monopile after N loading cycles under constant cyclic lateral loading $H = 30\%H_u$ - Comparison of the results of Li et al. (2015) [42] and the study model for two sets of parameters: $b_1 = 0.1$, $b_2 = 8$ and $b_1 = 0.05$, $b_2 = 5$

To the author's knowledge, no cyclic triaxial test in compression was performed on the soil of Li et al. (2015) [42]. Thus, parameters b_1 and b_2 were calibrated differently. The same method as Kuo (2008) for the pile test of Hettler (1981) [29] was used (subsection 3.3.2): parameters b_1 and b_2 were calibrated on the cyclic pile test of Li et al. (2015) [42].
An upper and lower bound of the pile head displacement is obtained with the test data. The parameter set $b_1 = 0.1$ and $b_2 = 8$ provides the upper bound and the parameter set $b_1 = 0.05$ and $b_2 = 5$ provides the lower bound.

The study model provides results in agreement with the pile test of Li et al. (2015) [42]. Verifying the study model with the pile test of Li et al. (2015) [42] confirmed the capacity of the study model to estimate the pile lateral displacement under cyclic loading for non-disturbed homogeneous and multi-layered sand.

6.4 Discussion about 1-g experiments

The three pile tests of Hettler (1981) [29], Achmus et al. (2007) [1] and Li et al. (2015) [42] are 1-g experiments. 1-g experiments are performed on reduced models in a laboratory or on natural soils. The stress distribution in the soil is not identical to full-scale condition. Scaling and thus comparing results with a real-size pile is therefore difficult (Klinkvort et al., 2012 [36]). The 1-g experiments are a very practical approach to assess the soil behaviour under cyclic loading as the whole pile-soil system can be created artificially and at lower costs. However, they only capture the behaviour of monopiles for small scale conditions.
There are two other types of pile experiments: the Ng experiments and the full scale testing.
Ng experiments are more representative of the large scale conditions. Ng experiments are performed on reduced models in a centrifuge facility. In a centrifuge, the gravitational forces are increased so that the soil stresses in the small-scale model are equivalent to the soil stresses of an offshore wind monopile. The centrifuge test is designed for representing the behaviour of a real size monopile by implementing a scaling procedure. The scaling procedure can be complex.
Full scale testing tends to reproduce the most accurately the pile behaviour. However they are very costly experiments (Klinkvort et al., 2012 [36]).
Validating the study model on Ng experiments or full scale testing would reinforce the validation procedure of this study and would bring more insights about the method ability to capture the behaviour of offshore wind monopiles under cyclic loading.
Appendix E summarizes the variability of the soil, pile and load parameters of the reference model and pile tests used for validating the study model.

6.5 Conclusion

In this chapter, the study model was validated over three pile tests. The study model proved to provide results in agreement with the SDM of Kuo (2008) [39] and three 1-g experiments. For some load cases, the study model showed a closer fit with the test data compared to Kuo (2008) [39].
A sensitivity study was carried out on parameters b_1 and b_2 of the SDM. Parameter b_1 has a determining impact on the pile head displacement whereas the impact of b_2 is less important. For two of the pile tests, no cyclic triaxial test in compression was available for calibrating the parameters b_1 and b_2. Thus, parameters b_1 and b_2 were calibrated on the test data with satisfying results.

Chapter 7

Design integration

As the study model was validated in the previous chapter, it can be integrated to a design framework. To do so, the study model is adapted to the input data available in the early-design procedure. Two models are adapted: a model for homogeneous soil and a model for multi-layered soil. The aim of this chapter is to compare the results of the study models with other cyclic methods.
First, the reference model of the design exercise is presented and the model adaptation to the design framework is explained. The cyclic methods of the design exercise will be presented and the results will be compared with the study models. Afterwards, the total rotation of the pile will be assessed based on the results of the two study models. Finally, parameters b_1 and b_2 from literature will be classified from the highest to the smallest estimate of pile lateral displacement. The 1D model will be calibrated with the highest estimate of the pile lateral displacement.

7.1 Reference system

In this section, the reference system is introduced.
At early design phase, limited soil data are available. The soil parameters are derived from CPT tests and correlations, exploratory boreholes and lab tests. In the reference model, the soil consists of layers of sand. The soil parameters are summarized in Table 7.1. For an offshore wind project, the soil data of the reference system are very homogeneous.
The pile dimensions are presented in Table 7.2. Table 7.3 presents the load case. The lateral loading corresponds to 100% of ULS loading.

	Soil input parameters								
	[m]	[m]	$[kN/m^3]$	[°]	[-]	[°]	[-]	[-]	$[kPa]$
Layer No.	zTop	zBot	γ'	ϕ'	c	ψ	ν	R_{inter}	E
1	0	1	6,54	41	0,1	11	0,26	0,67	39600
2	1	2,6	8,29	42	0,1	12	0,25	0,67	68800
6	2,6	3,7	8,25	40	0,1	10	0,26	0,67	87200
4	3,7	5,2	9,79	43	0,1	13	0,24	0,67	100400
5	5,2	6,36	10,04	42	0,1	12	0,25	0,67	113600
6	6,36	8,56	10,03	38	0,1	8	0,28	0,67	119600
7	8,56	9,78	10,56	40	0,1	10	0,26	0,67	144400
8	9,78	10,84	10,38	41	0,1	11	0,26	0,67	165200
9	10,84	11,94	10,38	39	0,1	9	0,27	0,67	154400
10	11,94	15,84	11,34	41	0,1	11	0,26	0,67	192800
11	15,84	18,6	11,44	40	0,1	10	0,26	0,67	210400
12	18,6	22,7	10,93	38	0,1	8	0,28	0,67	205200
13	22,7	24,8	11,06	38	0,1	8	0,28	0,67	228800
14	24,8	29,88	10,69	36	0,1	6	0,29	0,67	222800
15	29,88	35,8	10,53	35	0,1	5	0,3	0,67	223200
16	35,8	41,82	10,8	35	0,1	5	0,3	0,67	248800
17	41,82	46,16	11,05	36	0,1	6	0,29	0,67	282800
18	46,16	50,66	10,7	31	0,1	1	0,2	0,8	268800

Table 7.1: Soil input parameters for the reference system (CPT data)

	Pile input parameters							
	Pile geometry					Pile parameters		
Model	D (m)	L (m)	h (m)	h/L	t_p (m)	E_p (kPa)	w_p (kN/m^3)	ν_p
Study model	9.5	28	55.2	2	0.08	2,10E+08	68.5	0.2

Table 7.2: Pile input parameters for the reference system

	Load input parameters		
Load case	H (MN)	M (MNm)	V (MN)
1	14.5	800	24.525

Table 7.3: Load input parameters for the reference system

7.2 Model adaptation to design framework

The Stiffness Degradation Method (SDM) of Achmus et al. (2009) [2] was developped for homogeneous dense sand (mono-layer soil). By validating the pile test of Li et al. (2015) [42] with the study model in section 6.3, the SDM is expected to be valid for homogeneous multi-layered dense sand. Two models have been developped for the design framework: a model for homogeneous soil and a model for multi-layered soil.

7.2.1 Homogeneous soil model

For the homogeneous soil model, the soil characteristics in Table 7.1 are averaged to obtain a single set of soil parameters. The stress-dependent stiffness of the SDM is calibrated on the CPT stiffness values like Figure 7.1. Table 7.4 presents the parameters of the homogeneous soil model for the reference model.

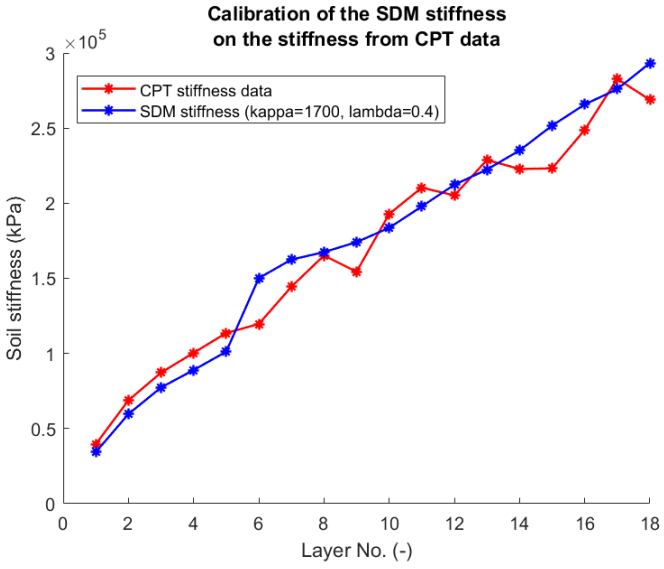

Figure 7.1: Calibration of the stiffness parameters κ and λ on the CPT stiffness

Soil input parameters							
γ' (kN/m^3)	ϕ (°)	c	ψ (°)	ν	R_{inter}	κ	λ
10,2	38,7	0,1	8,7	0,27	0,68	1700	0,4

Table 7.4: Soil input parameters of the homogeneous model

7.2.2 Multi-layered soil model

In reality, the soil is not homogeneous. CPT tests, exploratory boreholes and lab tests assess the soil properties for different depths. The test data allow the identification of soil layers. Table 7.1 presents the usual data available during the design phase. Therefore, the study model was adapted to correspond to the input parameters in Table 7.1. The following measures were applied to the study model:

- **Create soil layers according to Table 7.1**
  Stiffness parameters κ and λ are abandonned. Instead, the stiffness of Table 7.1 is used in the study model. Every soil layer is assigned top and bottom layer depths, soil effective unit weight γ', friction angle ϕ, dilatancy angle ψ, cohesion c, Poisson's ratio ν, interface coefficient R_{inter} and stiffness E_s.
- **Assign corresponding layer input parameters to the clusters**
  In the multi-layered soil model, the input parameters of every layer are assigned to the clusters located in the layer.

7.3 Comparison with current design practices

To assess the impact of the SDM on the cyclic design of offshore wind monopiles, the two study models are compared with existing methods that assess the cyclic behaviour of monopiles. First, three cyclic methods are presented: the codified procedure, the method of Dührkop (2009) [23] and the method of Garnier (2013) [27]. Then, the results of the cyclic methods for the reference system are compared with the results of the two study models.

7.3.1 Cyclic design practices

The results of the three cyclic methods were obtained as follows:

- **Static analysis with 3D FE model**
  First, the static analysis is calculated with PLAXIS 3D. The input parameters used for this exercise are the data of the reference system presented in section 7.1.
- **Calibration of the 1D model**
  The 1D model is calibrated with the results of the 3D FE model. The pile response of the 1D model is used as the reference pile deflection shape that is representative of the static analysis ($N = 1$ cycle).
- **Application of cyclic ratios**
  The cyclic deflection curves of the pile are obtained by calibrating the 1D model with cyclic ratios from the literature (DNVGL-ST-0126 [24]; Dührkop, 2009 [23]; Garnier, 2013 [27]).

Codified procedure

As presented in subsection 2.3.2, the codified procedure for the design of offshore wind monopiles under cyclic loading consists of cyclic p-y curves (API, 2011 [8], DNVGL-ST-0126 [24]). Equation 2.3 presents the standard equation of the cyclic p-y curves. This cyclic method does not account for the pile geometry and thus the more rigid behaviour of offshore wind monopiles. The cyclic p-y curves do not account either for the number of cycles N and the loading amplitude.

Dührkop (2009)

Based on 1-g pile tests and numerical simulations, Dührkop (2009) [23] reduced the first cyclic degradation factor A of the standard p-y curve in Equation 2.3. The experiments were carried out on almost rigid piles in sand under cyclic loading (Albiker et al., 2017 [4]). In Equation 2.3, the first cyclic degradation factor is reduced to:

$$A_{cycl} = r_a(3 - 1.143\frac{z}{D}) + 0.343\frac{z}{D} \leq 0.9 \tag{7.1}$$

Where r_a decreases from 0.3 to 0 for respectively $N = 10^2$ to $N = 10^5$ cycles, z is the depth and D is the pile diameter. With this method, the p-y curves account for the pile geometry with the pile diameter D and the embedded length L (depth z). The number of cycles N is accounted for by using the factor r_a. However, the

cyclic degradation factor of Dührkop (2009) [23] does not depend on the loading amplitude.
The cyclic degradation factor A_{cycl} is normalised with the static coefficient of the p-y curves (Equation 2.3):

$$A_{stat} = 3.0 - 0.8 - \frac{z}{D} \geq 0.9 \tag{7.2}$$

Where z is the depth and D is the pile diameter.
Figure 7.2 presents the normalised cyclic degradation factor A_{cycl}/A_{stat} in function of depth for the standard p-y curve and the approach of Dührkop (2009) [23] for $N = 10^2$, $N = 10^3$, $N = 10^4$ and $N = 10^5$ loading cycles. Dührkop (2009) [23] assumes that the cyclic p-y curves ($A_{cycl} = 0.9$) are valid for $N = 10^2$ cycles. Thus, at $N = 10^2$ cycles, the cyclic degradation factor of Dührkop (2009) [23] is identical to the factor of the codified procedure.

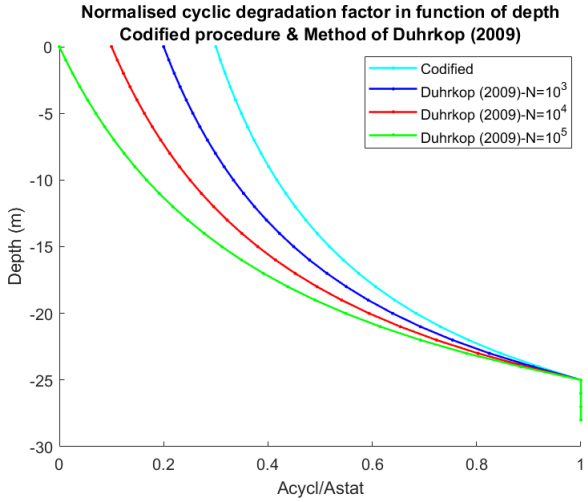

Figure 7.2: Normalised cyclic degradation factor A_{cycl}/A_{stat} in function of depth - Comparison of the cyclic coefficient of the codified procedure and the method of Dührkop (2009) [23] for $N = 10^2$, $N = 10^3$, $N = 10^4$ and $N = 10^5$ loading cycles

From mudline to $z = 2.625D$, the normalised cyclic degradation factor A_{cycl}/A_{stat} increases with depth. Then, from $z = 2.625D$ to the pile tip, the normalised cyclic degradation factor A_{cycl}/A_{stat} is equal to 1 and remains constant over depth.
From $N = 10^2$ to $N = 10^5$ cycles, the normalised cyclic degradation factor of Dührkop (2009) [23] decreases. In Equation 2.3, the decrease of the first cyclic degradation coefficient A_{cycl} decreases the soil resistance p. Thus, the pile lateral displacement increases with the number of cycles N.
With Equation 7.1, the reduction of the cyclic factor is only applied to the first factor A in Equation 2.3. The second factor A in the tanh function is the cyclic factor of the codified procedure ($A_{cycl} = 0.9$). Thus, the common recommendation is to use the representative load and the number of cycles that an OWT can experience (Dührkop, 2009 [23]).

Garnier (2013)

Garnier (2013) [27] developped cyclic degradation coefficients for p-y curves. The cyclic coefficients are based on centrifuge experimental data (section 6.4). The cyclic degradation coefficients are presented in Table 7.5. The method of Garnier (2013) [27] accounts for the pile geometry with the pile diameter D and the embbeded length L (depth z). The cyclic degradation coefficient r_c is also dependent of the number of cycles N and the loading amplitude H_{cycl}/H_{max}. The method of Garnier (2013) [27] is validated until 10^3 cycles.

Relative depth $\frac{z}{D}$	**Degradation coefficient** r_c
$0 < \frac{z}{D} < 1.5$	$r_c = 1 - (0.034 * ln(N) + 0.24 * H_{cycl}/H_{max})$
$1.5 < \frac{z}{D} < 3$	$r_c = 1 - (0.017 * ln(N) + 0.12 * H_{cycl}/H_{max})$
$3 < \frac{z}{D} < 5$	$r_c = 1 - (0.008 * ln(N) + 0.06 * H_{cycl}/H_{max})$
$\frac{z}{D} > 5$	$r_c = 1$

Table 7.5: Degradation coefficients r_c developped by Garnier (2013) [27]

Figure 7.3 presents the cyclic degradation coefficient in function of depth for $N = 10^2$, $N = 10^3$, $N = 10^4$ and $N = 10^5$ cycles. As the SDM corresponds to the loading conditions of $H_{cycl}/H_{max} = 0.5$, the cyclic coefficient r_c of Garnier (2013) [27] was determined accordingly. According to Garnier (2013) [27], this loading corresponds to the worst case scenario in one-way loading.
The degradation coefficient r_c of Garnier (2013) [27] is depth-dependent and varies from a depth range to another (Table 7.5). From mudline to $\frac{z}{D} > 1.5$, the degradation coefficient r_c is constant over depth. At $\frac{z}{D} = 1.5$, the degradation coefficient r_c reaches a new level and remains the same from $z = 1.5D$ to the pile embedded length L.
From 10^2 to 10^5 cycles, the degradation coefficient r_c decreases. Reducing the degradation coefficient r_c decreases the soil resistance. Thus, the pile lateral displacement increases with the number of cycles N.

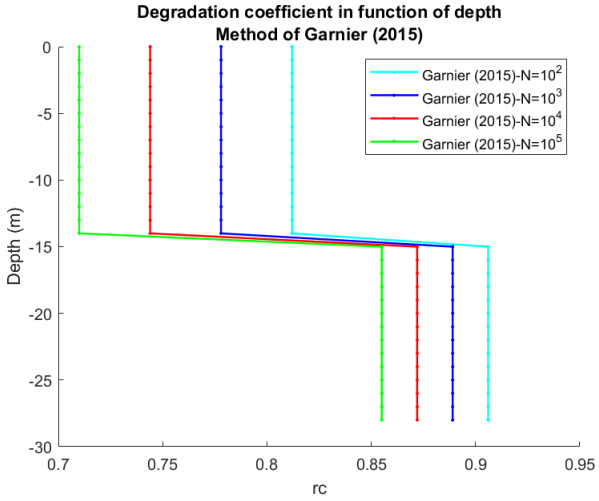

Figure 7.3: Cyclic degradation coefficient r_c in function of depth for $N = 10^3$, $N = 10^4$ and $N = 10^5$ cycles, based on the method of Garnier (2013) [27]

7.3.2 Static analysis

The results of the static analysis ($N = 1$) of the two study models and the 1D model are presented in Figure 7.4.

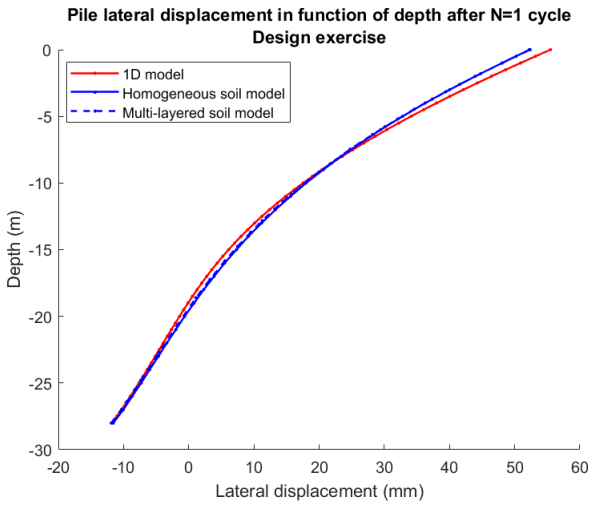

Figure 7.4: Lateral displacement of a monopile after N=1 cycle (design exercise) - Results comparison between the study models and the 1D model

The results of the multi-layered soil model are in agreement with the results of the homogeneous soil model. As the soil data used for this design exercise are very homogeneous, the parameters variation of the multi-

layered soil model does not impact significantly the pile-soil response. Moreover, on Figure 7.4, the results of the study models are in agreement with the results of the 1D model. Thus, the cyclic analysis can be realised.

7.3.3 Cyclic analysis

In this study, the homogeneous and multi-layered soil models use the average parameters $b_1 = 0.20$ and $b_2 = 5.76$ for dense sand (subsection 3.3.2).
Figure 7.5 and Figure 7.6 compare the pile deflection shapes of the study models with the results of the method of Garnier (2013) [27], the method of Dührkop (2009) [23] and the codified procedure for $N = 10^2$, $N = 10^3$ and $N = 10^4$ cycles.

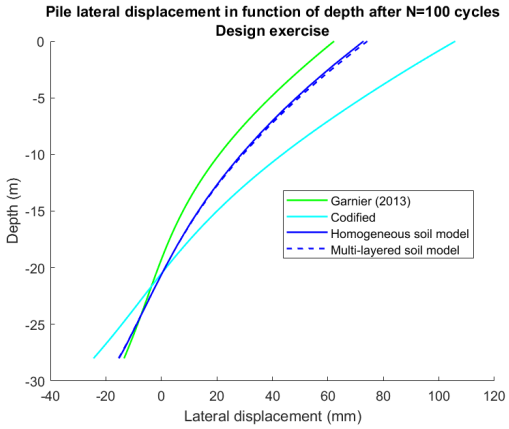

Figure 7.5: Lateral displacement of a monopile after $N = 10^2$ cycles (design exercise) - Results comparison between the study models and the method of Garnier (2013) [27], Dührkop (2009) [23] and the codified procedure

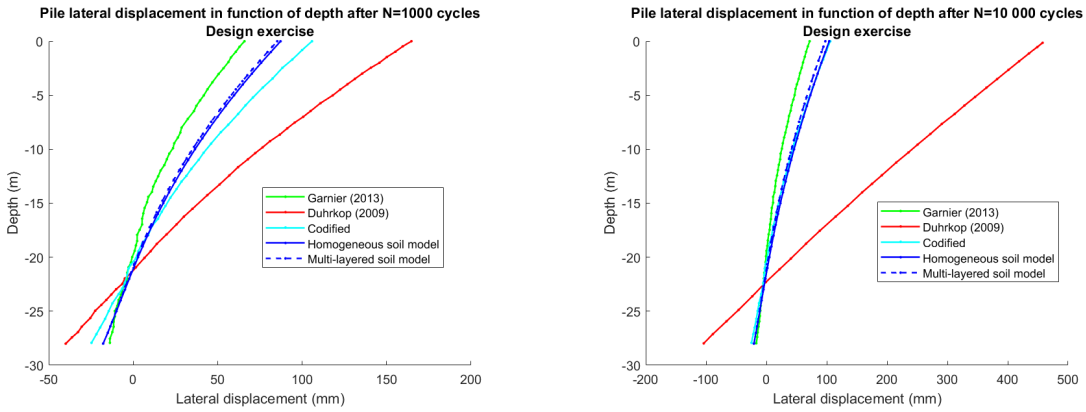

(a) $N = 10^3$ cycles (b) $N = 10^4$ cycles

Figure 7.6: Lateral displacement of a monopile after N cycles (design exercise) - Results comparison between the study models and the method of Garnier (2013) [27], Dührkop (2009) [23] and the codified procedure

The observations about Figure 7.5 and Figure 7.6 are summarized as follows:

- **Multi-layered and homogeneous soil models**
  For $N = 10^2$, $N = 10^3$ and $N = 10^4$ cycles, the results of the multi-layered soil model are in agreement with the results of the homogeneous soil model. They are in agreement because the soil data are very homogeneous.
  From $N = 10^2$ to $N = 10^4$ cycles, the offset between the pile deflections slightly increases. In the homogeneous soil model, the soil data are averaged to obtain a single set of soil parameters and the stiffness is calibrated on the CPT stiffness with a reasonable fit (subsection 7.2.1). This procedure is responsible

for the slight offset between the pile deflections of the two study models. As the fit between the CPT stiffness and the calibrated stiffness of the homogeneous soil model is not exact, the stiffness degradation procedure enhances the offset between the pile deflections of the two models.

- **Codified procedure**
  For $N = 10^2$ and $N = 10^3$ cycles, the study models provide smaller pile lateral deflections compared to the codified procedure. The pile lateral displacement of the codified procedure is reached by the study models at $N = 10^4$ cycles.
  The codified procedure does not account for the number of cycles, the loading amplitude and the geometry of the pile. Thus, the codified procedure is recommended for conditions that are representative of the loading spectrum. In the reference system, the loading $H = 14.5MN$ represents 100%ULS. Applying 10^4 times the load $H = 14.5MN$ is not representative of the loading spectrum of an OWT. The representative loading is expected to be much smaller. This observation proves the tendency of the codified procedure to overestimate significantly the pile lateral displacement.

- **Dührkop (2009) [23]**
  At $N = 10^2$ cycles, the pile deflection of Dührkop (2009) [23] is identical to the pile deflection of the codified procedure because the two methods use the same cyclic degradation factor (section 7.3.1).
  At $N = 10^3$ and $N = 10^4$ cycles, the pile deflection of Dührkop (2009) [23] increases with the number of cycles. The method provides the highest pile deflection of the design exercise.
  This observation is coherent with section 7.3.1. The method of Dührkop (2009) [23] reduces the cyclic coefficient of the codified procedure ($A_{cycl} = 0.9$). At $N = 10^2$ cycles, the codified procedure already provides a conservative estimation of the pile lateral displacement. As reducing the cyclic degradation factor decreases the soil resistance p, the pile lateral displacement increases. Thus, reducing the cyclic degradation factor of the codified procedure amplifies the displacement overestimation of the codified procedure.

- **Garnier (2013) [27]**
  For $N = 10^2$, $N = 10^3$ and $N = 10^4$ cycles, the method of Garnier (2013) [27] provides the smallest estimation of the pile lateral displacement. In overall, the results of the study models and Garnier (2013) [27] are in agreement. This result was expected as Garnier (2013) [27] and the study model account for the number of cycles, the loading amplitude and the pile geometry.
  Garnier (2013) [27] developped cyclic coefficients for p-y curves based on centrifuge pile tests. The testing piles had similar dimensions to offshore wind monopiles. Thus, the method of Garnier [27] is expected to provide more rigid pile response compared to methods based on slender piles like the codified procedure.

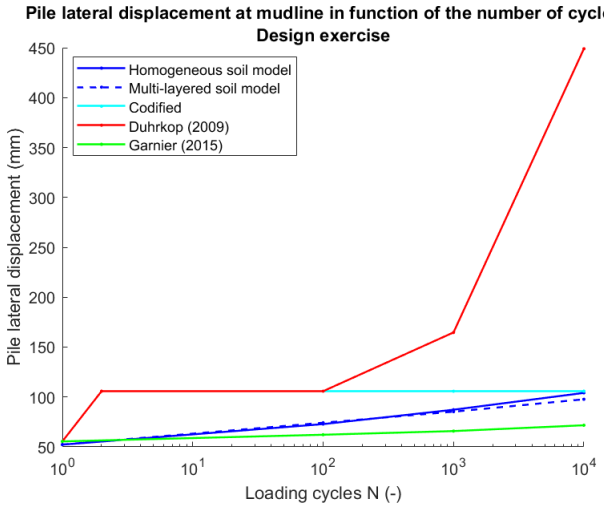

Figure 7.7: Pile lateral displacement at mudline after N cycles (design exercise) - Results comparison between the study models and the method of Garnier (2013) [27], Dührkop (2009) [23] and the codified procedure

Figure 7.7 presents the pile lateral displacement at mudline from 1 to 10^4 cycles. From $N = 1$ to $N = 10^3$ cycles, the results of the two study models are in agreement with Garnier (2013) [27]. At $N = 10^4$ cycles, the results of the study model are similar to the codified approach.
Whereas the method of Garnier (2013) [27] is calibrated on centrifuge pile tests, the two study models are validated on 1-g pile tests. Both methods account for the pile geometry, the loading amplitude and the number of cycles. The method of Garnier (2013) [27] holds until $N = 10^3$ cycles. Obtaining similar results for the method of Garnier (2013) [27] and the study model (SDM) from $N = 1$ to $N = 10^3$ cycles confirms the ability of the study model to model the rigid behaviour of offshore wind monopiles under lateral cyclic loading.

7.4 SLS assessment - Total rotation

In this section, the total rotation of the pile at mudline is calculated for the two study models. The Serviceability Limit State (SLS) is assessed by calculating the tilt at the pile head. The tolerance is 0.5°. Because the study model focuses on modelling the soil behaviour under cyclic loading, the pile above mudline and the load excentricity have for only purpose to represent the bending moment created by the load. Thus, in this study, the total rotation is calculated at mudline.
As observed in subsection 7.3.3, the pile response after cyclic loading is not perfectly rigid. Thus, below mudline, the pile experiences a curvature. The pile curvature does not allow the calculation of the total tilt with the embedded length L.
The total rotation will then be calculated with the following formula:

$$sin(\theta_N) = \frac{u_{z1} + u_{z3}}{D} \tag{7.3}$$

- **Vertical displacement at mudline of the side beams** $u_{z1} + u_{z3}$
  The vertical displacement u_z at mudline of the two side beams 1 and 3 is extracted.

- **Constant diameter** D
  By applying a load on the pile, the perfectly rounded shape of the pile tubular tends to flatten and the diameter is not constant. This effect is caused by the ovalisation. For this study, the pile is considered constant and no ovalisation is considered.

Figure 7.8 presents the total rotation of the pile after N cycles. The results of the homogeneous soil and multi-layered soil model are in agreement.
The tolerance for the SLS check is 0.5°. The two models provide a total rotation below 0.5°. The monopile passes successfully the SLS check. The study model is able to perform SLS check.

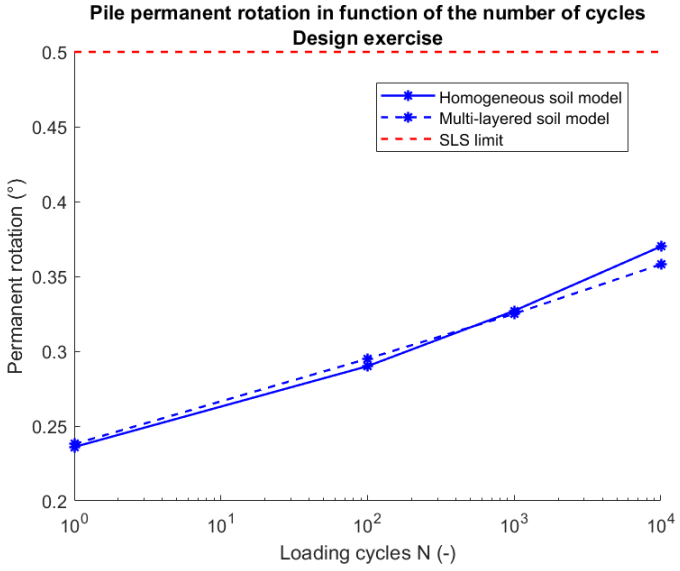

Figure 7.8: Total pile rotation after N cycles - Comparison between the homogeneous and multi-layered soil models

7.5 Calibration of the 1D model with the SDM

During the early-design phase, p-y curves remain the main tool for the design of offshore wind monopiles (subsection 2.3.2). As recommended by design standards (DNVGL-ST-0126 [24]), they must be calibrated on a 3D FE model. In this section, the possibility of calibrating the 1D model of section 7.3 with the SDM is investigated.
As the results of the homogeneous soil model and the multi-layered soil model are in agreement (section 7.3) and the multi-layered soil model corresponds to the early-design requirement, this study is investigated with the multi-layered soil model. The study is carried out for the parameters of the reference system presented in section 7.1.
A first study is carried out to determine the set of parameters b_1 and b_2 that provide the highest and most probable estimates of the pile lateral displacement. Afterwards, the 1D model is calibrated based on the selected pile deflection shapes.

7.5.1 Highest and most probable estimates

During the early-design phase of an OWT, cyclic triaxial tests data are generally not available. Thus, a calibration of the parameters b_1 and b_2 on cyclic triaxial test is not possible. This subsection aims to determine sets of parameters that provide a prompt estimation of the pile lateral displacement under cyclic loading.
In this study, the highest and most probable estimates of the pile lateral displacement are determined among different sets of parameters b_1 and b_2 for dense sand. Table 7.6 presents the sets of parameters that are investigated. This study focuses on five sets of parameters b_1 and b_2. Appendix F classifies the parameters sets b_1 and b_2 for dense sand that are available in the literature from the highest to the smallest estimate.

Set No.	b1 (-)	b2 (-)
1	0.12	0.32
2	0.12	0.5
3	0.1	8
4	0.05	5
5	0.20	5.76

Table 7.6: Sets of parameters b_1 and b_2 for determining the highest and most probable estimate of the pile lateral displacement of the reference system

In Table 7.6, the parameter sets 1, 2, 3, 4 and 5 correspond respectively to the parameters b_1 and b_2 of Hettler (1981) [29], Achmus et al. (2007) [1], the lowest and highest bounds of Li et al. (2015) [42] and the average parameters determined by Kuo (2008) [39] for dense sands (chapter 3, chapter 6).

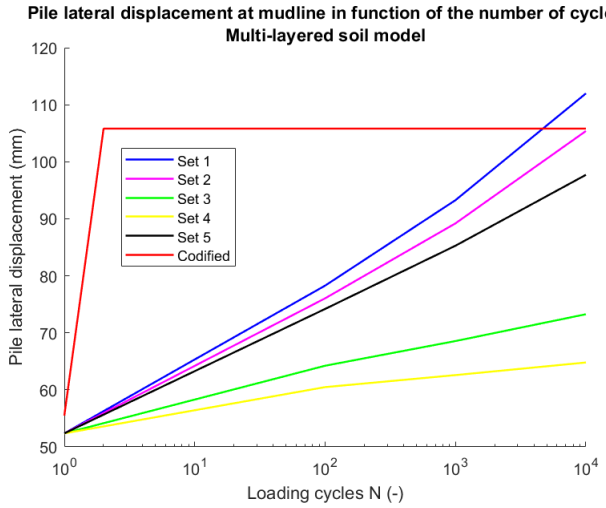

Figure 7.9: Pile lateral displacement at mudline in function of the number of cycles for 5 sets of parameters b_1 and b_2 obtained with the multi-layered soil model

Figure 7.9 presents the pile lateral displacement at mudline for the 5 sets of parameters b_1 and b_2. The pile lateral displacement at mudline of the codified procedure is plotted as reference. In overall, the SDM pile lateral displacements are smaller than the displacements of the codified procedure. At $N = 10^4$ cycles, the parameter set 1 provides a slightly higher estimate than the codified procedure.
The highest estimate of the pile lateral displacement at mudline is obtained with the parameter set 1. The most probable estimate of the pile lateral displacement at mudline is determined as the parameter set that provides the most centered estimation within the displacement range. In this study, parameter set 5 corresponds to the most probable estimation of the pile lateral displacement.

7.5.2 Calibration of the SDM results on the 1D model

The 1D model was calibrated with the pile lateral displacement at mudline for the SDM highest estimate (set 1). Figure 7.10 presents the calibrated curve for the highest estimate of the pile lateral displacement at mudline. The lateral displacement of the study model and the 1D model are in agreement.

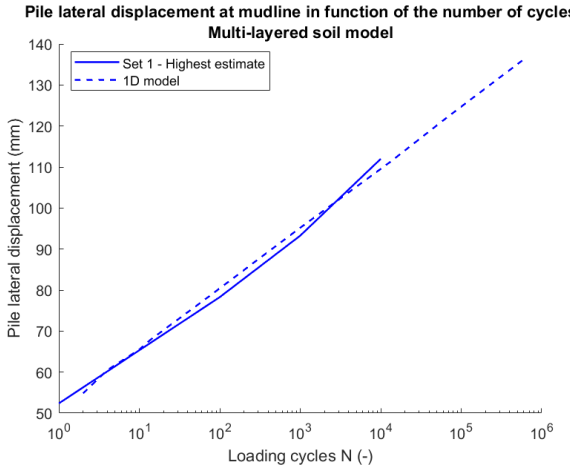

Figure 7.10: Pile lateral displacement at mudline in function of the number of cycles - Calibration of the 1D model on the highest estimate

Figure 7.11 presents the pile lateral displacement in function of depth at $N = 10^2$ and $N = 10^3$ cycles for the study model (highest and most probable estimates), the codified procedure and the calibrated 1D model.

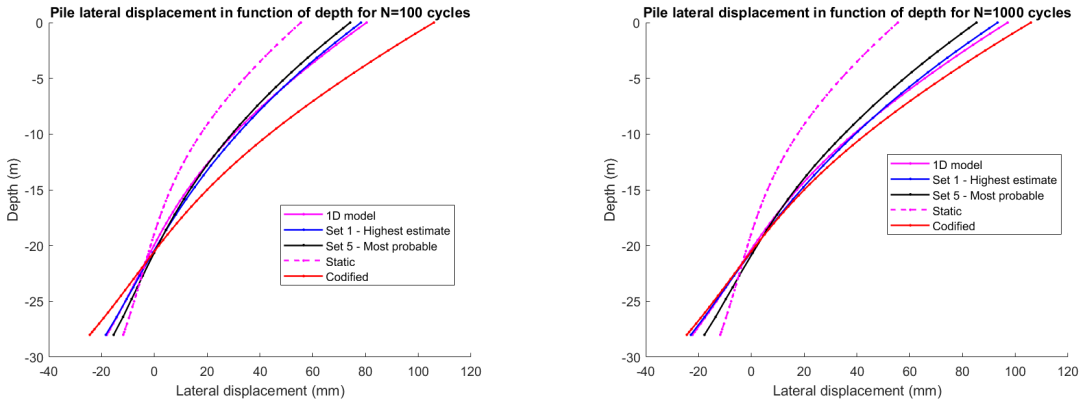

(a) $N = 10^2$ cycles (b) $N = 10^3$ cycles

Figure 7.11: Pile lateral displacement in function of depth after N loading cycles - Results comparison between the study model (highest and most probable estimates), the codified procedure and the 1D-model

The calibrated 1D model provides a close fit with the SDM highest estimate for $N = 10^2$ and $N = 10^3$ loading cycles. Thus, the calibrated 1D model provides a smaller estimation of the pile lateral displacement compared

to the codified procedure.
By calibrating the 1D model on the results of the study model (SDM), the 1D model accounts for the number of cycles, the loading amplitude and the pile geometry. With this method, the 1D model provides a less conservative estimation of the pile lateral deflection under cyclic loading. As advised by the standards, the 1D model was calibrated on a FE model (DNVGL-ST-0126 [24]).
The 1D model is successfully calibrated for the reference system of section 7.1. Further studies are required to determine if the calibration is valid for different soil, loading and pile parameters.

7.6 Conclusion

In this chapter, a design exercise was investigated. The study model was extended to two different soil models: the homogeneous soil model and the multi-layered soil model. In the case of very homogenous soil conditions, the two models provide results in agreement.
The results of the study models were compared with the results of three cyclic methods: the codified procedure, the method of Dührkop (2009) [23] and the method of Garnier (2013) [27]. The two study models provide results in agreement with the method of Garnier (2013) [27]. The SDM and Garnier (2013) [27] account for the loading amplitude, the pile geometry and the number of cycles. Moreover, the methods were verified on pile test data with rigid piles. The two methods estimate a smaller pile head displacement compared to the codified procedure.
A Serviceability check (SLS) was performed with the study model. The results of the study model were below the SLS limit. Thus, the SDM can be used for performing SLS check.
Finally, parameters b_1 and b_2 that provide the highest and most probable estimates of the pile lateral displacement at mudline were determined from literature. The 1D model was successfully calibrated with the highest estimate of the pile lateral displacement. With this procedure, the 1D model accounts for the loading amplitude, the number of cycles and the pile geometry.

Chapter 8

Conclusions and Recommendations

8.1 Conclusions

In this research, the Stiffness Degradation Method (SDM) of Achmus et al. (2009) [2] and Kuo (2008) [39] was implemented into the FE software PLAXIS 3D with an automated routine coded in Python. The procedure was verified by comparing results with the reference system of Kuo (2008) [39]. Once verified, the study model was validated against three pile tests. As part of a design exercise, the results of the study model were compared with the results of codified and published cyclic approaches. The parameter sets b_1 and b_2 that provide the highest and most probable estimates of the pile lateral displacement were determined. Finally, the 1D model was calibrated with the highest estimate of the pile lateral displacement.

In the light of the main objectives of this research:

1. **Objective 1 - Literature overview**: Select a numerical method that assesses the cyclic behaviour of a monopile in sand under cyclic loading and corresponds to the early-design requirements of an offshore wind monopile.
2. **Objective 2 - FE implementation**: Ease the method application by implementing the procedure on a widely-used FE software by the mean of an automated routine coded in Python.
3. **Objective 3 - Validation**: Identify the strengths and limitations of the study model by comparing results with pile test data.
4. **Objective 4 - Design integration**: Assess the cyclic impact of the study model on a reference system.

The following main conclusions were drawn:

- The SDM corresponds to the requirements of an early design procedure:
  - Based on drained cyclic triaxial tests in compression, the SDM can model the cyclic behaviour of drained sand from shakedown to ratcheting.
  - The SDM requires a limited set of parameters that can be obtained from standard geotechnical tests. Parameters b_1 and b_2 are calibrated on cyclic triaxial tests in compression. Parameters b_1 and b_2 can also be calibrated with cyclic pile test data as long as the parameters remain in the same parameter range of cyclic triaxial tests. In case cyclic triaxial test data are not available for a specific soil, sets of parameters b_1 and b_2 from literature are classified from the highest to the smallest estimate of pile lateral displacement.
  - The SDM requires limited computation times for a FE model.
- The SDM was successfully implemented into the FE software PLAXIS 3D by the mean of an automated routine coded in Python. The soil stiffness was degraded by updating the soil material within the soil clusters. The study model was verified against the results of a published reference system (Kuo (2008) [39]) for two different pile embedded lengths. The results of the study model were in agreement with the results of Kuo (2008) [39] even though differences were observed. The study model provides a stiffer pile-soil response than the reference model because the soil stiffness is overestimated. The degraded stiffness overestimation is attributed to the initial stiffness mismatch and the use of soil clusters.
  - The study model uses a different soil model than the user-defined material (UMAT) created for the SDM. The linear elastic material with Mohr-Coulomb failure criterion and stress-dependent stiffness is modelled in this study with the Mohr-Coulomb constitutive model along with soil layers

with depth-dependent stiffness. Whereas the stresses at phase 0 and phase 1 are identical between the study model and the original SDM, the resulting stress-dependent stiffness is higher in the study model. Thus, the results indicate that the two models calculate the stiffness differently.

  - In this study, the soil stiffness is degraded by updating the soil stiffness in the soil clusters. By averaging the stiffness over the clusters, the degraded stiffness is smoothed and some accuracy is lost. Refining the clusters layout improves the results of the study model in comparison with Kuo (2008) [39].
  - As a result of the stiffness overestimation and the use of the clusters, the study model provides closer results to Kuo (2008) [39] for the long pile than for the short pile. The impact of the stiffness overestimation is greater on the short pile ($\frac{L}{D}$ = 2.73) than on the long pile ($\frac{L}{D}$ = 5.3) because the short pile opposes less resistance to the loading and is thus more affected by the stiffness overestimation.

- The study model was validated by back-calculating three 1-g pile tests: Hettler (1981) [29], Achmus et al. (2007) [1] and Li et al. (2015) [42].
  - The numerical results of the study model are in agreement with the results of the pile tests. For some loading conditions, the study model provides a closer fit with the test results than Kuo (2008) [39]. This trend is attributed to the degraded stiffness overestimation from the FE implementation.
  - The impact study performed on parameters b_1 and b_2 indicates that b_1 has a decisive impact on the pile lateral displacement whereas parameter b_2 has less impact.
  - The study model is validated on mono-layered and multi-layered dense sand.

- The study model was adapted to an early-design framework.
  - Two numerical models were developped for the design exercise: the homogeneous and multi-layered soil models. The multi-layered soil model is adapted to the data that are available during an early-design phase. The homogeneous and multi-layered soil models provide results in agreement.
  - The study model was compared with three cyclic methods: the codified procedure, the method of Dührkop (2009) [23] and the method of Garnier (2013) [27]. The method of Garnier (2013) [27] and the study model account for the loading amplitude, the number of loading cycles and the pile geometry. They provide similar results. The codified procedure and the method of Dührkop (2009) [23] estimate higher lateral displacement compared to the study model. Thus, the study model is a less conservative cyclic approach for determining the pile lateral displacement.
  - Parameters b_1 and b_2 that are available in the literature are classified from the highest to the smallest estimate of pile lateral displacement.
  - The 1D model can be calibrated with the pile deflection curves of the study model. With this procedure, the 1D model accounts for the number of cycles, the loading amplitude and the pile geometry.

8.2 Recommendations

This section presents the recommendations for the use of the study model and recommendations for further research.

8.2.1 Recommendations for the use of the study model

This section presents different recommendations for the use of the study model:

- Sets of parameters b_1 and b_2 are classified in this study. They are classified from the highest to the smallest estimate of pile lateral displacement. Because the study model underestimates the pile lateral displacement compared to the SDM, it is recommended to use parameters b_1 and b_2 that provide the highest estimate of pile lateral displacement. This recommendation is reinforced for small piles ($\frac{L}{D} \approx 3$) as the stiffness overestimation has more impact on them.

- A cluster layout is recommended in this study. In this study, the cluster layout could not be refined further because of limitation in the computer capacity. Thus, the user is required to check if a refinement of the cluster layout is possible depending on the computer capacity.

- The study model is validated on 1-g pile tests. 1-g pile tests are not scaled to represent large monopiles. Thus, for using the study model in an early-design procedure, the results should be confirmed with published cyclic practices that were validated on Ng pile tests or field tests.
  Verifying the study model on Ng and large scale pile tests would ensure the definitive validation of the study model.

- The validation of the study model for multi-layered conditions was performed on remarquably homogeneous dense sands. Thus, in case of less homogeneous sand, the use of the multi-layered soil model requires cautiousness and further validation.
  In case some small layers of clay (maximum 1m depth) are interspersed in the sand layers, they could be discarded for running the study model. However, as the effect of the clay layers was not investigated in this study, their impact is unknown. For such case, the results of the study model require cautiousness and can only a provide a first indicative estimation of the pile lateral displacement. Thus, in the case where small layers of clay are discarded, the study model estimation requires further study.

- Calibrating the 1D model on pile deflection curves from the study model is a promising procedure because it provides smaller pile lateral displacement compared to the codified procedure. However, this new design procedure is not validated. It requires further studies and additional verification on pile tests for variable soil, pile and loading conditions.

8.2.2 Recommendations for future research

This section presents different recommendations for future research:

- Accessing the script of the User-defined Material (UMAT) of the SDM (Kuo, 2008 [39]) would enable to determine precisely the differences between the SDM and the study model.

- Extending the literature database of parameters b_1 and b_2 would assist the user for chosing the most adapted parameters. Enlarging the database enables the study of possible correlations between the soil parameters and SDM parameters b_1 and b_2.

- Studying the possible extension of the SDM to two-way cyclic loading would provide insight about the capability of the method to fully cover the different types of cyclic loading. The study would include a calibration of parameters b_1 and b_2 on cyclic triaxial tests in compression and extension.

- Extending the study model to variable amplitude loading.

- Comparing the results of the study model with other explicit numerical methods that assess the cyclic behaviour of monopiles in sands.

- Studying the possible extension of the SDM to a more advanced soil constitutive model like HSsmall.

Bibliography

[1] Achmus, M., Kuo, Y.S. and Abdel-Rahman, K. (2007). Behavior of large diameter monopiles monopile under cyclic horizontal loading. *12th International Colloquium on Structural and Geotechnical Engineering (ICSGE)*.

[2] Achmus, M., Kuo, Y.S. and Abdel-Rahman, K. (2009). Behavior of monopile foundations under cyclic lateral load. *Computers and Geotechnics*, 36(5), pp. 725-735. Elsevier BV.

[3] Adhikari, S. and Bhattacharya, S. (2012). Dynamic Analysis of Wind Trubine Towers on Flexible Foundations. *Shock Vib 2012*; 19:37-56.

[4] Albiker, J., Achmus, M., Frick, D. and Flindt, F. (2017). 1g model tests on the displacement accumulation of large-diameter piles under cyclic lateral loading. *Geotechnical Testing Journal*, Vol. 40, No. 2, pages 173-184.

[5] Alonso-Marroquin, F. and Herrmann, H. J. (2004). Ratcheting of granular materials. *Physical Review Letters*, 92(5):054301.

[6] Andersen, K. H., Puech, A. A. and Jardine, R.J. (2013). Cyclic resistant geotechnical design and parameter selection for offshore engineering and other applications. *Proceedings of TC 209 Workshop - 18th ICSMGE*, pages 9-45, Paris, France.

[7] Andersen, K. H. (2015). Cyclic soil parameters for offshore foundation design. In Meyer, V., editor, *Frontiers in Offshore Geotechnics III*, pages 5-82, Oslo, Norway. Taylor & Francis Group.

[8] API. (2011). *Recommended Practice 2 GEO*. API, 1220 L Street, NW, Washington, DC 20005, Geotechnical and Foundation Design Considerations.

[9] Arany, L., Bhattacharya, S. and Adhikari, S. (2015) An analytical model to predict the natural frequency of offshore wind turbines on three-spring flexible foundations using two different beam models. *Soil Dynamics and Earthquake Engineering 2015*, 74:40-5.

[10] Arany, L., Bhattacharya, S., Macdonald, J., Hogan, S.J. (2017). Design of monopiles for offshore wind turbines in 10 steps. *Soil Dynamics and Earthquake Engineering 92*, 126-152.

[11] Bhattacharya, S. (2014). Challenges in design of foundations for Offshore Wind Turbines. *Engineering & Technology Reference*.

[12] Bhattacharya, S., Nikitas, G., Arany, L., Nikitas, N. (2017). Soil-Structure Interactions (SSI) for Offshore Wind Turbines. *The Institution of Engineering and Technology*.

[13] Bouzid, D.A., Bhattacharya, S. and Dash, S.R. (2013). Winkler springs (p-y curves) for pile design from stress-strain of soils: FE assessment of scaling coefficients using the mobilized strength design concept. *Geomechanics and Engineering*, Vol. 5, No. 5, pp. 379-399.

[14] Brinkgreve, R.B.J. (2005). Selection of soil models and parameters for geotechnical engineering application. *Geo-Frontiers Congress 2005*, Austin, Texas, United States.

[15] Brinkgreve, R.B.J. and Engin, E and Swolfs, WM. (2013). PLAXIS 3D 2013 user manual. *Plaxis bv, Delft*.

[16] Burd, Harvey J and Taborda, David MG and Zdravković, Lidija and Abadie, Christelle N and Byrne, Byron W and Houlsby, Guy T and Gavin, Kenneth G and Igoe, David JP and Jardine, Richard J and Martin, Christopher M and others. (2019). PISA design model for monopiles for offshore wind turbines: application to a marine sand. *Géotechnique*, Vol. 70, pp. 1048-1066.

[17] Byrne, BW and McAdam, Ross A and Burd, HJ and Houlsby, GT and Martin, Chris M and Beuckelaers, WJAP and Zdravkovic, L and Taborda, DMG and Potts, DM and Jardine, RJ and others. (2015). PISA: new design methods for offshore wind turbine monopiles. *Offshore Site Investigation Geotechnics 8th International Conference Proceeding*. pp. 142-161.

[18] Chern, J-C. (1985). *Undrained response of saturated sands with emphasis on liquefaction and cyclic mobility*. Phd thesis, University of British Columbia.

[19] Chong, S.-H. and Santamarina, J. C. (2016). Sands subjected to repetitive vertical loading under zero lateral strain: accumulation models, terminal densities, and settlement. *Canadian Geotechnical Journal*, 53(12):2039-2046.

[20] De Gennaro, V., Canou, J., Dupla, J.C. and Benahmed, N. (2004). Influence of loading path on the undrained behaviour of a medium loose sand. *Canadian Geotechnical Journal*, T03-082.

[21] Della, N., Belkhatir, M., Arab, A., Canou, J. and Dupla, J-C. (2014). Undrained Monotonic Response and Instability of Medium-Dense Sandy Soil. *Marine Georesources & Geotechnology*, 1521-0618.

[22] Depina, I., Le, T.M.H., Eiksund, G., Benz, T. (2015). Behavior of cyclically loaded monopile foundations for offshore wind turbines in heterogeneous sands. *Computers & Geotechnics*, No. 65, 266-277.

[23] Dührkop, J. (2009). *Zum Einfluss von Aufweitungen und zyklischen Lasten auf das Verformungsverhalten lateral beanspruchter Pfähle in Sand*. Phd thesis, Institute for Geotechnical and Construction Engineering, Hamburg University of Technology.

[24] DNV-GL (2018). *Support structures for wind turbines - DNVGL-ST-0126*. DNV GL AS, Norway.

[25] Frick, D. and Achmus, M. (2019). Model tests on the behaviour of monopiles under genereral cyclic lateral loading. *2nd International Conference on Natural Hazards & Infrastructure*, 23-26 June, 2019, Chania, Greece.

[26] Frick, D. and Achmus, M. (2020). An experimental study on the parameters affecting the cyclic lateral response of monopiles for offshore wind turbines in sand. *Soils and Foundations*, Vol. 60, Issue 6, pp. 1570-1587.

[27] Garnier, A. (2013). Advances in axial cyclic pile design: Contribution of the SOLCYP project. *Proceedings of TC 209 Workshops - 18th ICSMGE*, Paris, France, pp. 59-68.

[28] Goldscheider, M. (1977). Shakedown and incremental collapse of structures in dry sand bodies. *Proceedings of Dynamical Methods in Soil and Rock, Plastic and Long-Term Effects in Soils 1977*.

[29] Hettler,A. (1981). Deformations of stiff and elastic foundation structures in sand under monotonous and cyclic loading. *Veröffentlichungen des Instituts für Bodenmechanik und Felsmechanik der Universität Fridericiana in Karlsruhe*, Heft 9.

[30] Huurman,M., (1996). Development of traffic induced permanent strain in concrete block pavements. *Heron 1996*.

[31] Idriss, I.M., Bobry, R., Singh, R.D. (1978). Non-linear behavior of soft clays during cyclic loading. *Journal of the Geotechnical Engineering Division, ASCE*, Vol. 104, No. 12, pp. 1427-1447.

[32] Jagodnik, V., Kraus, I., Ivanda, S., Arbanas, Z. (2020). Behaviour of Uniform Drava River Sand in Drained Condition - A Critical State Approach. *Applied Sciences 2020*, 10, 5733.

[33] Jalbi, S., Arany, L., Salem, A., Cui, L., Bhattacharya, S. (2019). A method to predict the cyclic loading profiles (one-way or two-way) for monopile supported offshore wind turbines. *Marine Structures 63*, 65-83.

[34] Kallehave, D., Byrne, B.W., Leblanc, C., Mikkelsen, K.K. (2015). Optimization of monopiles for offshore wind turbines. *A Mathematical Physical and Engineering Sciences 373*.

[35] Kaltekis, K and Panagoulias, S and van Dijk, BFJ and Brinkgreve, RBJ and da Silva, M Ramos (2019). Comparative concept design study of laterally loaded monopiles. *Journal of Physics: Conference Series*; 1222(1), pp. 012027.

[36] Klinkvort, R. T., Leth, C.T. and Hededal, O. (2012). Centrifuge modelling of monopiles in dense sand at The Technical University of Denmark. *Conference proceedings of the 2nd European conference on Physical Modelling in Geotechnics (EUROFUGE 2012)*, TU Delft.

[37] Klinkvort, R. T. and Hededal, O. (2013). Lateral response of monopile supporting an offshore wind turbine. *Geotechnical Engineering*, Vol. 166, Issue GE2, pp. 147-158.

[38] Komusanac, I. Wind Energy in Europe in 2019: Trends and Statistics (2020). Technical report. *WindEurope*.

[39] Kuo, Y-S. (2008). On the behavior of large-diameter piles under cyclic lateral load. Phd thesis, Leibniz Universität Hannover, Heft 65.

[40] Leblanc, C., Houlsby, G. T. and Byrne, B.W. (2010). Response of stiff piles in sand to long-term cyclic lateral load. *Géotechnique 60*, No. 2, pages 79-90.

[41] Li, Z., Haigh, S.K. and Bolton, D. (2010). Centrifuge modelling of mono-pile under cyclic lateral loads. *7th International Conference on Physical Modelling in Geotechnics*, Zurich, Vol.2, 965-970.

[42] Li, W., Igoe, D. and Gavin, K. (2015). Field tests to investigate the cyclic response of monopiles in sand. *Proceedings of the Institution of Civil Engineers: Geotechnical Engineering 68*, Issue GE5, pp. 407-421.

[43] Lin, S. and Liao, J. (1999). Permanent strains of piles in sand due to cyclic lateral loads. *Journal of Geotechnical and Geoenvironmental Engineering (ASCE)*, 120(1), 225-244.

[44] Little R.L., Briaud, J. (1988). Full scale cyclic lateral load tests on six single piles in sand. *Miscellaneous Paper*, No. GL-88-27, Texas A&M University, College Station, TX.

[45] Liu, H., Abell, J. A., Diambra, A. and Pisano, F. (2019). Capturing cyclic mobility and preloading effects in sand using a memory-surface hardening model. In Silvestri & Moraci (Eds.), *Earthquake Geotechnical Engineering for Protection and Development of Environment and Constructions (Proceedings in Earth and Geosciences)*. Rome: Associazione Geotecnica Italiana.

[46] Liu, H. (2020). *Constitutive modelling of cyclic sand behaviour for offshore conditions*. Phd thesis, Delft University of Technology.

[47] Long, J.H., Vanneste, G. (1994). Effects of cyclic lateral loads on piles in sand. *Journal of Geotechnical Engineering*, Vol. 120, No.1, pp. 33-42.

[48] Matlock, H. (1970). Correlations for design of laterally loaded piles in soft clay. *Offshore Technology in Civil Engineering's Hall of Fame Papers from the Early Years*, pp. 77-94.

[49] Murphy, G., Igoe, D., Doherty, P. and Gavin, K. (2018). 3D FEM approach for laterally loaded monopile design. *Computers and Geotechnics, 100*, 76-83.

[50] Nanda, S., Arthur, I., Sivakumar, V., Donohue, S., Bradshaw, A., Keltai, R., Gavin, K., Mackinnon, P., Rankin, B. and Glynn, D. (2017). Monopiles subjected to uni- and multi-lateral cyclic loading. *Geotechnical Engineering 2017*; 170(GE3):246-58.

[51] Narsilio, A. and Santamarina, J. (2008). Terminal densities. *Géotechnique*, 58(8):669.

[52] Niemunis, A., Wichtmann, T. and Triantafyllidis, T. (2004). Explicit accumulation model for cyclic loading. *International Conference on Cyclic Behaviour of Soils and Liquefaction Phenomena*, Bochum.

[53] Pasten, C., Shin, H. and Santamarina, J.C. (2014). Long-term foundation response to repetitive loading. *Journal of Geotechnical and Geoenvironmental Engineering*, 140(4):04013036.

[54] Panagoulias, S. and Brinkgreve, R.B.J. and Minga, Elini and Burd, H.J. and McAdam, R.A. (2018). Application of the PISA framework to the design of offshore wind turbine monopile foundations. *WindEurope 2018 conference at the Global Wind Summit*, Hamburg, Germany.

[55] Panagoulias, S., Hosseini, S., Brinkgreve, R.B.J. and Burd, H.J. (2019). Design of laterally-loaded monopiles in layered soils. *Proceedings of the 2nd International Conference on Natural Hazards & Infrastructure*, Athens: National Technical University of Athens.

[56] Peralta, P. and Achmus, M. (2010). An experimental investigation of Piles in Sand subjected to Lateral Cyclic Loads. *7th International Conference on Physical Modelling in Geotechnics (ICPMG 2010)*, Zurich, Switzerland.

[57] Poulos, H.G. and Hull, T. (1989). The role of geotechnical geomechanics in foundation engineering. *Foundation Engineering: Current principles and practices*, ASCE, Reston, 2 (1989), pp. 1578-1606.

[58] Puech, A., Canou, J., Bernardini, C., Pecker, A., Jardine, R. and Holeyman, A. (2012). SOLCYP: A four-year joint industry project on the behaviour of piles under cyclic loading. *Offshore Site Investigation and Geotechnics: Integrated Technologies - Present and Future*, SUT-OSIG-12-26.

[59] Rascol, E. (2009). *Cyclic Properties of Sand: Dynamic Behaviour for Seismic Applications*. Phd thesis, Ecole Polytechnique Fédérale de Lausanne.

[60] Reese, L.C., Cox, W.R. and Koop, F.D. (1975). Field testing and analysis of laterally loaded piles in stiff clay. *Proceedings of the VII Annual Offshore Technology Conference*; pp. 672-690. Houston, Texas, 2(OTC 2312).

[61] Rosquoet, F., Thorel, L., Garnier, J. and Canepa, Y. (2007). Lateral cyclic loading of sand-installed piles. *Soils and Foundations*, Vol. 47, No. 5, pp. 821-832.

[62] Rudolph, C., Grabe, J., Bienen, B. (2014). Response of monopile under cyclic lateral loading with a varying load direction. *Proceedings of the 8th international conference on physical modelling in geotechnics*, Perth: CRC Press.

[63] Shajarati, A., Sorensen, K. W., Nielsen, S. K., Ibsen, L.B. (2012). Behaviour of Cohesionless Soils During Cyclic Loading. *DCE Technical Memorandum No. 14*. Department of Civil Engineering, Aalborg University.

[64] Smith, M. (2009). ABAQUS/Standard User's Manual, Version 6.9. Dassault Systèmes Simulia Corp, Providence, RI.

[65] Sorensen, S. P. H., Brodbaek, K. T., Moller, M. and Augustesen, A.H. (2012). *Review of Laterally Loaded Monopiles Employed as the Foundation for Offshore Wind Turbines*, Department of Civil Engineering, Aalborg University. DCE Technical reports No. 137.

[66] Thieken, K., Achmus, M. and Lemke, K. (2015). A new static p-y approach for piles with arbitrary dimensions in sand. *Geotechnik 38*, Heft 4. Ernst & Sohn: Verlag fur Architektur und technische Wissenschaften GmbH & Co. KG, Berlin.

[67] Ti, K.S., Huat, B.B.K., Noorzaei, J., Jaafar, M.S., Sew, G.S. (2009). A review of basic soil constitutive models for geotechnical application, EJGE, Vol. 14.

[68] Truong, P. and Lehane, B.M. (2015). Experimental trends to lateral cyclic tests of piles in sand. *Proceedings of the 3rd International Symposium on Frontiers in Offshore Geotechnics*, Oslo, Norway, vol. I, pp. 747-752.

[69] Truong, P., Lehane, B.M., Zania, V. and Klinkvort, R.T. (2019). Empirical approach based on centrifuge testing for cyclic deformations of laterally loaded piles in sand. *Geotechnique*, 69(2), 133-145.

[70] Vaid, Y. P., Chung, E. K. F. and Kuerbis, R.H. (1989). Preshearing and undrained response of sand. *Soils and Foundations*, 29(4):49-56.

[71] Venkatesh,N., Heeralal, M., Pillai, R. J. (2018). Resilient and permanent deformation behaviour of clayey subgrade soil subjected to repeated load triaxial tests. *European Journal of Environmental and Civil Engineering*, 2116-7214.

[72] Wichtmann, T. (2005). *Explicit accumulation model for non-cohesive soils under cyclic loading*. Phd thesis, Ruhr-Universität Bochum.

[73] Wu, X., Hu, Y., Li, Y., Yang, J., Duan, L., Wang, T., Adcock, T., Jiang, Z., Gao, Z., Lin, Z., Borthwick, A. and Liao, S. (2019). Foundations of offshore wind turbines: a review. *Renewable and Sustainable Energy Reviews 104*, pages 379-393.

[74] Yang, M., Luo, R. and Li, W. (2018). Numerical study on accumulated deformation of laterally loaded monopiles used by offshore wind turbine. *Bulletin Engineering, Geology and Environment*, 77:911-921.

[75] Zorzi, G., Richter, T., Kirsch, F., Augustesen, A.H., Ostergaard, M.U. and Sorensen, S.P.H. (2018). Explicit method to account for cyclic degradation of offshore wind turbine foundations using cyclic interaction diagrams. *14th EAWE PhD Seminar on Wind Energy*, Brussel, Belgium.

Appendices

Appendix A

Appendix A

Experiment parameters								
Name	Model	Soil	Pile	Prototype diameter (m)	Load eccentricity (e/d)	Pile penetration (L/d)	N [-]	ζ_c
Little and Briaud (1988) [44]	Full scale	Sand and clay (medium dense)	Flexible	[0.5, 1]	-	[0.41, 4.9]	20	0, 0.5
Long and Vanneste (1994) [47]	Full scale	-	Flexible	-	-	-	-	
Lin and Liao (1999) [43]	Full scale	Sand (loose, medium, dense)	Flexible	[0.15; 1.4]	Depends on tests	Depends on tests	100	[-1;0.5]
Rosquet et al. (2007) [61]	Ng	Dry dense to medium dense sand	Flexible	0,72	2,2	16,6	44	1
Cuellar et al. (2009) [**?**]	1g	Saturated sand	Rigid	7.5	4	4	5x10^6	1
Leblanc et al. (2010) [40]	1g	Drained loose sand	Stiff	4	4	5.4	8000 - 60 000	[-1;1]
Li et al. (2010) [41]	Ng	Dense dry sand	Stiff	5	14.4	5	1000	1
Klinkvort et al. (2012) [36]	Ng	Dry sand	Rigid	5	[2.5d;6.5d]	-	100 - 500	-
Klinkvort and Hededal (2013) [37]	Ng	Saturated and dry dense sand	Rigid	3	Constant: [2d;25d]		10 000	[-0.84;1]
Li et al. (2015) [42]	Calibrated model	Dense sand	Rigid	6	1.2	6.5	5000	1
Albiker et al. (2017) [4]	1g	Dry sand	Rigid	5 to 6	0.71	-	30 000	[-0.8;0.5]
Frick and Achmus (2019) [25]	1g	Sand	Rigid	4,5	[0.6 ; 0.8]	-	2500	[-0.75; 0.25]
Truong et al. (2019) [69]	1g	Saturated sand	Rigid	-	-	-	1500	
Frick and Achmus (2020) [26]	1g	Medium dense sand	Rigid	-	[0.6;1.2]	[6;8]	10 000	[-0.75; 1]

Table A.1: Summary table of cyclic pile tests in chronological order and their parameters

Appendix B

Appendix B

Method to determine b_1 and b_2 from drained cyclic triaxial test in compression
The recommendation is to determine parameters b_1 and b_2 from drained cyclic triaxial tests like in Figure B.1.

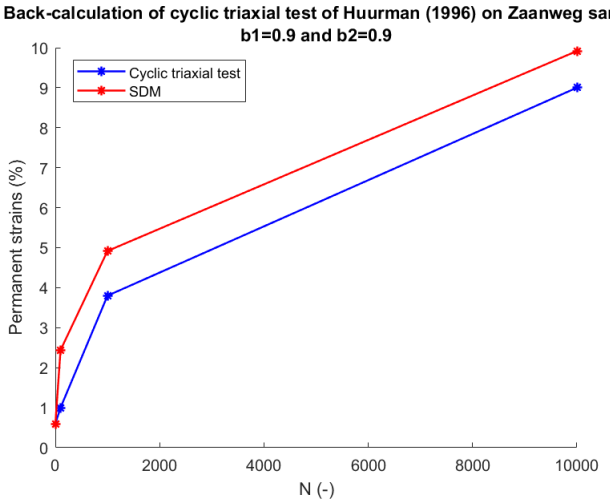

Figure B.1: Calibration of the parameters b1 and b2 on a cyclic triaxial test performed on Zaanweg sand from Huurman (1996)

The method is described as follow:

1. **Step1: Calculate the cyclic stress ratio X of the lab test**
   The cyclic stress ratio is determined with Equation 3.6. The cyclic major principal stress $\sigma_{1,cycl}$ is determined from the confining pressure $p = \sigma_3$ and the cyclic deviatoric stress q_{cycl}:

   $$\sigma_{1,cycl} = p + q_{cycl} \tag{B.1}$$

   The principal stress at failure is determined with the Mohr-Coulomb failure criterion in Equation 3.7.

2. **Step2: Calculate the permanent axial strains with the SDM empirical law**
   From the lab test, the permanent axial strains at $N = 1$ cycle are measured as the average axial strains at $N = 1$ cycle: $\epsilon_{p,N=1} = \epsilon_{avr,N=1}$. The empirical law of Equation 3.11 is used to calculate the strains after N loading cycles.

3. **Step3: Calibration of the strains calculated with the SDM power law on the triaxial test results**
   The permanent axial strains calculated during the triaxial test and with the SDM are plotted on the same graph like in Figure B.1. To obtain a good fit between the red and blue curves, the parameters b_1 and b_2 from which the SDM strains are determined are varied until reaching the optimized values.

Appendix C

Appendix C

In this appendix, the results of the homogeneous soil model of chapter 7 are compared fort two loading conditions:

- Axial and lateral loads are applied on top of the monopile (V)
- Only the lateral load is applied on top of the monopile (No V)

Figure C.1 presents the pile lateral displacement in function of depth for N=1, 100 and 10 000 cycles. The lateral displacement of the pile is slightly higher if no axial load is applied.

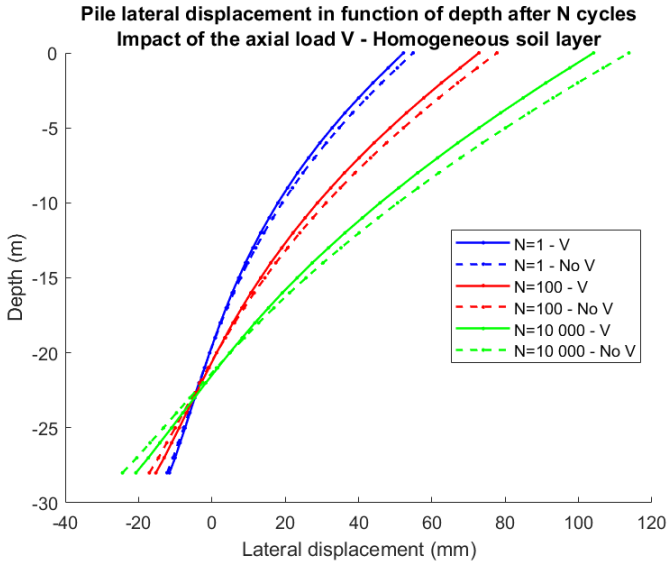

Figure C.1: Pile lateral displacement in function of depth for N=1, 100 and 10 000 cycles - Comparison of the results of the homogeneous soil model (chapter 7) with and without axial load

Appendix D

Appendix D

In this appendix, the FE models of the pile tests of Hettler (1981) [29], Achmus et al. (2007) [1] and Li et al. (2015) [42] are presented.

D.1 Pile test of Hettler (1981)

The dimensions of the FE model representing the settings of the pile test of Hettler (1981) [29] have been extended to a width and a length of respectively 10 times and 20 times the pile diameter D. The model depth is kept to 2 times the embedded length L. Figure D.1 presents the FE model.

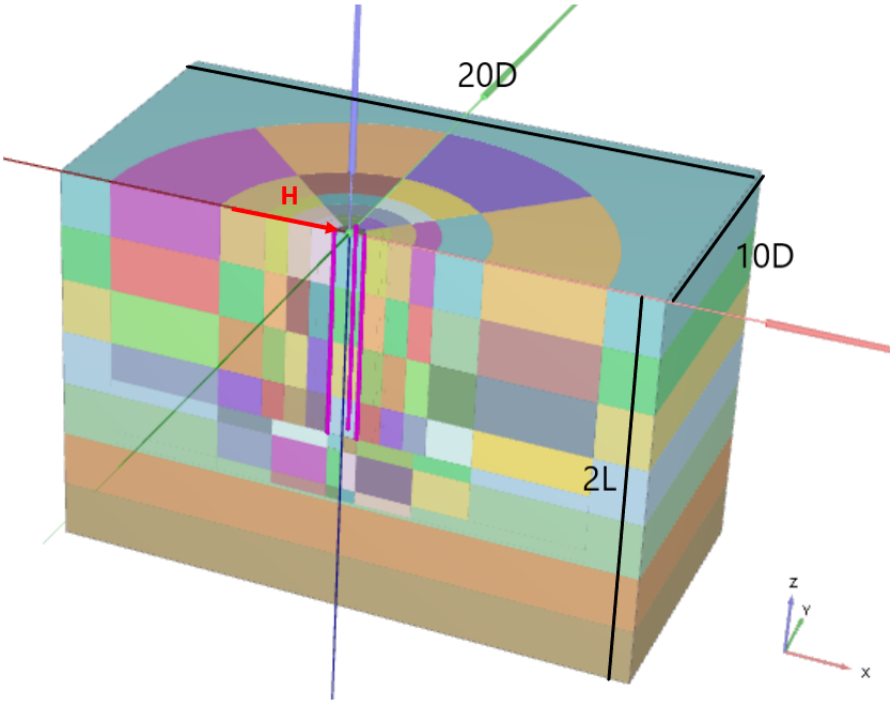

Figure D.1: FE model of the pile test of Hettler (1981) [29] - PLAXIS 3D View

The model parameters of the pile test of Hettler (1981) [29] are available in subsection 6.1.1. Table D.1 presents the dimensions of the cluster layout. The dimensions a and b are higher than the recommendation in section 5.3.5 because of the small size of the model. Using smaller clusters leads to collapse during the meshing procedure. The mesh coarseness is set to 0.075 (coarse mesh) as recommended in subsection 5.3.4.

Cluster layout - Pile test of Hettler (1981) [29]		
a (m)	b (m)	c (-)
0.05	[0.02;0.02;0.02;0.04;0.1]	4

Table D.1: Cluster layout of the FE model representing the settings of the pile test of Hettler (1981) [29]

The lateral loading H is determined as:

$$R_{Het} = \frac{H}{\gamma L^2 L_E} \tag{D.1}$$

Where γ is the soil unit weight, L is the embedded length and L_E is the elastic pile length:

$$L_E = \sqrt{\frac{E_p I_p}{\gamma L}} \tag{D.2}$$

Where E_p is the Young's modulus of elasticity of the pile, I_p is the moment of inertia of the pile, γ is the soil unit weight and L is the embedded length.
Table D.2 presents the three load cases of the pile test of Hettler (1981) [29].

Loading conditions - Pile test of Hettler (1981) [29]		
R_{Het}	H (N)	H/Hu
0,0804	47,18	66%
0,0446	26,17	36%
0,0292	17,14	24%

Table D.2: Load cases of the pile test of Hettler (1981) [29]

D.2 Pile test of Achmus et al. (2007)

The dimensions of the FE model of the pile test of Achmus et al. (2007) [1] are presented in Figure D.2. The width and the length of the model are respectively 10 and 20 times the pile diameter D. The depth is 2 times the pile embedded length L. The main parameters of the numerical model are presented in subsection 6.2.1. As the pile lateral displacement is measured 0.09m above the pile head, the three beams (subsection 4.3.3) are extended to 0.33m above mudline.

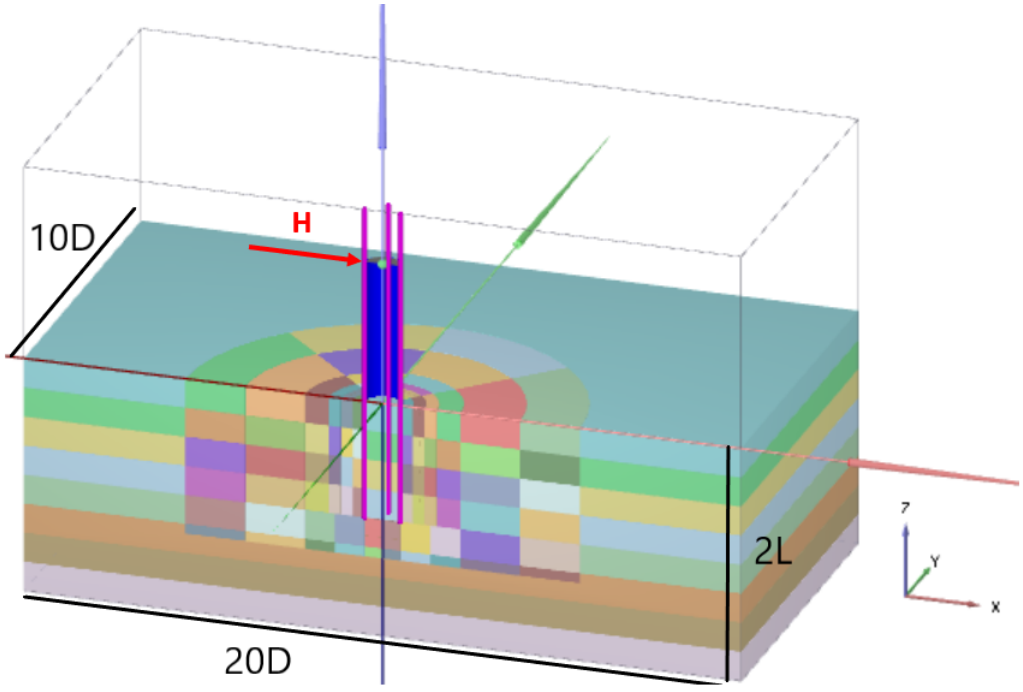

Figure D.2: FE model of the pile test of Achmus et al. (2007) [1] - PLAXIS 3D View

Table D.3 presents the dimensions of the cluster layout. Similar to section D.1, the parameters a and b are higher than the recommendations because smaller soil clusters would collapse during the meshing procedure of PLAXIS 3D. The mesh is coarse according to the recommendations of subsection 5.3.4.

Cluster layout - Pile test of Achmus et al. (2007) [1]		
a (m)	b (m)	c (-)
0.05	[0.02;0.02;0.02;0.04;0.1;0.1]	4

Table D.3: Cluster layout of the FE model representing the settings of the pile test of Achmus et al. (2007) [1]

The lateral loads of the pile test of Achmus et al. (2007) [1] are presented in Table D.4.

Loading conditions - Pile test of Achmus et al. (2007) [1]	
H (N)	H/Hu
16	40%
4	10%

Table D.4: Load cases of the pile test of of Achmus et al. (2007) [1]

D.3 Pile test of Li et al. (2015)

The dimensions of the FE model of the pile test of Li et al. (2015) [42] are presented in Figure D.3. The dimensions of the experiment tank were chosen as they were considered sufficently high to avoid boundary conditions. The width and the length are respectively 4.1m (12D) and 16.4m (48.2D). The depth of the model is the depth of the last layer of sand at 3.5m depth (1.6L). The main parameters of the model are presented in subsection 6.3.1.

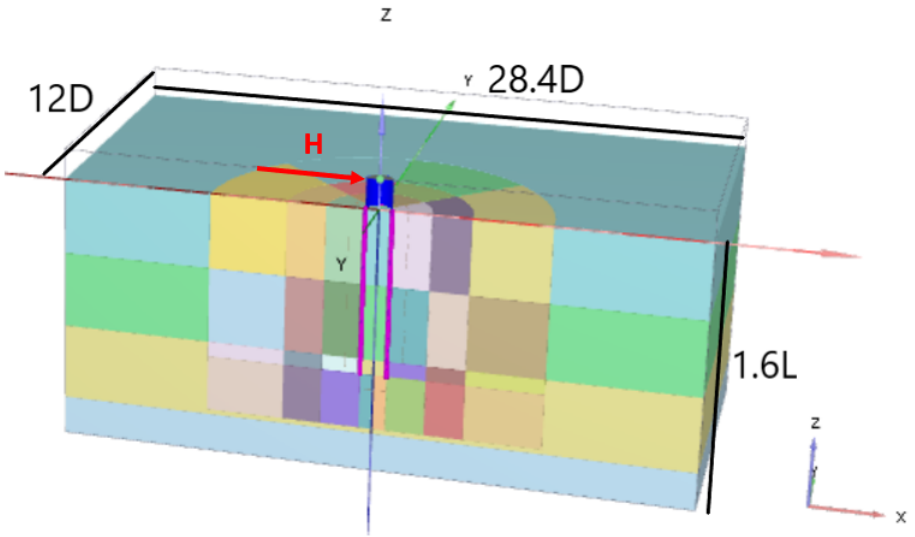

Figure D.3: FE model of the pile test of Li et al. (2015) [42] - PLAXIS 3D View

The cluster layout is presented in Table D.5. Dimension a is controlled by the depth of every sand layer (subsection 6.3.1). As the pile embedded length reaches the third layer, an extra layer of 0.2m is created to allow the clustering along the pile in the third layer. Clusters are then created below the pile. The mesh is coarse according to the recommendations of subsection 5.3.4.

Cluster layout - Pile test of Li et al. (2015) [42]		
a (m)	b (m)	c (-)
[1;1;0.2;0.5]	[0.5;0.5;1]	4

Table D.5: Cluster layout of the FE model representing the settings of the pile test of Li et al. (2015) [42]

Appendix E

Appendix E

		Soil properties							
		Submerged unit weight	Stiffness parameters		Friction angle	Dilatancy angle	Poisson's ratio	SDM parameters	
Model	Soil type	γ' (kN/m^3)	κ	λ	ϕ (°)	ψ (°)	ν	b_1	b_2
Kuo (2008) [39]	Dense sand	11	600	0.55	37.5	7.5	0.25	0.20	5.76
Hettler (1981) [29]	Dense sand	6.9	350	0.65	42	12.5	0.16	0.12	0.32
Achmus et al. (2007) [1]	Dense sand	9	300	0.65	37.5	7.5	0.25	0.12	0.5
Li et al. (2015) [42]	Dense sand	10	1000	0.4	51.2	17.7	0.20	0.1	8

Table E.1: Soil parameters of the reference models and pile tests on which the study model is validated

	Pile properties								
	Pile geometry						Pile parameters		
Model	D (m)	L (m)	h (m)	t_p (m)	h/L	L/D	E_p (kPa)	w_p (kN/m^3)	ν_p
Kuo (2008) [39]	7.5	20, 40	20	0.09	1	2.7 , 5.3	2.1E8	68	0.2
Hettler (1981) [29]	0.0259	0.185	0	0.003	0	7,1	2.1E8	68	0.2
Achmus et al. (2007) [1]	0.06	0.2	0.24	0.003	1,2	3,3	2.1E8	78	0.2
Li et al. (2015) [42]	0.34	2.2	0.40	0.080	0.18	6.5	2.1E8	68.5	0.3

Table E.2: Pile parameters of the reference models and pile tests on which the study model is validated

Loading conditions		
Model	V	H
Kuo (2008) [39]	10 MN	15 MN
Hettler (1981) [29]	X	66%, 36%, 24% H_u
Achmus et al. (2007) [1]	X	40%, 10% H_u
Li et al. (2015) [42]	X	30% H_u

Table E.3: Loading parameters of the reference models and pile tests on which the study model is validated

Appendix F

Appendix F

Figure F.1 presents the pile lateral displacement in function of the number of cycles for different sets of parameters available in literature. Table F.1 presents the classification of the parameters in function of the pile lateral displacement at mudline.

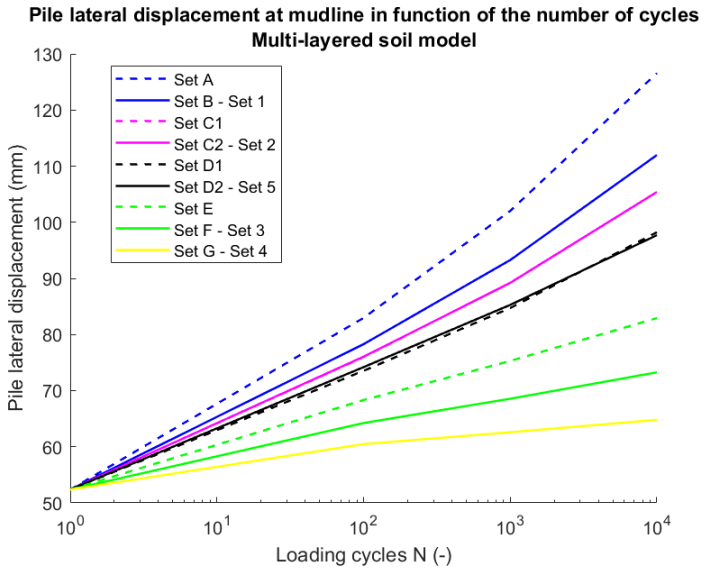

Figure F.1: Pile head displacement at mudline in function of the number of cycles - Multi-layered soil model

Rank	Researchers	b1	b2
A	Timmerman and Wu (1969)	0,1114	0
B - Set 1	Hettler (1981)	0,12	0,32
C1	Addo-Adebi (1980)	0,1607	1,56
C2 - Set 2	Achmus et al. (2007)	0.12	0.5
D1	Gaskin et al. (1979)	0,1265	0,98
D2 - Set 5	Average values of Kuo (2008)	0.20	5.76
E	McDonald and Raymond (1984)	0,16	21,4
F - Set 3	Li et al. (2015)- Upper bound	0,1	8
G - Set 4	Li et al. (2015)- Lower bound	0,05	5

Table F.1: Classification of the parameters b_1 and b_2 of the literature in ascending order in function of the pile lateral displacement in Figure F.1

Figure F.1 presents the variability of the pile lateral displacement at mudline for different sets of parameters b_1 and b_2. At $N = 10^4$ cycles, the highest estimate (set 1) of the pile lateral displacement is approximatively 2 times the displacement of the lowest estimate (set G). Thus, the impact of parameters b_1 and b_2 on the pile lateral displacement is significant.
The parameter set C1 ($b_1 = 0.1607$ & $b_2 = 1.56$) creates the same displacement as the parameter set C2 ($b_1 = 0.12$ & $b_2 = 0.5$). The same phenomenon is observed for the parameter set D1 ($b_1 = 0.1265$ & $b_2 = 0.98$) and the parameter set D2 ($b_1 = 0.20$ & $b_2 = 5.76$). Thus, different sets of parameters b_1 and b_2 can create similar

pile lateral displacement. This observation supports the hypothesis that a range of parameters b_1 and b_2 can represent the range of pile lateral displacement in sand.